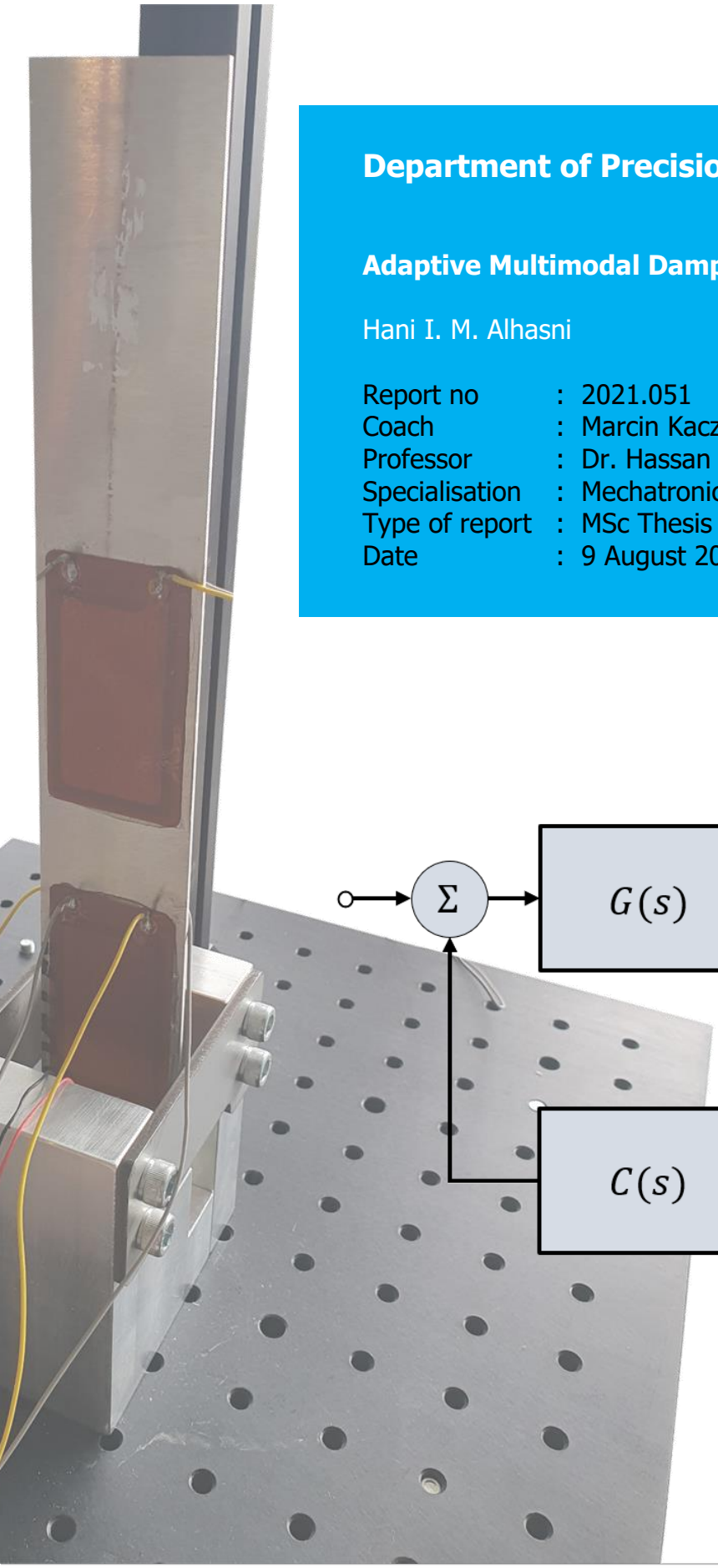

Department of Precision and Microsystems Engineering

Adaptive Multimodal Damping of Flexible Structures

Hani I. M. Alhasni

Report no : 2021.051
Coach : Marcin Kaczmarek
Professor : Dr. Hassan HosseinNia
Specialisation : Mechatronic System Design
Type of report : MSc Thesis
Date : 9 August 2021

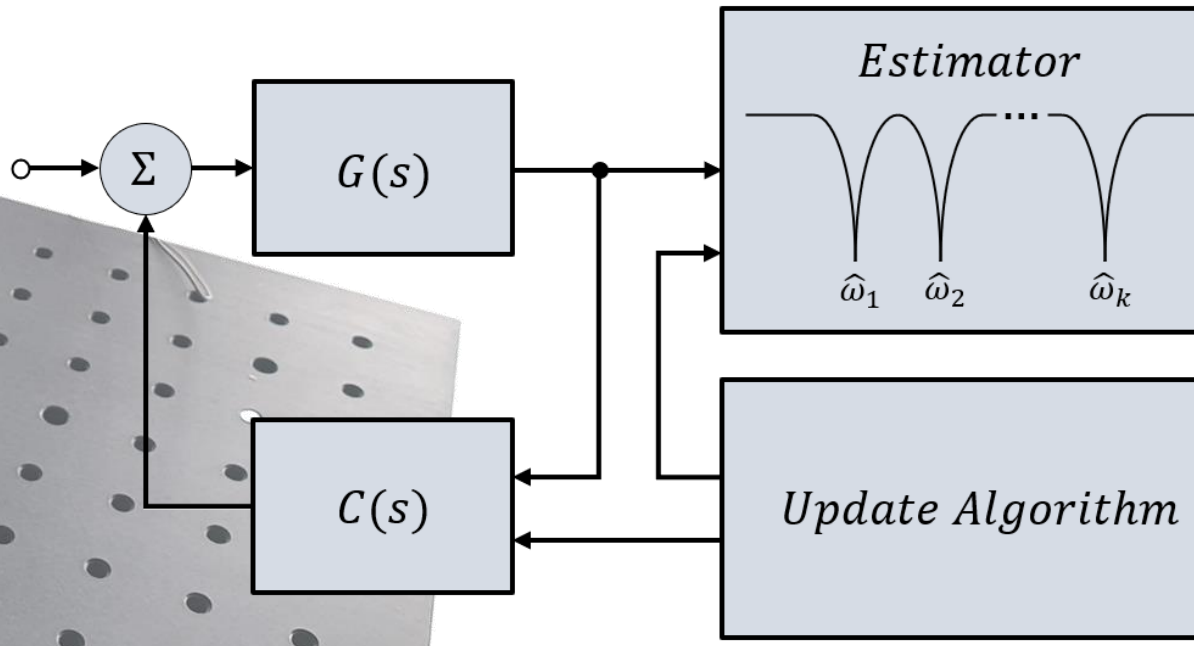

Adaptive Multimodal Damping of Flexible Structures

Hani I. M. Alhasni

Supervisors: Dr. Hassan HosseinNia
Marcin Kaczmarek

Committee: Dr. Andres Hunt
Dr. Barys Shyrokau
Dr. Hassan HosseinNia
Marcin Kaczmarek

Department of Precision and Microsystems Engineering
Faculty of Mechanical, Maritime and Materials Engineering
Delft University of Technology

This thesis is submitted for the degree of
Master of Science in Mechanical Engineering

August 2021

Acknowledgements

This thesis would not have been possible without all the supervision and support that I've received throughout this year-long commitment.

First and foremost, I would like to thank Dr. Hassan HosseinNia for allowing me to work on such an interesting topic, for his counsel, and for sharing invaluable practical knowledge with me. I would also like to thank Marcin Kaczmarek as my daily coach. Marcin made insightful comments, asked important questions, and encouraged active curiosity. Whenever I had doubts, Marcin always pointed me in the right direction. I am beyond grateful for the excellent supervision that I had for the duration of this thesis.

The environment at TU Delft and the PME department in particular was extremely supportive. I am thankful to everyone who helped me create my experimental setup, including Gideon, Spiridon, and Bradley from lab support and Dr. Andres Hunt for sharing tips on using piezoelectric materials. I would also like to thank my peers Mathew, Thomas, and everyone else working in the mechatronics lab for creating such a pleasant and helpful atmosphere, and participants of the Monday meetings for all the interesting discussions and helpful feedback.

Finally, I would like to thank my family for their endless support and my friends for the motivational atmosphere they helped create, especially during the pandemic. I could not have done it without them.

Abstract

The pursuit of faster and more precise mechatronic systems necessitates the use of inventive mechanical designs and advanced control schemes. In recent years, flexible elements have seen increased use as they enable the development of high-precision motion systems in a wide variety of applications ranging from semiconductor fabrication to precision surgery. Although these flexures provide ample benefits for systems that require lightweight elements and predictable behavior, structural vibrations can restrict their effectiveness in achieving precise positioning. This motivates the need for vibration suppression in motion systems, particularly those with flexible components. To that end, smart structures with embedded transducers and a suitable control algorithm can be used to actively damp the underlying structure's resonance modes, although time-varying parameters and uncertainties from various sources can degrade the performance of the vibration controller. In this thesis, an adaptive control scheme is developed to maintain the desired damping performance regardless of system variations. The method employs adaptive notch filters in a cascade arrangement to track multiple modal frequencies of a smart flexible structure, then tunes a positive position feedback controller for multimodal damping with a straightforward adjustment rule. The adaptation is shown to be fast, accurate, and efficient, with clear advantages in suppressing the vibrations of time-varying and uncertain systems. The method also provides key features absent from other adaptive damping implementations, including the ability to effectively estimate modal frequencies using brief transient signals typical of damped structures, as well as signals buried in noise. Finally, the adaptive scheme is validated experimentally with a flexible beam, showcasing its strong potential for practical applications.

Table of Contents

List of Figures

List of Tables

Nomenclature

Acronyms / Abbreviations

ALE Adaptive Line Enhancer

ANC Active Noise Cancellation

ANF Adaptive Notch Filter

AR Autoregressive (Model)

AVC Active Vibration Control

CANF Cascaded Adaptive Notch Filters

DOF Degree Of Freedom

DVF Direct Velocity Feedback

FFT Fast Fourier Transform

FIR Finite Impulse Response

GS Gain Scheduling

HAC High Authority Control

IIR Infinite Impulse Response

LAC Low Authority Control

LMS Least Mean Squares

MRAC Model Reference Adaptive Control

NDF Negative Derivative Feedback

PPF Positive Position Feedback

RLS Recursive Least Squares

SNR Signal-to-Noise Ratio

STFT Short-Time Fourier Transform

STR Self Tuning Regulator

VSS Variable Step Size

Chapter 1

Introduction

1.1 Background

Speed and precision are important performance objectives in high-tech mechatronic systems. As an example, photolithography machines must offer constantly improving throughput and resolution to keep pace with technological demand [1]. However, structural resonance modes occurring at specific frequencies can amplify disturbances and lead to undesirable mechanical vibrations, placing limitations on the performance of different machine components.

To alleviate this issue, stiffer and lighter structures are designed to shift the resonance modes beyond the frequency band of excitation, but there are limits to this approach stemming from design and material restrictions. Flexible structural elements, which are used in a growing number of applications including precision motion stages and deployable mechanisms, can introduce further complications. Flexures provide selective compliance, enable monolithic designs, largely eliminate friction, and offer improved mechanical repeatability through exact-constraint designs [2, 3]. Such structures are very lightly damped and, as a consequence, their flexible vibration modes are amplified. These vibrations must be attenuated in order to prevent system failure and achieve the desired performance. For example, flexible manipulators can have excessively long settling times and imprecise positioning if their oscillations are not sufficiently suppressed.

1.2 Vibration Control

Vibration suppression is a well-researched topic in various applications including flexible space structures, vehicle suspensions, atomic force microscopy, acoustic control, and active optics [5–8]. Suppression methods include vibration isolation, disturbance rejection, and

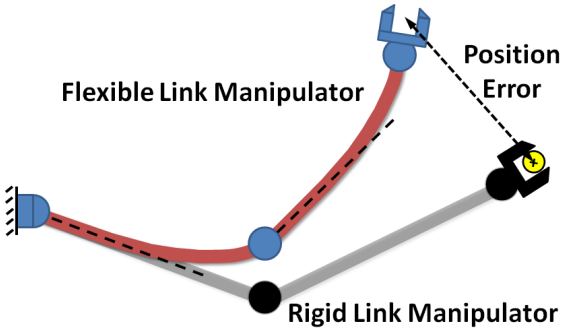

Figure 1.1: Flexible link manipulator [4].

dissipating vibration energy from the structure through damping. All of these methods fall under the wider umbrella of active vibration control (AVC) [8].

Vibration isolation is usually used to prevent the propagation of a particular disturbance with a clear transmission path to a target system. However, the structure's dynamics remain unchanged and disturbances from other sources may still excite it. Other methods directly counteract disturbances using a feedforward control configuration, usually employing adaptive algorithms like filtered-x least mean squares (FxLMS) [9]. However, a reference signal correlated to the disturbance must be available, and the disturbance rejection is localized with no guarantee of global suppression.

On the other hand, damping offers a comprehensive approach for controlling structural vibrations as the control effort is focused on attenuating the resonance modes. Damping can also be used to supplement vibration isolation methods. For example, both methods are used to suppress lens vibrations in photolithography machines [10]. Vibration isolation is used to prevent the transmission of disturbances from the floor to the wafer stepper, in which case acoustic vibrations become the dominant source of disturbances, making it necessary to damp the system as well.

From the wide array of vibration suppression strategies, this research focuses on active damping methods using smart structures with integrated actuators and sensors. Compared to passive methods which add damping through mechanical measures [11], active damping is more suitable for high-speed precision systems owing to the negligible amount of added mass and the lack of restrictions on the structure's design. The versatility provided by the control algorithm also enables the use of a plethora of advanced control techniques and facilitates damping of broadband resonance modes. Actively damped smart structures are thus able to provide superior vibration suppression capabilities.

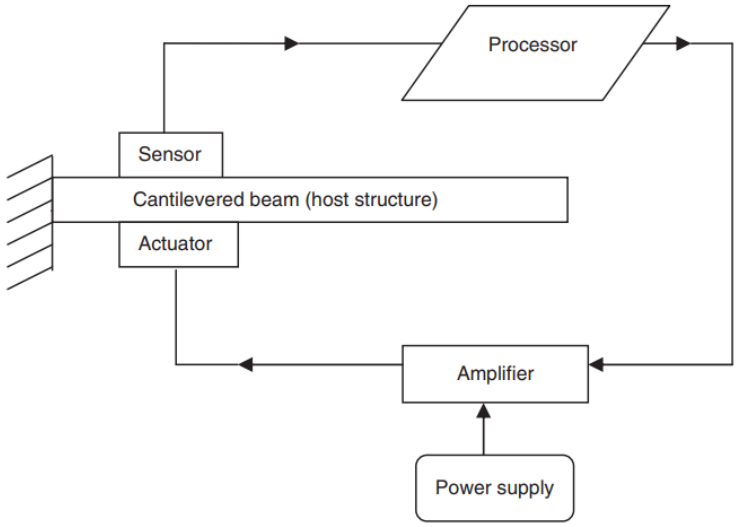

Figure 1.2: Block diagram of an actively damped smart structure [12].

1.3 Uncertain and Time-Varying Systems

A limitation of commonly used active damping methods is their ineffectiveness in compensating for uncertainties and systems variations. Exact controller tuning may be difficult due to uncertainties arising from model approximations, inaccurate system identification, or variations in manufacturing. In addition, some systems have time-varying dynamics which typical AVC schemes do not account for, such as manipulators with variable payloads or deflecting flexures with variable stiffness. Such parametric changes can shift the modal frequencies of the system and de-tune the vibration controller. As a result, the controller can either destabilize the system or deteriorate its active damping performance.

In order to properly control uncertain systems, either robust or adaptive control methods can be used. Each method has its own set of properties that makes it suitable for controlling a particular process. Robust control techniques used in active damping include integral resonant control [13, 14], $\mathscr{H}_\infty$ control [15, 16], and μ synthesis [17]. These methods ensure that the system remains stable and has sufficient performance when uncertainties are present. However, robust controllers have fixed parameters; they are designed for a predetermined and bounded uncertainty set, but do not adapt in real-time to system variations [18]. Sliding mode control, which is suitable for nonlinear systems, has also been used in AVC [19, 20]. The method exploits the phase plane of a system to define a switching function that adjusts the controller gain, ensuring that the system converges to the desired phase plane trajectories. However, this type of control can result in high frequency chattering and limit cycles [21] that require increased control complexity to eliminate [22].

In contrast to robust control, adaptive methods compensate for system variations by adjusting the controller parameters. When designing an adaptive controller, both the parameter estimation and controller adjustment methods need to be appropriately selected from a range of available options. The adaptive controller's performance is usually limited by the chosen parameter estimation method and its convergence speed.

While adaptive controllers are generally slower than robust controllers in responding to system variations, they are not limited to a particular uncertainty set. With a sufficiently fast and accurate estimator, adaptive methods can effectively provide optimal damping performance regardless of system variations. Robust controllers are suitable for applications where the range of uncertainties can be clearly defined or approximated, but even in those cases, the performance is likely to be sub-optimal across system variations. Robust controllers also rely on large loop gains to achieve robustness, which increases control effort and sensitivity to noise. For these reasons, the focus of this thesis is on adaptive control techniques for active damping.

1.4 Problem Statement

Structural resonance modes can introduce undesired vibrations that are particularly restrictive in flexible structures. In order to achieve the required tracking and motion performance, these modes can be actively damped using vibration control methods. However, the performance of a vibration controller may deteriorate in the presence of time-varying and uncertain systems, in which case an adaptive control scheme can be employed to ensure that the controller accounts for these variations and maintains the desired performance.

The aim of this research is to develop a simple yet effective method for adaptive structural damping. Particular attention is given to implementing the method for damping flexible structures with multiple target modes. It should be possible to obtain estimates using transient vibrations of actively damped structures, which requires a fast and accurate estimator and a simple adjustment law for the vibration controller. To ensure its accuracy, the estimator should have low bias, lack sensitivity to noise, and react to different rates of variation in system parameters. A crucial consideration is maintaining the stability of the system in cases where the estimation error is large. In addition, the computational complexity of the adaptive method should be kept to a minimum to ensure that adaptation occurs within a suitable timescale without requiring powerful processors. Computational efficiency can be particularly beneficial in applications with large-scale industrial operations or high complexity like distributed control. Finally, the method should have a simple tuning process for practical use.

1.5 Thesis Outline

This thesis is organized as follows:

- Chapter 2 introduces the fundamentals of structural vibrations, active damping, and adaptive control, and explores various methods that could be utilized in adaptive structural damping. The chapter also discusses previously investigated adaptive damping methods and provides the literature gap motivating this research.
- Chapter 3 presents the main contributions of this thesis in a journal paper format. The research motivation and concepts introduced in Chapters 1 and 2 are briefly summarized in the paper's introduction. Following that, the adaptive damping scheme is proposed, and its performance is investigated with simulations and an experimental setup using a flexible beam.
- Chapter 4 provides additional insights into the main contribution of this thesis.
- Chapter 5 offers concluding remarks and recommendations for future work.
- Finally, several appendices elaborate on the methods and experimental details used throughout this thesis, with the aim of providing further information should the reader require it.

Chapter 2

Literature Survey

This chapter provides background information and summarizes the literature reviewed for this thesis. It is structured as follows:

- Section 2.1 provides the necessary background on structural dynamics and concepts in vibration control, as well as the choice of controller for implementing the adaptive damping method.
- Section 2.2 introduces key concepts in adaptive control and discusses state-of-the-art adaptive methods used in vibration control. In addition, various parameter estimation and controller adjustment methods, as well as their strengths and limitations, are discussed in the context of adaptive damping.
- Section 2.3 elaborates on the literature gap and provides the motivation for the main contribution of this thesis.

2.1 Active Damping

2.1.1 Structural Dynamics

The equation of motion of a 1 degree of freedom (DOF) system is expressed as:

$$\ddot{\xi} + 2\zeta\omega_n\dot{\xi} + \omega^2\xi = k_n^2 f \tag{2.1}$$

where ξ is the generalized displacement, ζ is the damping ratio, ω_n is the natural frequency, k_n is a modal constant, and f is the applied force. System dynamics can be clearly analyzed in the frequency domain via a Laplace transformation of Equation 2.1 using the Laplace variable s to obtain the compliance transfer function:

$$G(s) = \frac{k_n^2}{s^2 + 2\zeta\omega_n s + \omega_n^2} \tag{2.2}$$

Continuous structures like flexures are distributed parameter systems with an infinite number of DOFs, meaning their dynamic behavior is governed by an infinite number of flexible modes. Figure 2.1 visualizes the modes of a simple continuous structure using various domains.

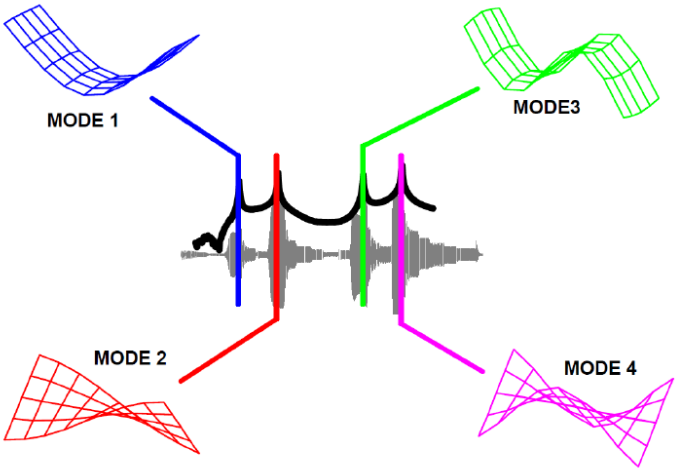

Figure 2.1: Structural mode visualization in the spatial, temporal, and frequency domains [23].

The use of modal coordinates is preferred for continuous systems as they simplify the dynamics of the structure into a linear combination of its vibration modes. In the vibration control of flexible structures, a certain number of non-negligible flexible modes within the control bandwidth are considered, and the rest of the modes are truncated from the model. This effectively approximates the continuous system as a summation of mass-spring-damper models each described by Equation 2.2

2.1.2 Collocation

In a collocated system, the actuator and sensor are attached to the same DOF by occupying the same physical location. To enable the exchange of energy between the active controller and the structure, the actuator and sensor signals must be dual power conjugates whose product describes the transfer of energy (for example, force actuators must be paired with translation sensors). Actuator-sensor pairs that are collocated and dual enable the use of control laws that supply only a finite amount of energy to the mechanical structure and thus provide a robustly stable control system [10].

The open loop transfer function of a truncated and collocated system at DOF l is given by:

$$G_{ll}(s) = \sum_{i=1}^{m} \frac{\phi_i(l)^2}{s^2 + 2\zeta_i \omega_{n,i} s + \omega_{n,i}^2} + R_{ll} \tag{2.3}$$

where i indexes m modes, which is the number of modes with frequencies within the control bandwidth, ϕ is the mass-normalized modal amplitude, and R_{ll} is a positive term that describes the quasi-static correction of higher frequency modes lying outside the bandwidth, also known as the residual mode term.

In the frequency domain ($s = j\omega$), G_{ll} is a monotonously increasing function of ω, resulting in an alternating resonance and anti-resonance pattern. This corresponds to the pole-zero interlacing seen in Figure 2.2. The benefits of this interlacing property are shown in the system's Bode plot (Figure 2.3). The phase is always between 0 and -180° and stability is guaranteed. In the case of system variations, the poles and zeros remain on the left hand plane, guaranteeing robust stability as well [8].

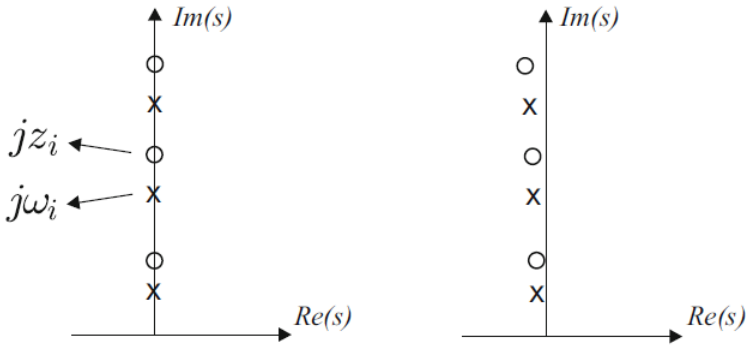

Figure 2.2: Pole-zero map of an undamped (left) and lightly damped (right) collocated structure [8].

Note that unless self-sensing actuators are used, exact collocation is not achievable in real systems [24]. Some nearly-collocated systems may have negative residual terms that affect the interlacing property, in which case robust stability is not guaranteed. In practice, near-collocation is sufficient for active damping purposes.

2.1.3 Piezoelectric Transducers

Piezoelectric materials generate mechanical strain proportional to externally-applied electric fields, and are commonly used as transducers in smart structures. They are light, stiff, highly sensitive, consume little power, have a wide frequency band, and can be easily integrated

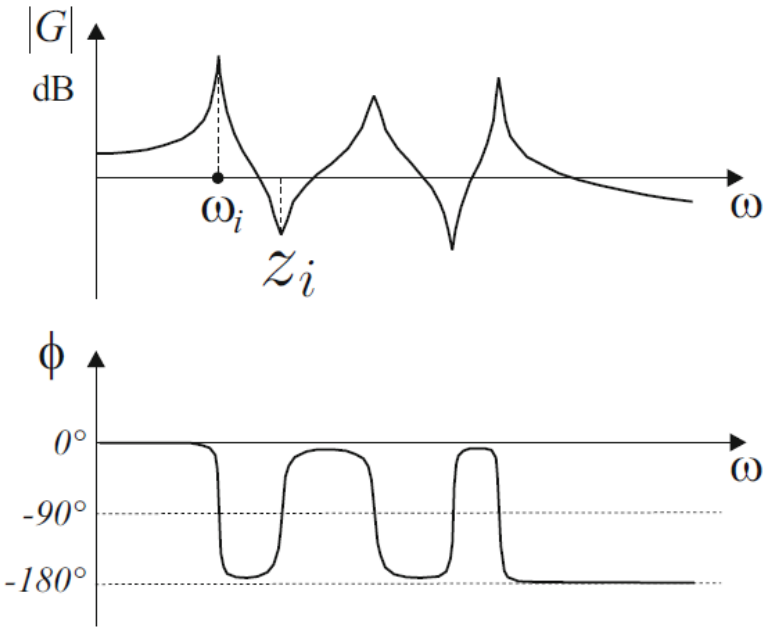

Figure 2.3: Bode plot of a lightly damped collocated structure [8].

into structures, making them suitable for precision and active damping applications [25]. As an example, bending transducers are usually bonded to beams and generate axial strain from an electric field applied in the poling direction P. This is shown in Figure 2.4.

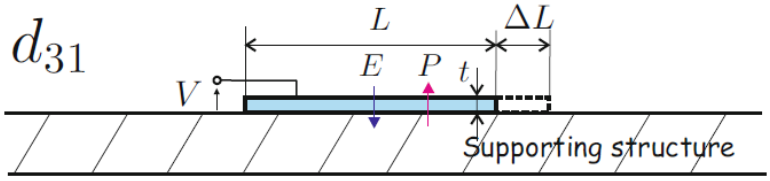

Figure 2.4: Piezoelectric bending transducer [8].

Actuator and sensor placement plays a large role in the performance of the active damping controller, and can be optimized based on different criteria. Examples include maximizing the applied modal forces and moments, minimizing the control effort, or maximizing the degree of observability [12]. Several criteria result in optimal placement at locations of maximum strain energy.

2.1.4 Spillover

The collocated system given by Equation 2.3 describes a system with a finite number of dominant modes and assigns a constant term to account for truncated higher frequency modes.

Control spillover refers to the excitation of these residual and otherwise uncontrolled modes by feedback control, which can generally degrade the performance of the closed loop system [8].

The ideal behavior of an active vibration controller would be to target a specific mode and leave the response of the uncontrolled modes unchanged, which cannot occur in practice due to spillover. Uncontrolled modes can change in magnitude and their resonance frequencies can shift, making it more difficult to tune controllers for multimodal control. The effects of spillover strongly depend on the feedback control scheme used, and should be taken into account when selecting a control method.

2.1.5 Control Authority

Control authority refers to the ability of the actuators to shift the closed loop poles of the system. Active damping requires little control effort and does not substantially affect the system dynamics, which makes it a low authority control (LAC) method. On the other hand, motion control is a high authority control (HAC) method as it requires high gain and has significant influence on the closed loop poles. In a HAC/LAC strategy, active damping is used to improve the bandwidth of the motion controller and make it more robust to parametric variations [26]. Figure 2.5 shows an example of such a control structure.

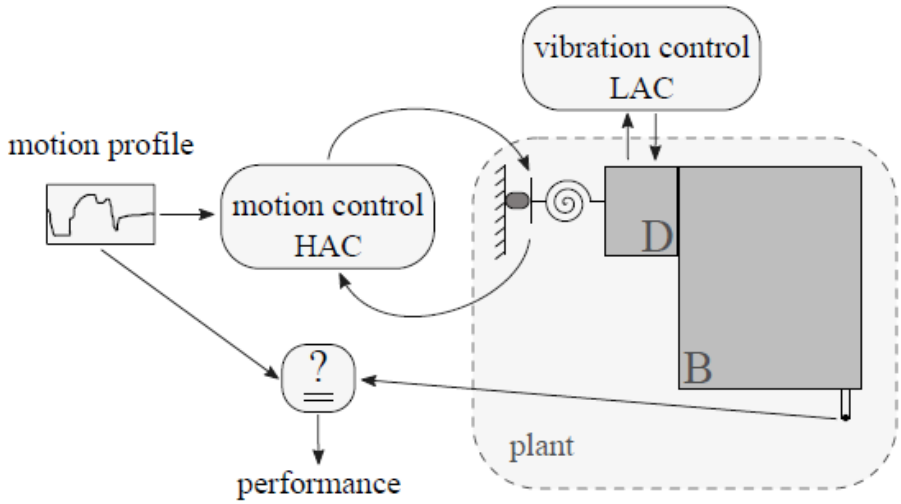

Figure 2.5: HAC/LAC structure with motion control and active damping [26].

LAC methods require limited knowledge of the system, as opposed to HAC methods which require a well-defined model. In the case of collocated active damping, robust stability can be theoretically achieved without any information about the system. However, achieving

the desired performance may require knowledge of the system (e.g., natural frequencies) and applied disturbances, in addition to suitable degrees of controllability and observability [8].

2.1.6 Vibration Controller

A suitable controller $C(s)$ is required to actively damp a structure with the transfer function given by Equation 2.3. A simple way to achieve this is through direct velocity feedback (DVF) [27]. However, DVF has several limitations. Its constant feedback gain gives it insufficient high frequency roll-off, and finite actuator dynamics might affect closed loop stability and performance. DVF also utilizes high control force at all frequencies. It is more advantageous to restrict control effort in the frequency range of interest and avoid actuator saturation.

To solve the problems associated with DVF, Goh and Caughey [28] proposed the positive position feedback (PPF) control method to focus control effort on the modal frequencies and reduce sensitivity to high frequency dynamics. PPF works by measuring a generalized displacement signal y which is positively fed back through a second order low pass filter to counteract the disturbance d. Figure 2.6 shows a block diagram of the PPF control loop with filter frequency ω_f, damping ratio ζ_f, and gain g used to damp a single mode of a collocated structure.

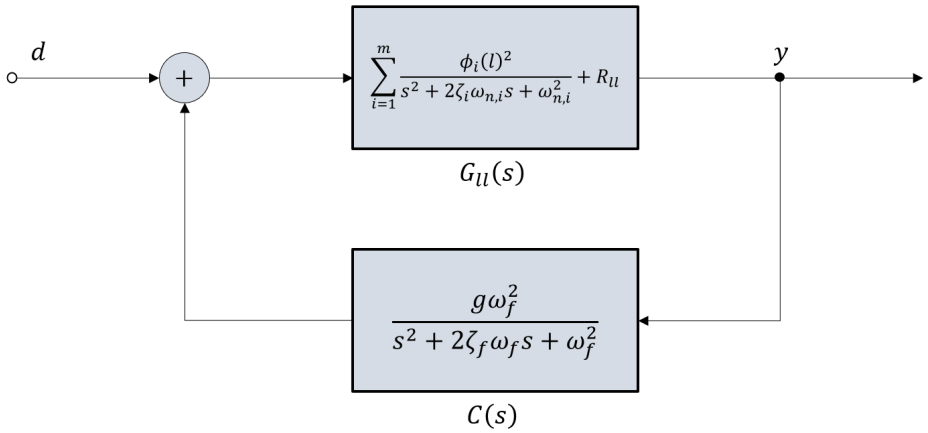

Figure 2.6: PPF block diagram.

For sufficient damping performance, the PPF second order filter is tuned such that $\omega_f = \omega_n$ and $\zeta_f > \zeta$. Bode plots of the plant $G(\omega)$, controller $C(\omega)$, and closed loop $T(\omega)$ are shown in Figure 2.7. When a disturbance excites a mode of a structure with a perfectly tuned PPF controller, the structure phase shifts the disturbance by $-90°$, and the controller phase shifts the measured position signal once again by $-90°$. The control force is thus

a periodic counter-vibration signal with equal frequency to the disturbance. The low pass filter lifts the periodic disturbance from the rest of the vibration spectrum and ignores high frequency dynamics. This can be seen as providing active flexiblity at frequencies lower than ω_f, active damping around ω_f, and active stiffness at frequencies higher than ω_f.

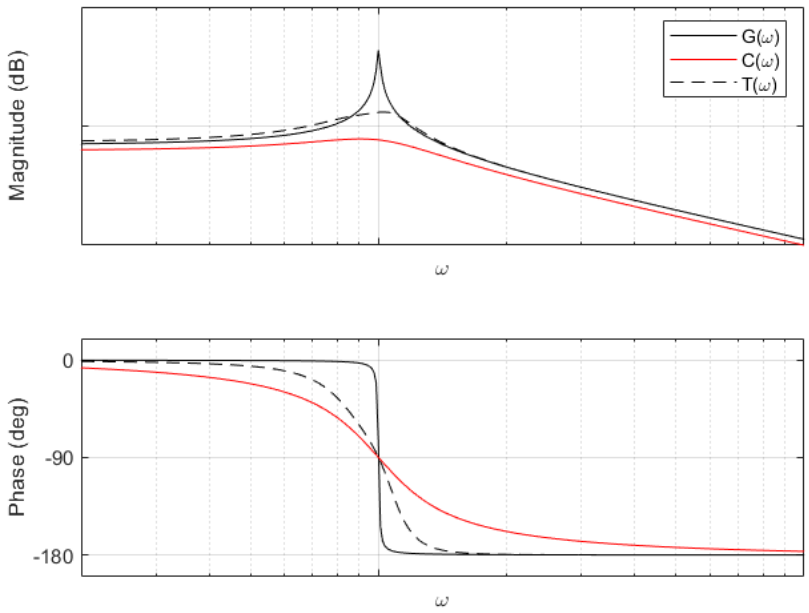

Figure 2.7: Bode plot of a 1 DOF plant, PPF controller, and the closed loop system.

Increasing the feedback gain increases closed-loop damping, but comes at the expense of the gain margin. The gain determines the magnitude of the added counter-vibrations, and a large enough value will cause the system to become unstable. The closed loop stability condition is given by $0 < gG(0) < 1$ [8].

Multiple PPF filters placed in parallel can be used to damp multiple modes. However, low frequency spillover occurs as a result of the active flexibility provided by PPF as seen in Figure 2.8. When damping the second mode, the first mode changes in magnitude and frequency and quasi-static amplification occurs, but the third mode is unaffected as there is no high frequency spillover. Thus when designing a multimodal PPF controller, filters targeting higher frequency modes should be tuned first. Several methods were developed to deal with the issue of PPF spillover, including the use of bandpass filters [7, 29, 30] and fractional order control [31].

Leo and Griffin [32] provide an in-depth approach to PPF design through pole allocation and describe the effects of varying the different PPF parameters. They conclude that the PPF filter frequency ω_f is the key design parameter, as the closed loop damping performance is

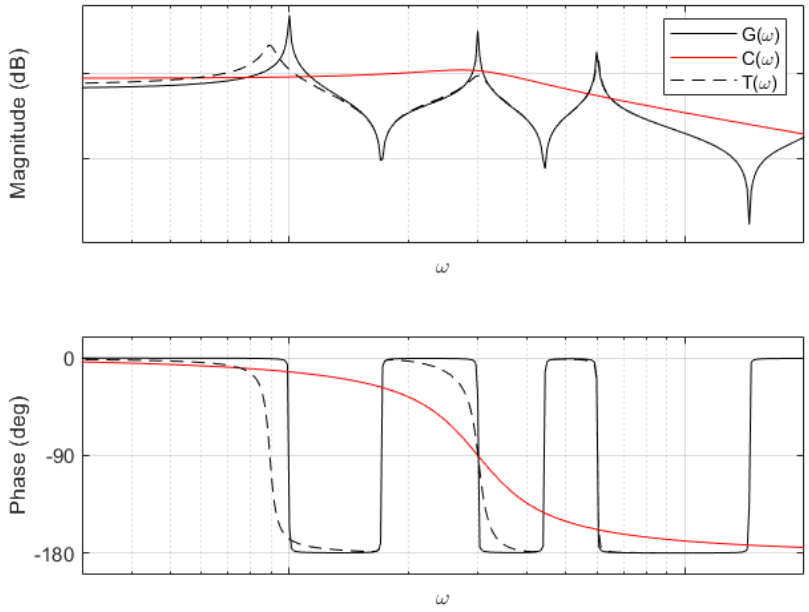

Figure 2.8: Bode plot showing the effects of PPF spillover on uncontrolled system dynamics.

highly sensitive to small changes in ω_f. PPF can be made robust against system variations by widening the filter bandwidth close to the mode, but the damping performance can suffer as a result.

Other suitable collocated active damping methods include negative position feedback [33, 34], integral resonant control [35, 36, 14, 37], and negative derivative feedback [38, 39]. Each method comes with its own set of advantages and disadvantages in terms of spillover, control effort, and required knowledge of model parameters. In this thesis, PPF is used in the development of the adaptive damping scheme for a variety of reasons:

- Minimal knowledge about the structure is required, and the performance depends mostly on the selection of one parameter, the filter frequency ω_f, which has a simple tuning relationship with respect to the mode frequency ($\omega_f = \omega_n$). If the modal frequencies can be tracked, then the adjustment mechanism of the adaptive controller becomes a trivial problem.

- Stability is maintained in case the estimation of ω_n is inaccurate and the PPF filter is incorrectly tuned, as the stability of PPF is solely dependent on its gain. The lack of high frequency spillover with PPF is also an advantage in such cases.

- PPF is a low-authority control method, where the control effort is focused at the mode frequencies.
- Strain measurements from integrated piezoelectric sensors can be used directly in PPF without additional differentiation/integration steps.
- An adaptive scheme developed for PPF as the vibration controller can be potentially applied in other modal collocated damping methods, where knowledge of the mode frequencies can be used to tune the controller.

2.2 Adaptive Damping

As discussed in Section 1.3, a suitable adaptive damping scheme is required to compensate against uncertainties and variations in structural dynamics. In addition, low frequency spillover caused by PPF and nonlinearities from piezoelectric transducers can make it difficult to accurately tune filters for multimodal damping as the closed loop poles shift in frequency. For these reasons, it is essential to use adaptive control to track the frequencies of the modes and tune the PPF filters accordingly.

Åström and Wittenmark define an adaptive controller as "a controller with adjustable parameters and a mechanism for adjusting the parameters" [40]. The adaptive control problem is to find a method of adjusting a controller when the characteristics of the process and its environment are unknown or changing. Fixed gain controllers are not able to deliver the desired performance in such cases, making it necessary to use adaptive control. The steps for designing an adaptive controller are given by [40, p. 27]. These are discussed here in the context of adaptive damping.

Step 1: Characterize the desired behavior of the closed loop system.

The desired behavior of the closed loop system is to retain its damping performance regardless of system variations or uncertainties, where the desired damping performance is specified by the control designer.

An example of undesirable behavior is shown in Figure 2.9. Here, the vibration controller is initially tuned to damp 3 modes of a time-varying collocated structure, and the structural response has a 2% settling time of about 0.19 s. This is a vast improvement when compared to the settling time of the undamped structure, which is about 0.73 s. However, as time passes, the structural modes shift in frequency, and the performance of the PPF controller with fixed parameters starts to deteriorate. The modes are each shifted by 25% at the 2 s

mark, causing them to lose about 2 dB of peak attenuation with a settling time of 0.23 s. At the 4 s mark, a 50% variation in the modes causes an additional 2 dB amplification and a settling time of 0.31 s, which is about 60% higher than that of the tuned system. An adaptive vibration controller would behave to counter such changes in performance and maintain the desired damping levels.

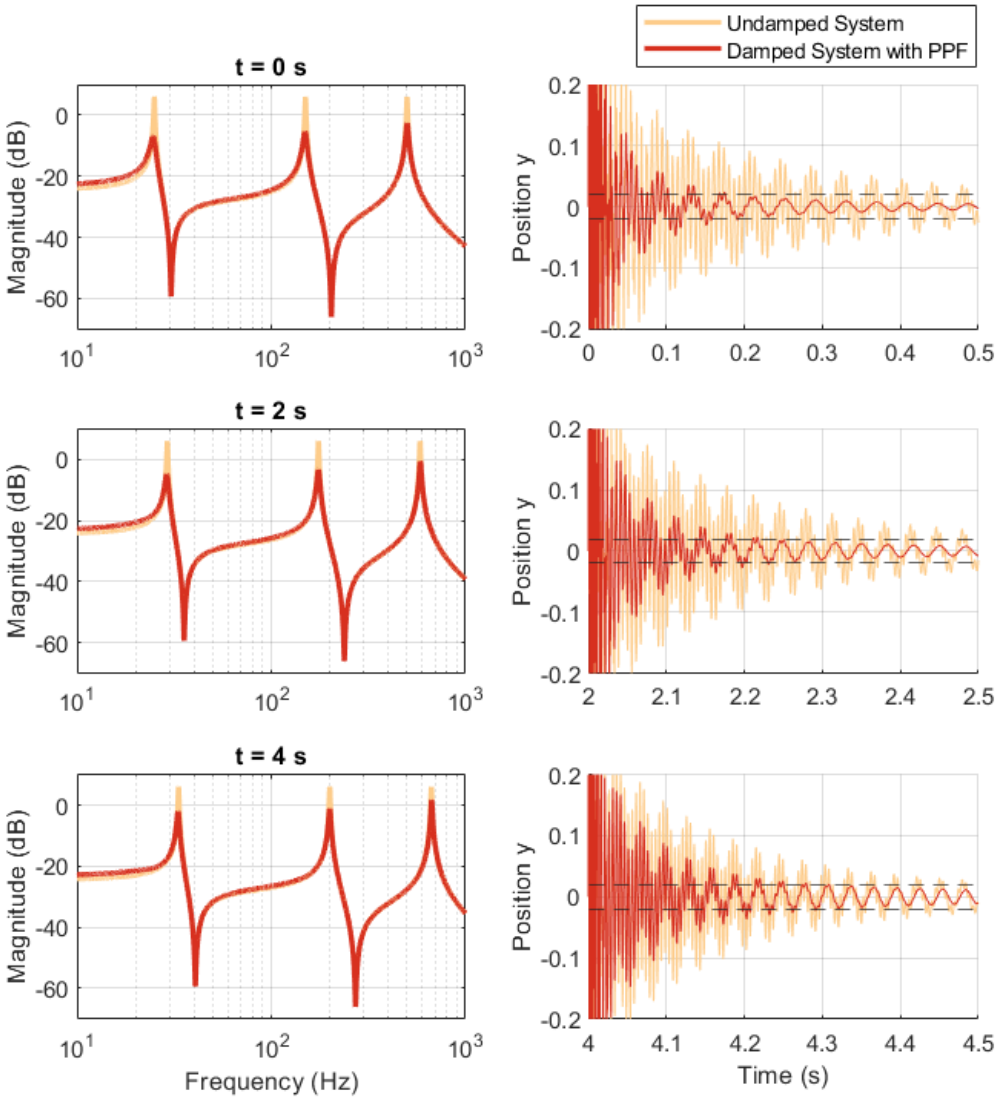

Figure 2.9: Effects of active damping controller de-tuning.

Step 2: Determine a suitable control law with adjustable parameters.

As discussed in Section 2.1.6, PPF control will be used for active damping.

Step 3: Find a mechanism for adjusting the parameters.

The adjustment mechanism is discussed in Section 2.2.1 and the estimation method is discussed in Section 2.2.2.

Step 4: Implement the control law.

2.2.1 Adaptive Scheme

Commonly used adaptive schemes are listed here:

- **Gain scheduling (GS)** changes the controller parameters based on certain predetermined operating conditions that describe the process variations. This works especially well when there is a measurable variable that provides information about the operating point. A mapping is then established between the measurement and controller parameters, either with a function or a lookup table [40]. The control structure is shown in Figure 2.10.

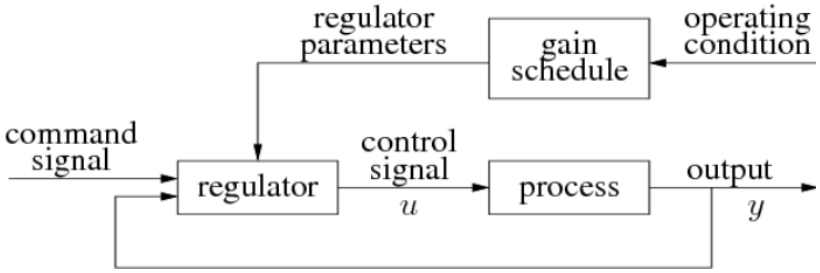

Figure 2.10: Gain scheduling block diagram.

  GS is generally used to control systems with predictable variations, or nonlinear systems by computing linear approximations at different operating points like in autopilot systems. In AVC, it has been implemented in a disturbance rejection scheme by using the observed disturbance model to adjust the controller [41].

- **Model reference adaptive control (MRAC)** sets the performance specifications using a reference model that meets those specifications. In other words, the reference model provides the desired response of the system to a command signal, which is fed to both the reference model and the actual system. A diagram of the MRAC structure is shown in Figure 2.11.

  The key MRAC problem is to find an adjustment mechanism that minimizes the error $e = y - y_m$ and results in a stable system. Baz and Hong [43] use MRAC to adjust

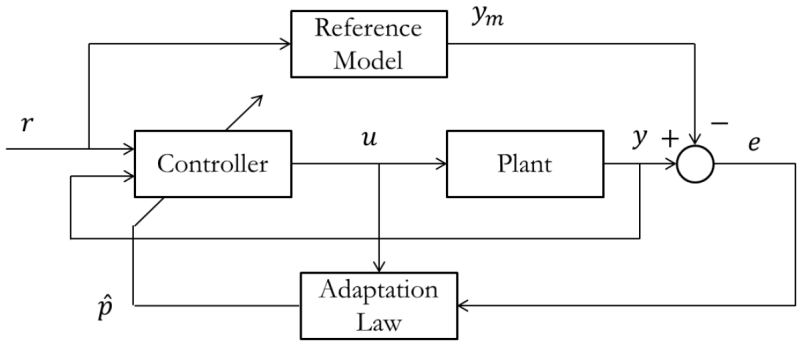

Figure 2.11: MRAC block diagram [42].

PPF parameters, where the reference behavior is given by a third order system with an optimal integral of time multiplied by absolute error (ITAE).

- **Self tuning regulators (STR)** combine online identification and controller design to adaptively control a system. The identification method aims to obtain accurate estimates of the plant model which are then used to design the controller. There are many variations in the choice of design and estimation methods, leading to many different possible combinations. The STR method makes use of the certainty equivalent principle, where the estimates are treated as if they were equal to the true parameters of the system. The STR structure is shown in Figure 2.12.

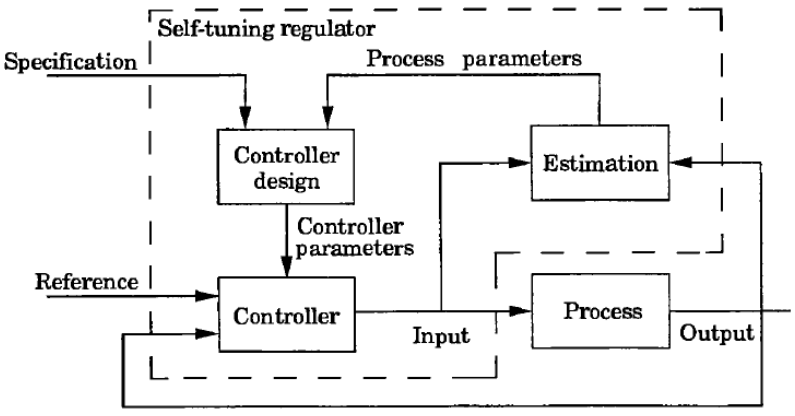

Figure 2.12: STR block diagram [40].

A popular controller design method is adaptive pole placement, which adaptively places the closed loop poles such that the desired dynamics are achieved. In some applications, it is possible to eliminate the separate identification and controller design steps and instead directly update the controller parameters [44].

For adaptive PPF tuning, the filter frequency ω_f is the key design parameter, and for sufficient damping it should be tuned to be equal to the mode frequency ω_n. When controlling multiple modes, each parallel PPF filter should be tuned to the frequency of the corresponding mode. STR is the most suitable scheme in this case as it enables the use of estimates of the system (in this case, modal frequencies) in order to tune PPF parameters through a simplified form of pole placement. As the system adapts to changes in modal frequencies, the controller design step is considerably simplified since the filter frequencies can be simply set equal to the estimated mode frequencies. The proposed adaptive damping control and identification loop is shown in Figure 2.13.

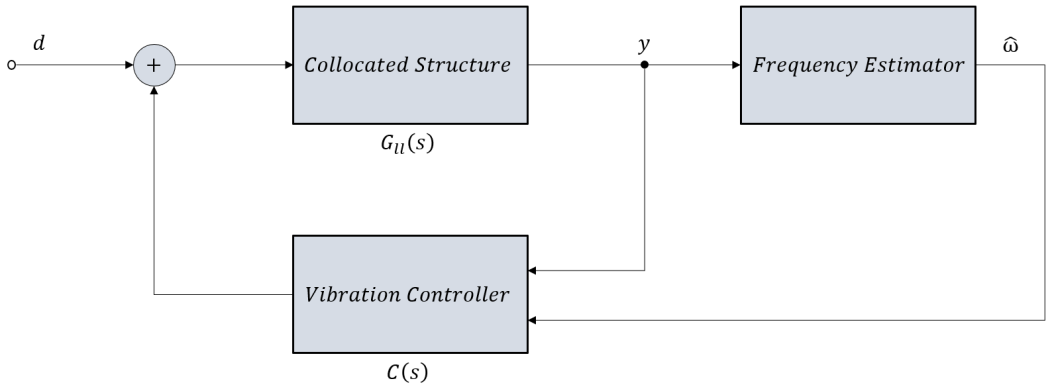

Figure 2.13: Adaptive damping block diagram.

Because the collocated layout used in active damping guarantees robust stability, uncertainties in the estimates which lead to incorrect tuning cannot destabilize the system in theory. Owing to the low pass filtering action of the PPF, high frequency spillover is avoided, so underestimated frequencies do not pose an issue. However, if the PPF is tuned at a frequency higher than the actual frequency, low frequency spillover may amplify the modes which can cause performance to quickly deteriorate. Consequently, the estimation method must be as accurate as possible.

2.2.2 Modal Frequency Estimation

The goal of this section is to explore various methods to be used for modal frequency estimation. Since information about disturbances is usually unavailable in active damping applications, this is an output-only estimation problem. It should be possible to estimate modal frequencies when a structure experiences broadband excitations and by using its damped transient response. The observability of modes, which depends on the placement of sensors, is also an important factor for achieving effective estimation.

Online parameter estimation is more challenging than offline estimation since the measured signal is provided to the estimator during regular operation of the system. This places fundamental constraints on how well the online estimator can perform as the availability of sufficient information is limited. In order to obtain estimates, the structure must be persistently excited, but this is usually not an issue in motion control applications particularly when the system operates at high speeds. Nevertheless, in cases where the frequencies have changed during a pause in the excitation, the estimator must quickly converge to the values of the modal frequencies when the system is excited once again.

Another aspect to be considered in frequency estimation is the structure's dynamic response. For instance, some structures exhibit closely-spaced modes that can be misinterpreted as a single mode due to their proximity. This can occur because of the structure's geometry, particularly in cases where there is some degree of symmetry like plates or parallel mechanisms. The presence of dynamic imbalances or multiple components that share similar natural frequencies can also give rise to closely-spaced modes [45]. In these cases it is crucial to keep track of the mode frequencies and spacing in order to tune the active damping controller accordingly. Figure 2.14 shows examples of structures where this phenomenon can occur.

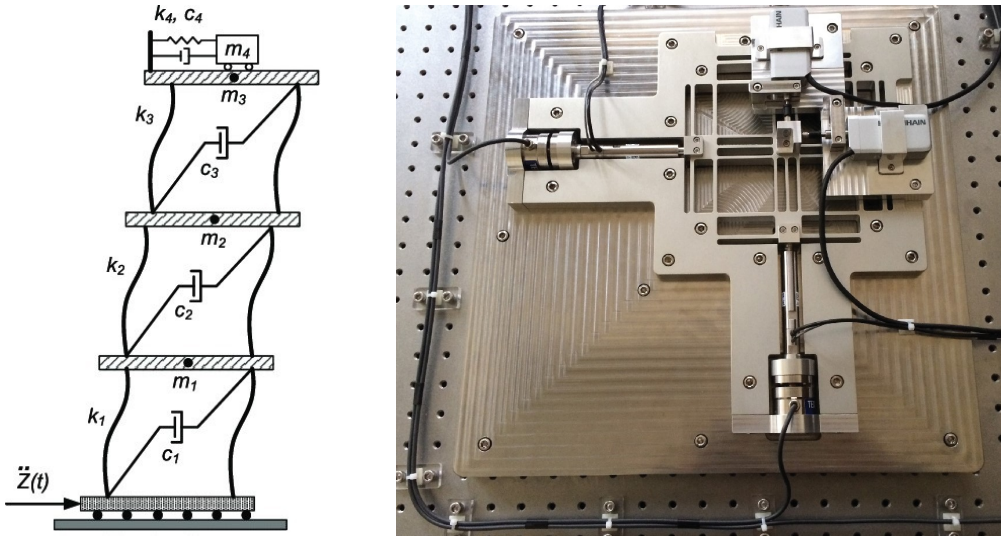

(a) Three-story building [46]. (b) Compliant stage [47].

Figure 2.14: Examples of structures with closely-spaced modes.

The relative magnitude of the modes (dynamic range) can also affect the estimator's ability to detect them. If one mode is significantly lower in magnitude than another, its contribution to the amplitude of the system response is also reduced and the damped signal decays quickly, making it more difficult to estimate. Active damping is usually used to attenuate the most

prominent modes, but the relative magnitudes become an issue when multiple modes need to be adaptively damped. Mainly, the convergence speed when estimating low magnitude modes can be slow [48].

There are two main approaches for frequency estimation or tracking. One method is to identify the system and extract the frequencies of the poles. This can be done parametrically with adaptive filters, requiring prior knowledge of the general structure of the model. The frequencies can also be non-parametrically estimated from the frequency spectrum of the response. Some of these methods are introduced in this section, with additional details and other methods discussed in Appendix A.

Short-Time Fourier Transform

The short-time Fourier transform (STFT) utilizes the fast Fourier transform (FFT) on portions of the output signal to obtain its frequency spectrum as a function of time. Although this method can provide accurate estimates and is simple to implement, it has several limitations:

- A block of data must be collected for each estimate, which can be inefficient in real-time operations.
- Introducing the window function improves the time resolution, but degrades the frequency resolution.
- The fixed window length means that the time and frequency resolutions are fixed for the entire length of the signal.
- Occurrence of spectral leakage and biased frequency estimates.

STFT has seen frequent use in AVC and similar applications:

- Creasy et al. [7, 29] use PPF for acoustic energy absorption in acoustic cavities and payload fairings. An STR scheme is implemented to track and update filter parameters where STFT obtains the frequencies of zeros around each target pole and uses these values to update the frequencies of the PPF filters. STFT is implemented using a buffer to accumulate measurements. The resulting controller is able to track about 20% changes in the mode frequencies, with an implementation time of about 0.4 s. However, a running average of the estimates is used to maintain stability, which increases the implementation time to about 8 s.
- Mahmoodi et al. [49] use a modified PPF to control a cantilever beam and adapt the filter gain and frequency. The authors use STFT and pick the peaks with the highest

magnitudes to update the filter frequencies. An MRAC scheme is also used to derive a control law and provide additional control force when needed. Adaptation takes about 0.9 s since sufficient amounts of data need to be stored in the buffer for accurate estimation.

Parametric System Identification

Online system identification is usually used in adaptive control schemes. This is done with adaptive, auto-tuning filters that use certain algorithms to update their coefficients based on changes in the system. The algorithms minimize a certain cost function, which is usually the mean square error between the output of the adaptive filter and the desired signal. The filter's coefficients converge to a solution when the cost function is minimized. The filter then repeats this process at each sampling period as new data becomes available. The block diagram of this process is shown in Figure 2.15.

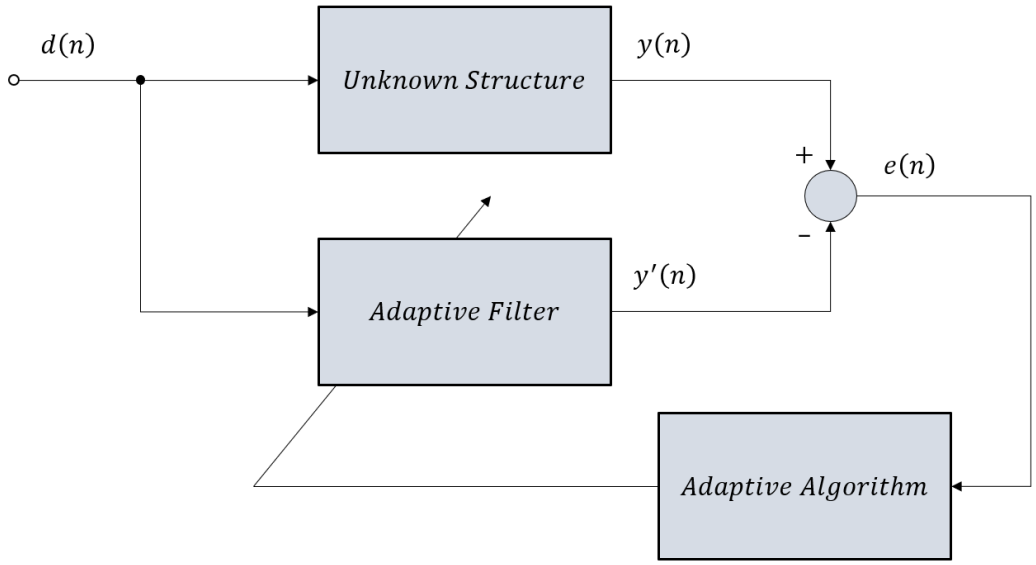

Figure 2.15: Real time parametric system identification block diagram.

Different algorithms are available to determine the update used for obtaining the next estimates. The choice of algorithm usually depends on the desired convergence performance, computational complexity, and filter stability. Examples include the least mean squares (LMS) and recursive least squares (RLS) algorithms.

Parametric system identification has been implemented in various AVC applications:

- Rew et al. [48] use RLS to estimate an autoregressive (AR) model of a plate structure and Bairstow's root-finding algorithm to decouple the modes for frequency extraction.

The estimates are then used to tune a PPF controller for attenuating 3 modes of the structure when it is excited using a banded random signal. The convergence speed was in the order of milliseconds to seconds, and was found to be slower and more biased when estimating modes with lower magnitudes.

- Malik et al. [50] use the filtered-u least mean squares (FuLMS) method to track the natural frequency and damping ratio of a single mode of a structure and update a PPF controller. The downside of this approach is that it requires accurate information on the disturbance and its source, which can be impractical.

- As for more recent developments, Ma and Ding [51] use time-dependent AR models, functional subspaces, and ridge regression to track fast dynamic changes and obtain up to 4 natural frequencies. The method achieves improved model parsimony (identification with a small amount of data). In the experimental setup, 15 accelerometers are used to measure the structural response in order to reduce the computational load of the algorithm. A proper functional subspace and several parameters must also be selected to ensure accurate identification. Such advanced methods are promising, but the complexity and computational load are largely increased for a small improvement in performance.

Adaptive Line Enhancers

The adaptive line enhancer (ALE) was developed to address different problems regarding the retrieval of sinusoidal signals, including the enhancement of signals buried in noise and tracking signals with time-varying frequencies. Building on the concept of active noise cancellation (ANC), Widrow et al. [52], Griffiths [53], and others developed the ALE to track instantaneous frequencies with minimal prior knowledge about the signal. Both ANC and ALE methods separate periodic and stochastic components in a signal, but ANC methods require measurements of the signal and an additional reference input that is correlated to the noise, whereas ALE methods use a single measurement of the signal [54].

A block diagram of the ALE structure is shown in Figure 2.16. The input signal $y(n)$ is filtered by an adaptive filter which outputs the signal $y'(n)$. The error $e(n)$ between the input and filtered signals is then minimized by an adaptive algorithm which usually uses time domain gradient algorithms to continuously update the adaptive filter coefficients. By selecting an appropriate adaptive filter structure, the resulting output $y'(n)$ becomes an enhanced (i.e., noiseless) estimate of the input $y(n)$. The difference between parametric system identification and ALE methods is that in the former, the filter approximates the

system model, whereas in the latter, filter adaptation is used for signal enhancement and frequency tracking.

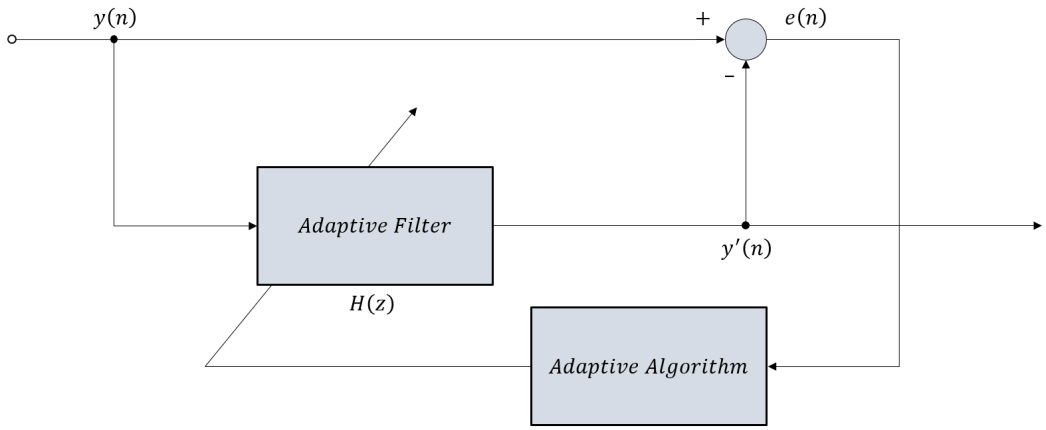

Figure 2.16: ALE block diagram.

ALEs can be efficiently used for frequency tracking and extended to track multiple sinusoids. For example, a bandpass filter with unity gain and zero phase shift at its center frequency can be used as the adaptive filter in Figure 2.16. This results in a notch filter between the input signal and the error term. When the error is minimized, the adaptive notch filter (ANF) converges to the frequency of the signal. There are countless improvements and variations of the ALE scheme that use different filter types, algorithms, and structures to improve its performance. As an example of the improvements made, Hsu et al. [55] developed an ALE method that guarantees globally convergent estimation for all frequency values. In addition, ANFs in parallel [56], cascade [57], or lattice [58] structures can be used to simultaneously track multiple frequencies.

The small estimation bias and the signal-to-noise ratio (SNR) improvements provided by ALEs allow them to track frequencies accurately. Certain ALEs can directly provide frequency estimates from their filter coefficients, bypassing the need to use pre-filters, root-finding algorithms, or transfer function evaluation in contrast to parametric system identification. Furthermore, ANFs usually update a single filter coefficient per estimated frequency, which effectively halves the number of adapted parameters when compared to estimating a structural model of the form given by Equation 2.3.

ANFs have not seen much use as estimators in AVC applications. Mahmoodi et al. [59] use an ANF to estimate the response frequency of a beam and adjust an acceleration feedback vibration controller. The structure is excited periodically at a particular mode frequency and then changed to a different mode frequency, and the ALE is able to detect this change and tune the AVC controller accordingly. However, the potential of using ALEs for

multimodal tracking in active damping with transient signals has not been investigated, and its performance has not been explored in different active damping scenarios.

ANFs may also be used directly to damp the modes of a structure [60–65]. However, using notch filters for mode suppression can cause pole-zero flipping if they are not tuned exactly, which can cause a closed loop pole to move into the positive real plane and lead to instability [8]. In contrast, using ANFs to estimate modal frequencies and adaptively tune PPF filters provides a control scheme with robust stability. As discussed in Section 2.1.6, systems damped with PPF remain stable regardless of the adapted filter frequency.

2.3 Research Gap

Based on the background information and methods discussed thus far, the desired properties of the frequency estimator can be summarized as follows:

- **Multiple mode tracking.** This is important for damping flexible structures where broadband dynamic modes are excited and must be suppressed. All the discussed methods are able to track multiple modes.

- **Real-time operation with fast, accurate, and efficient estimation.** Real-time implementation in adaptive damping applications requires estimation to be fast and accurate, especially when estimates must be obtained using brief transient signals and high precision is required. The estimation speed and accuracy depend on the properties and parameter settings of the estimator itself, the number of parameters to be estimated, the capabilities of the hardware used, and the sampling frequency. STFT-based methods must collect sufficient amounts of data before analyzing a signal, while the other methods update with each sample. To extract modal frequencies from the STFT spectra, additional algorithms might be required like interpolation to enhance the estimates. Both ANFs and parametric system identification methods exhibit slower convergence when estimating low-magnitude modes, but there are measures to combat this. System identification methods usually update more filter coefficients to estimate the same number of frequencies as ANFs. They also require pre-filtering or additional operations after estimation to extract the frequencies from decoupled equations, whereas ANFs can directly obtain the frequency estimates from filter coefficients without additional computations. ANFs are generally less computationally complex than other methods [66].

- **Detects closely-spaced modes.** This necessitates a suitable frequency resolution, which STFT lacks. In ANFs, this property depends on the bandwidth of the notch filter, which can be adjusted.
- **Wide dynamic range.** Parametric system identification schemes used in active damping applications have shown that lower magnitude modes are slower to estimate. ANFs are able to estimate modes with different magnitudes by varying the step size of the update algorithm used for each notch, although prior knowledge of the mode magnitudes is required.
- **Sufficient frequency tracking range.** All frequency estimates are limited by the sampling frequency. Parametric system identification and ANF estimates are generally able to converge to the "correct" frequencies starting from large initial distances. The tracking range is not a relevant property for STFT methods as they rely on spectral data to obtain frequency estimates.
- **Noise sensitivity.** Parametric system identification methods are highly sensitive to noise, while ALEs have good noise attenuation. STFT methods do not filter out noise, but usually this does not significantly affect the peaks of the spectrum. ALEs can be used to pre-filter signals used as inputs for the other estimation methods, but this is slightly redundant as ALEs can simultaneously enhance signals and accurately estimate their frequencies.
- **Minimal or straightforward parameter selection/tuning.** In order to implement adaptive damping control with suitable generality, it would be beneficial to have a simple parameter selection process for the estimator and require a minimal amount of knowledge about the system to be controlled. ANFs and parametric identification methods usually have a low number of parameters that can be fixed at certain values, especially when the nature of frequency variation is consistent. An adaptive step size in the update equation or RLS covariance-resetting [67] can be used if there are large changes in the timescale of frequency variation. An example of this is a change in the mass of a payload causing sudden and large variation in the modal frequencies which the estimator should be able to track. STFT-based methods require the choice of a suitable window size, which can be difficult without approximately knowing the extents of frequency variation in the system.

A vast majority of the literature investigates adaptive damping for the case of single mode damping. Few studies have investigated adaptive multimodal damping methods, but the majority of these utilize RLS in AR-based parametric system identification which is

computationally intensive, sensitive to noise, requires root-finding or pre-filtering, and suffers from inaccuracy when estimating modes with lower magnitudes. STFT-based methods are relatively slow since sufficiently long blocks of data must be used for accurate spectral analysis.

The problem of implementing an adaptive scheme for AVC applications with suitable properties relating to performance, simplicity, and practical implementation leaves much to be desired. The potential of using ANFs for multimodal frequency estimation has not yet been investigated in AVC applications. ANFs therefore present an underutilized and promising option for multimodal frequency estimation in active damping. They provide a direct estimation method which outputs the instantaneous frequencies of a signal, and can provide fast and unbiased estimates in an efficient manner. They also require a low number of tuning parameters and are insensitive to noise.

Based on the literature gaps discussed above, the objectives of this research are:

- Develop an adaptive vibration control scheme using PPF for damping multiple modes of flexible structures and a suitable ANF estimator to ensure the effective estimation of modal frequencies.
- Focus on practical implementation details such as the use of damped transient signals for estimation, fast and accurate convergence of estimates, computational efficiency, ability to estimate closely-spaced modes, dynamic range, tracking range, noise sensitivity, and simple parameter tuning.
- Validate the adaptive damping scheme and investigate its performance and behavior in different conditions using simulations and experimental tests.

Chapter 3

Adaptive Multimodal Damping of Flexible Structures

3.1 Introduction

Speed and precision are important performance objectives in mechatronic systems where high throughput and motion resolution are desired. For example, wafer scanners used in the semiconductor industry are crucial in enabling modern technological development through the continuation of Moore's law, and must consequently keep up with the demand for microchips while maintaining nanometer-level precision. However, vibrations due to structural resonance modes can limit the performance of such systems as they can induce undesirable oscillations. These vibrations are particularly problematic in systems that utilize flexures, where structural damping is sacrificed to achieve lightweight, minimally constrained designs with high repeatability. Vibration suppression is thus necessary to counteract the excitation of lightly damped flexible modes and obtain the desired performance.

Structural resonances can be attenuated by damping the structure passively or actively. Passive damping methods use mechanical measures like elastomer layers or tuned mass dampers. However, these solutions are only effective within a narrow range of frequencies and can add significant mass to lightweight structures. Active damping methods utilizing low-mass actuators, sensors, and multimodal control algorithms are better suited for such applications. These are often referred to as active vibration control (AVC) methods.

One of the main issues in commonly used AVC methods is the lack of robustness against uncertainties and systems variations. For example, a manipulator with a variable payload or a deflecting flexure will have time-varying dynamics which typical AVC schemes do not account for. In addition, uncertainties may arise from model approximations, inaccurate

system identification, or variations in manufacturing. As a result, the detuned controller can either destabilize or deteriorate the active damping performance of the system.

Two main approaches have been used to implement robust AVC. The first option involves the use of robust controllers designed with fixed parameters to ensure stability and suitable performance in the presence of uncertainties. Previously investigated solutions include integral resonant control [13, 14], $\mathscr{H}_\infty$ synthesis [15, 16], and μ synthesis [17]. These methods were shown to be effective but rather limited since designing a suitable controller requires a priori knowledge of the system model and its uncertainties. The resulting performance varies across uncertainties and is only sufficient within a predetermined and bounded uncertainty set.

In contrast, adaptive methods can be used to achieve robustness by adaptively tuning a vibration controller with minimal a priori knowledge of the structure. Given accurate estimates of the system parameters, an adaptive controller with a suitable adjustment law can maintain the desired damping performance for virtually any variation or uncertainty. Adaptive control has attracted much attention in AVC [68, 32, 69, 70, 50, 71–73].

The practical implementation of AVC for flexible structures requires a simple yet effective estimation method to track the frequencies of multiple resonance modes and use the estimates to adaptively tune a vibration controller in real time. Frequency tracking should be possible using readily available measurements from the AVC loop without requiring knowledge of disturbances as they can be difficult to measure. For effective vibration suppression, the estimates must converge accurately and in the same timescale as the vibration response of the structure, particularly if it is characterized by the quickly decaying transient response of actively damped structures like flexible manipulators. Other desired properties of the estimator include low computational complexity, operation in low signal-to-noise ratios (SNR), and having a minimal number of parameters to be manually adjusted.

The estimation and tracking of multiple frequency components of a signal in real time has been widely investigated, with applications ranging from power systems [74] and mechanical fault detection [75] to autonomous driving [76]. Non-parametric methods based on the fast Fourier transform (FFT) have been used to estimate modal frequencies for AVC and active noise control applications [29, 49, 77]. FFT provides a simple approach for time-frequency analysis, but it requires sufficiently long datasets to provide accurate estimates, suffers from spectral leakage, and has poor resolution for identifying modes with closely spaced frequencies. Several methods improve on these limitations, but they come at the cost of increased computational burden [78].

On the other hand, parametric methods use prior knowledge about the model structure and update the estimation parameters with each sample, allowing for fast, high-resolution

estimation. In AVC, Rew et al. use recursive least squares (RLS) to estimate an autoregressive (AR) model of a plate structure for multimodal damping with an adaptive positive position feedback (PPF) controller [48]. However, AR estimation is highly sensitive to noise and can provide inaccurate estimates. Such methods also require additional steps in the form of pre-filtering or a root-finding algorithm to separate the estimated transfer function into its modal components and determine the mode frequencies [79].

The problem of implementing an adaptive scheme for AVC applications with suitable properties relating to performance, simplicity, and practical implementation leaves much to be desired. In this paper, we aim to fill that gap by using adaptive notch filters in a cascade structure (CANF) to track the frequencies of multiple structural resonance modes, then tune a modal vibration controller using the estimates. In this work, PPF control is used to test and demonstrate the method. Adaptive notch filters (ANF) have been used to directly damp resonance modes [60–65], but inexact ANF tuning for mode suppression can cause pole-zero flipping and destabilize the system. An ANF was also used to track the frequency of a single mode for PPF tuning [59]. However, the potential of using ANFs for multimodal frequency estimation has not yet been investigated in AVC applications.

The developed adaptive scheme is shown to be stable regardless of the estimation accuracy, and the PPF controller can be easily tuned with the estimated frequencies using a simple adjustment rule. The CANF estimator provides fast and accurate convergence, even in low SNR, and directly provides estimates of each frequency without requiring additional decoupling steps. Instead of computing a large number of filter coefficients, the update algorithm of the CANF adapts a single parameter for each mode to be actively damped. In addition, a variable update step size is used to account for time-varying signal amplitudes, adapt to different frequency tracking scenarios, and simplify the process of manual parameter selection.

The remainder of this paper describes the proposed method in detail then investigates its performance in tracking and damping multiple modes of a flexible structure. Section 3.2 briefly introduces some principles of active damping and PPF control. Section 3.3 introduces the CANF method used for frequency estimation and discusses the overall adaptive scheme. Section 3.4 investigates the performance of the developed method using simulations, and Section 3.5 presents experimental results obtained by adaptively damping a flexible beam with piezoelectric transducers. Finally, Section 3.6 provides some concluding remarks and insights into potential future work.

3.2 Active Damping with Positive Position Feedback

The transfer function describing the compliance of a structure with a single degree of freedom (DOF) can be represented in the Laplace domain as:

$$G(s) = \frac{k_n^2}{s^2 + 2\zeta\omega_n s + \omega_n^2} \tag{3.1}$$

where s is the Laplace variable, k_n is a modal constant, ζ is the damping ratio, and ω_n is the natural frequency. Continuous systems like flexible structures exhibit an infinite number of elastic modes and their dynamics can be expressed as a linear combination of the system's modes. For such systems, collocated control, where actuators and sensors are located at the same DOF, is often employed to ensure robust open loop stability [10]. This is clear when the collocated open loop transfer function $G_{ll}(s)$ is analyzed at a given DOF l:

$$G_{ll}(s) = \sum_{i=1}^{m} \frac{\phi_i(l)^2}{s^2 + 2\zeta_i\omega_{n,i}s + \omega_{n,i}^2} + R_{ll} \tag{3.2}$$

where i indexes m modes, ϕ is the mass-normalized modal amplitude, and R_{ll} is a quasi-static approximation of high frequency dynamics called the residual mode. This model describes a system with a finite number of dominant modes and assigns a constant term to approximate truncated high frequency modes outside the control bandwidth. As shown in Figure 3.1, $G_{ll}(s)$ exhibits an alternating pattern of poles and zeros on the left half plane and its phase never falls below $-180°$, showcasing the stability benefits of using collocated control. This remains the case regardless of system variations, guaranteeing robust stability of the plant [8].

An ideal active vibration control method would be able to damp certain modes of a structure and leave other dynamics unchanged. However, feedback action may lead to spillover and excite modes outside the control bandwidth, making it more difficult to design controllers for multimodal damping. The goal is thus to find a suitable vibration controller $C(s)$ that actively damps multiple modes of $G_{ll}(s)$ without affecting its robust stability or significantly exciting uncontrolled modes. To that end, positive position feedback (PPF) was originally proposed by Goh and Caughey to overcome the stability limitations of conventional velocity feedback in the presence of unmodelled dynamics [28]. Figure 3.2 shows a block diagram of the PPF control loop used to damp a single mode of a collocated plant.

Here, d is the disturbance acting on the structure, y is a position output, and $C(s)$ is the transfer function of the PPF filter, a second-order low pass filter with gain g, cutoff frequency ω_f, and damping ratio ζ_f. Although PPF can be designed using optimal control methods, the

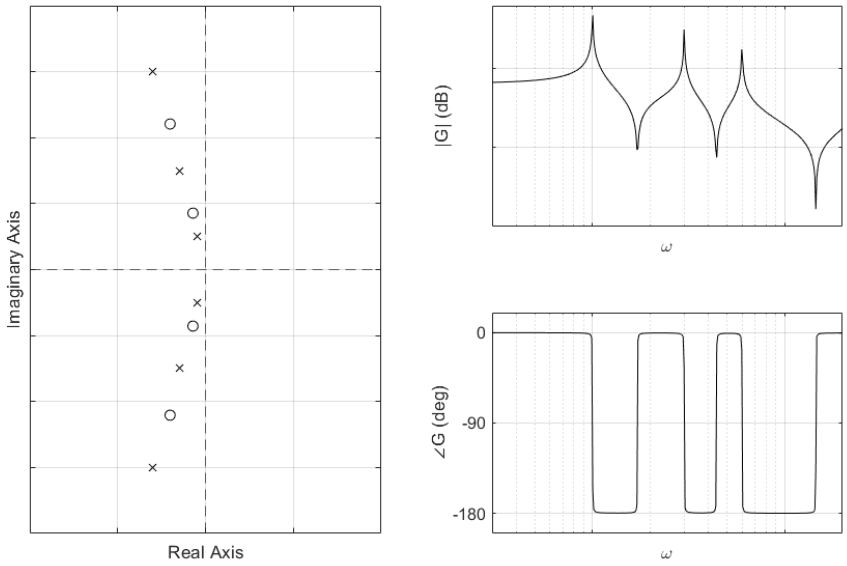

Figure 3.1: Pole-zero map and Bode plot of a structure with collocated actuation and sensing.

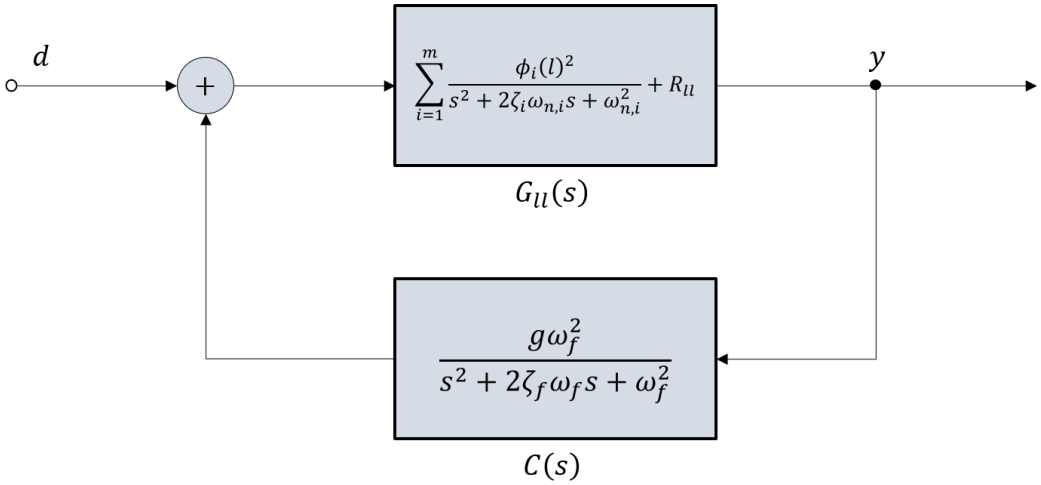

Figure 3.2: PPF block diagram.

following tuning rule is sufficient for damping structures and is used throughout this paper [32, 80]:

$$\omega_f = \omega_n \tag{3.3}$$

The filter damping ratio ζ_f and feedback gain g are chosen such that the targeted resonance peak is sufficiently damped. The gain value also determines the stability of the system with the following condition [8]:

$$0 < gG(0) < 1 \tag{3.4}$$

In practice, this condition does not restrict the damping performance since large gain values are not normally used.

The closed loop transfer function of interest describing the relationship between the disturbance input and position output is:

$$T(s) = \frac{G(s)}{1 - C(s)G(s)} \tag{3.5}$$

Figure 3.3 is used to highlight the properties of PPF for tuning the 2nd mode of a collocated structure. The root locus plot shows that all poles remain on the left half plane except for one branch that moves towards the positive real axis, representing the effect of violating the condition given by Equation 3.4. The magnitude plot shows that apart from successfully damping the 2nd mode, PPF only causes spillover at frequencies lower than its cutoff frequency ω_f. This lack of high frequency spillover is a major benefit of using PPF, as the damping performance is insensitive to both known and unknown high frequency dynamics. Finally, the phase plot provides intuitive insight into the workings of PPF. When a disturbance excites a structural mode and the position measurement is passed through a second-order low pass filter tuned to that mode, the resulting control signal is -180° shifted in phase relative to the original disturbance, providing a periodic counter-vibration signal equal to the disturbance in frequency but opposite in direction.

Multiple PPF filters placed in parallel can be used to damp multiple modes using a single actuator. However, control spillover makes it difficult to tune filters for low frequency modes. Figure 3.3 shows that coupling from damping the 2nd mode causes the 1st mode to shift in magnitude and frequency, in addition to amplifying the quasi-static region. Several methods were developed to decrease spillover and facilitate the design of multimodal PPF, including the use of bandpass filters [7, 29, 30] and fractional order control [31].

Leo and Griffin [32] concluded that the PPF filter frequency is the key design parameter, since small changes in its value result in large changes in the closed loop damping ratio. The controller gains may also be fixed as the frequency varies without much variation in performance [48]. The method can be made more robust by increasing ζ_f to widen the filter bandwidth close to the target mode, but this comes at the cost of reduced mode suppression [81]. Opting for adaptive PPF can provide a powerful solution for a variety of reasons:

- PPF can be difficult to tune in the multimodal damping case due to time-varying parameters, control spillover, actuator nonlinearities, among other reasons. An adaptive scheme circumvents this issue.

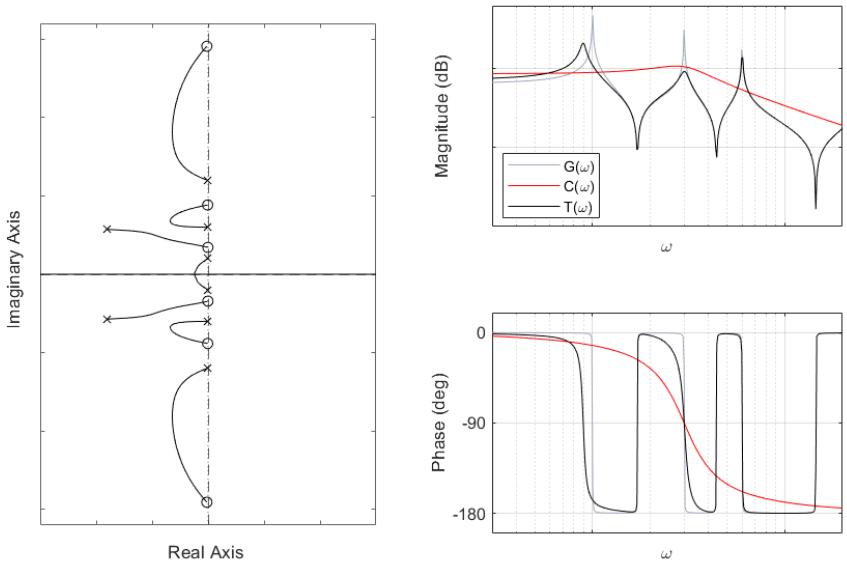

Figure 3.3: PPF root locus and Bode plots showing stability and damping action in the frequency domain.

- PPF performance is mostly sensitive to the filter frequency ω_f. Since minimal structural knowledge is needed, full system identification is not necessary. This allows the use of efficient frequency trackers for estimation and does not require the use of complex adjustment mechanisms as the tuning rule is simple: $\omega_f = \omega_n$.

- PPF is a low authority control method. The control effort is focused on the mode frequencies and its influence on other system dynamics is relatively low. In cases where the frequency tracker gives inaccurate estimates and incorrectly tunes the PPF filter, the collocated layout maintains robust stability and the high frequency roll-off of PPF avoids potential performance and stability degradation caused by high frequency dynamics.

In addition, an efficient adaptive scheme developed for PPF tuning can be applied either partially or fully to other AVC methods where the mode frequencies can be used as tuning parameters, including negative position feedback [33], integral resonant control [35, 37], and negative derivative feedback [38].

3.3 Modal Frequency Estimation with Cascaded Adaptive Notch Filters

In this section, adaptive line enhancement (ALE) is investigated for tracking multiple frequencies for PPF tuning. ALE is a spectral estimation technique developed to address different problems regarding the retrieval of sinusoidal signals, including the enhancement of signals buried in noise and tracking unknown signals with time-varying frequencies. Building on the concept of active noise cancellation, Widrow et al. [52], Griffiths [53], and others developed the ALE to enhance noise-corrupted signals with minimal a priori knowledge about the input signal. Figure 3.4 shows a block diagram of a typical ALE.

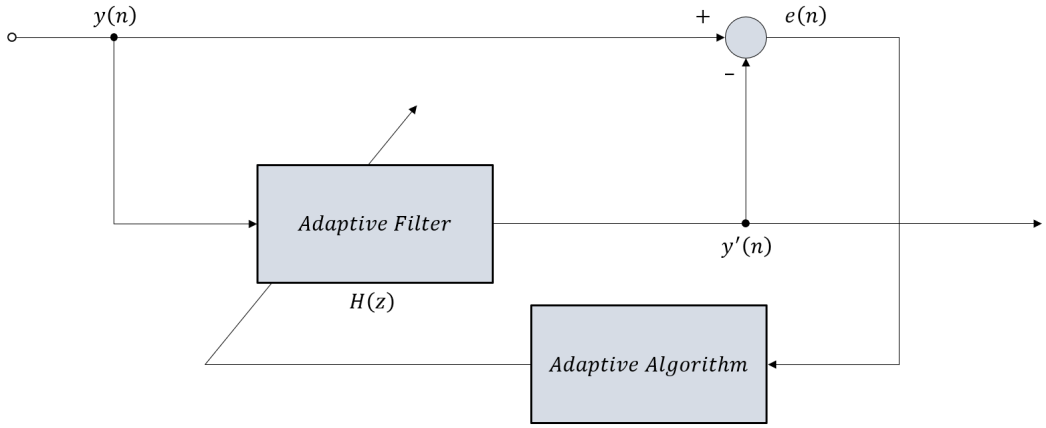

Figure 3.4: ALE block diagram.

The aim of the adaptive filter $H(z)$ is to enhance the input signal $y(n)$ at discrete time n by filtering out its noise components. This is done by minimizing the error signal between the input signal and the output $y'(n)$ of the adaptive filter using a certain adaptive algorithm.

For PPF tuning, the generalized position of the excited underdamped structure is used as the input to the ALE. This response consists of a sum of frequency components to be estimated given by the following equation:

$$y(n) = \sum_{i=1}^{k} A_i(n) sin(\omega_{0,i}(n)n) + v(n) \tag{3.6}$$

where i indexes k frequency components, $A(n)$ is the time-varying amplitude, ω_0 is the time-varying frequency, and $v(n)$ consists of other signal components which can be considered as Gaussian white noise. Depending on its structure, the ALE's adaptive filter can efficiently track the instantaneous frequencies $\omega_{0,i}$ of the signal that it is enhancing as it is decomposed into its separate components.

Several ALE structures and filter types have been explored, including finite impulse response (FIR) and infinite impulse response (IIR) filters [54]. An FIR filter requires a larger number of filter weights to provide adequate line enhancement performance compared to an IIR filter. As a result, despite its more complex structure, the smaller IIR filter length means fewer parameters to be adapted and generally better numerical behavior [82]. Additionally, FIR filters require further computations to determine the frequency estimates from the filter coefficients, whereas IIR filter coefficients can directly provide this information [83].

The IIR ALE developed by Kwan and Martin [84] is used here for its stability, simplicity, quick convergence, and computational efficiency in tracking multiple frequency components [66]. For operation with a single frequency component, the adaptive filter $H(z)$ in Figure 3.4 has the transfer function of a bilinearly transformed second-order bandpass filter given by:

$$H(z) = \frac{Y'(z)}{Y(z)} = \frac{1-r^2}{2}\frac{(1+z^{-1})(1-z^{-1})}{1-2rcos(\omega_p)z^{-1}+r^2z^{-2}}; \quad 0 \ll r < 1 \tag{3.7}$$

where r is the pole radius and ω_p is the normalized pole frequency. This structure can be more intuitively described by analyzing the transfer function between the input to the ALE and the error, given by the following equation:

$$N(z) = \frac{E(z)}{Y(z)} = 1 - H(z) \tag{3.8}$$

As shown by Figures 3.5 and 3.6, $N(z)$ is a constrained notch filter with a bandwidth determined by r and a zero-transmission frequency at ω_p. The zeros are set to lie on the unit circle and the poles are constrained by the radius r to lie on a line between the origin and the zeros. This ensures stability, prevents numerical issues through zero-pole cancellations, and simplifies the adaptation process [85]. A suitable constant value of r can be chosen to fix the notch bandwidth, leaving ω_p to be updated using an adaptive algorithm. The central notch frequency converges to the input signal frequency ω_0 as the error is minimized, making it an adaptive notch filter (ANF).

It is also possible to establish a linear relationship between the adapted parameter and the notch frequency [84]. This is done with the following substitutions:

$$\alpha = \sqrt{1+r^2-2rcos(\omega_p)} \quad and \quad \beta = 1-r^2 \tag{3.9}$$

which gives the following bandpass filter transfer function:

$$H(z) = \frac{\beta}{2}\frac{(1+z^{-1})(1-z^{-1})}{1-(2-\beta-\alpha^2)z^{-1}+(1-\beta)z^{-2}} \tag{3.10}$$

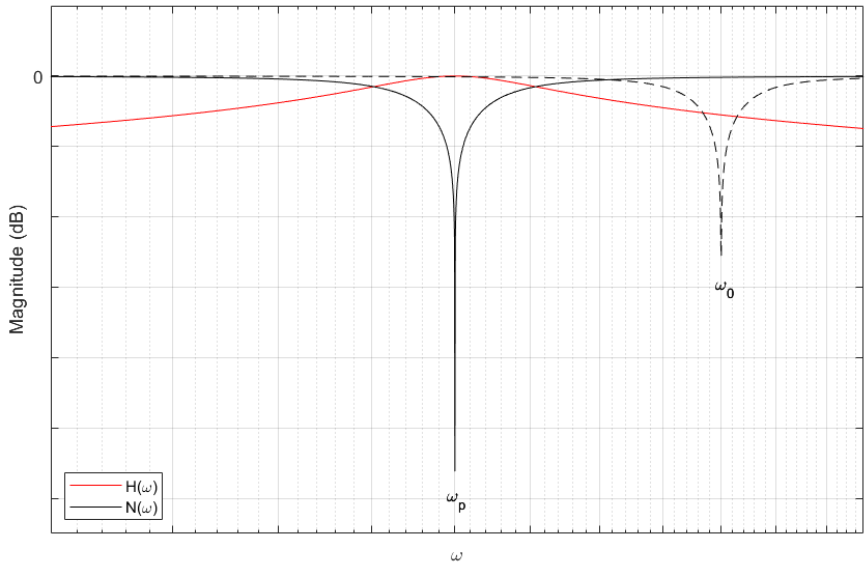

Figure 3.5: Magnitude transfer function of a second-order ANF.

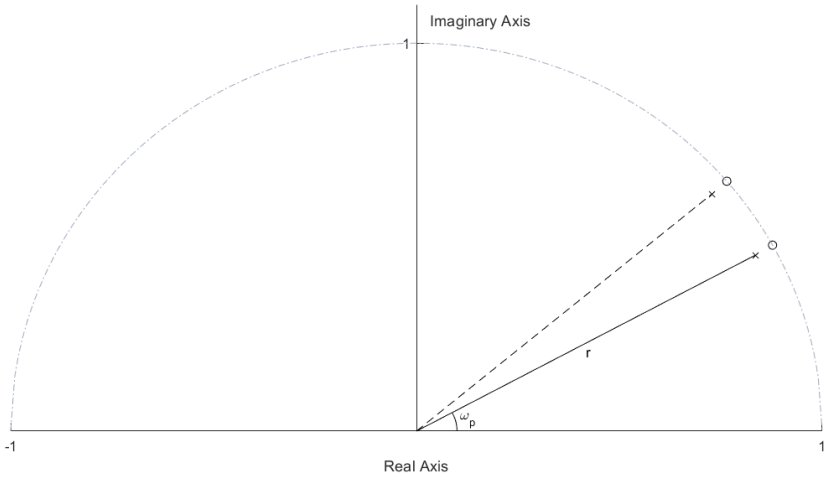

Figure 3.6: Pole-zero configuration of a second-order ANF.

The normalized frequency estimate is then obtained through its relation to the new parameters α and β:

$$\hat{\omega} = 2sin^{-1}\left(\frac{\alpha}{2\sqrt{1-\frac{\beta}{2}}}\right) \approx \alpha\left(1+\frac{\beta}{4}\right) \tag{3.11}$$

where the linear approximation applies for small values of α and β. The value of β is only related to r and is thus fixed, whereas α is related to ω_p and should be updated. The update equation is based on a least-squares solution for minimizing $||e(n)^2||$:

$$\alpha(n+1) = \alpha(n) - \mu e(n) s'(n) \tag{3.12}$$

where μ is a fixed step size and $s'(n)$ is a sensitivity signal describing the gradient of the error with respect to the parameter α. The sensitivity signal $s'(n)$ can be easily obtained from intermediate signals of the bandpass filter $H(z)$ as shown by Figure 3.7.

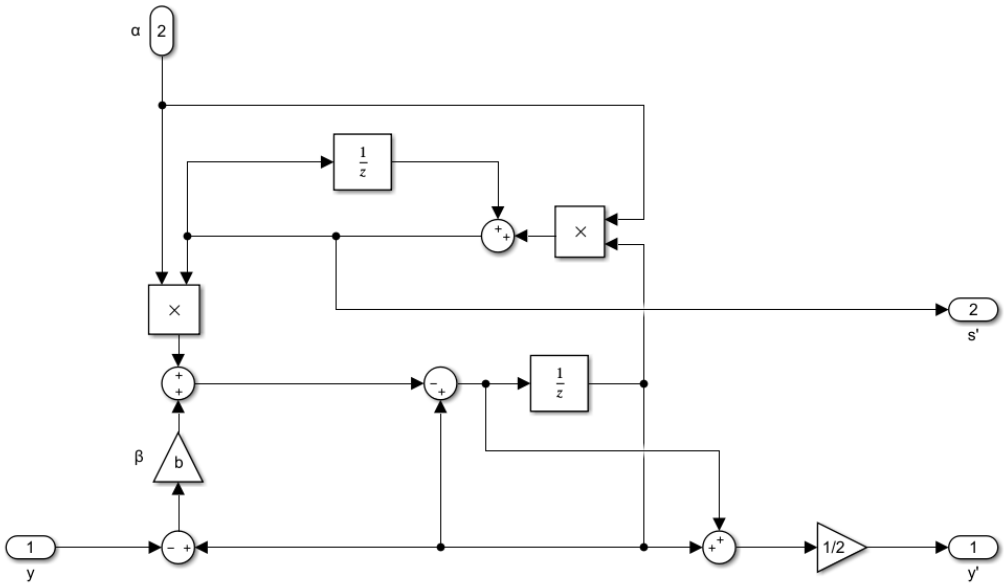

Figure 3.7: Signal flow diagram of $H(z)$.

To keep the update independent of the amplitude and enable greater dynamic range, the update can be normalized using the sensitivity signal, making the estimator particularly suitable for estimating frequencies from transient signals and tracking modes with various magnitudes. The normalized equation is:

$$\alpha(n+1) = \alpha(n) - \mu \frac{e(n)s'(n)}{||s'(n)||^2 + \delta} \quad 0 < \delta < 1 \tag{3.13}$$

where δ is a constant to prevent numerical issues from division.

To extend the ANF application for tracking multiple frequencies, the cascaded ANF (CANF) structure shown in Figure 3.8 can be used to obtain the different sensitivity terms associated with each frequency component. The resulting transfer function is that of a notch comb filter. For the estimation of k frequencies, $k(k+1)/2$ bandpass filters ($H_i(z)$) and k

sensitivity filters ($S_i(z)$) are required. For example, 9 total filters are required to track 3 frequencies.

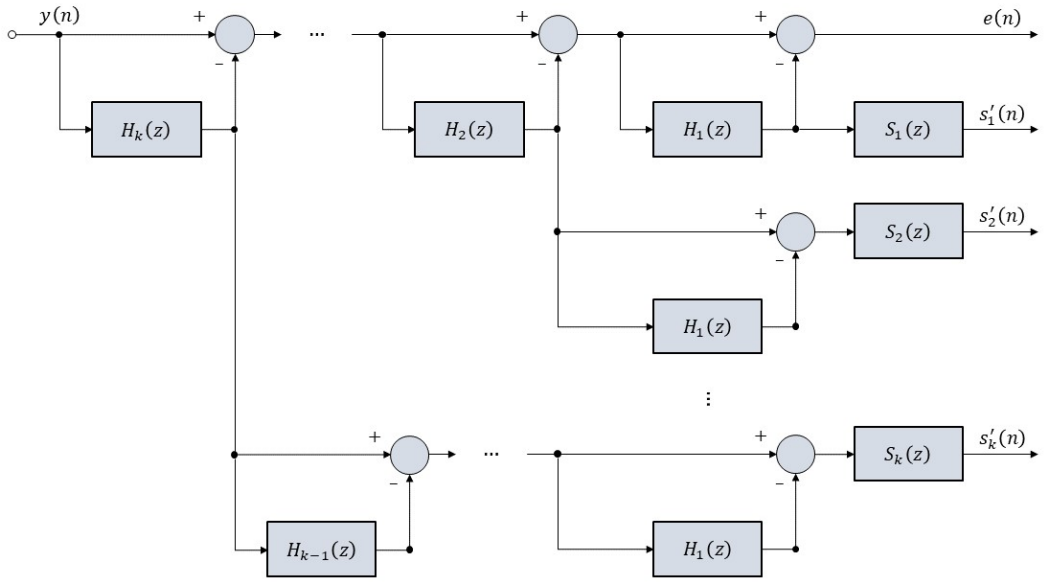

Figure 3.8: Cascade structure of adaptive notch filters.

The advantage of the CANF structure over other parallel [56] and cascade [57] structures is that all filters are updated using the last error signal, which allows for estimates with small bias, avoids frequency tracking conflicts, is computationally efficient, and does not require further root-finding as the frequencies are directly obtained from the updated filter coefficients.

Once converged, the sensitivity outputs are orthogonal which allows for an approximation of the Gauss-Newton algorithm to be used with less computational burden. As a result, only k parameters are updated using k decoupled equations of the form given by Equation 3.13, each used to update a single parameter α_i corresponding to a bandpass filter $H_i(z)$. The Gauss-Newton approximation can become slow when estimates are far from convergence, but remains faster than alternatives like the steepest descent approach typically used in least mean squares filters [84].

When the rate of frequency variation is unknown, the fixed step size used to update each notch can become a limiting factor. In cases where the modal frequencies are far from the initial estimates or vary substantially in a short amount of time, the step size must be large enough to converge quickly to a suitable estimate. In other cases where the estimates have converged or are slowly drifting, the step size must be small enough to prevent excessive oscillations and steady-state errors in the estimate. To solve this issue, a time-varying step size is implemented using the method developed by Mayyas and Momani [86]. The method

adjusts the step size based on the notch distance from the target by minimizing the mean squared error of the coefficient α:

$$E[e_\alpha^2] = E[(\alpha^*(n) - \alpha(n))^2] \tag{3.14}$$

The step size used in Equation 3.13 is determined at each time step by the following equation:

$$\mu(n) = \frac{|\eta(n)|}{\rho(n)} = \frac{1}{\kappa}\frac{|\gamma\eta(n-1) + (1-\gamma)e(n)e(n-1)|}{\gamma\rho(n-1) + (1-\gamma)e^2(n)(s'^2(n) + \varepsilon)}; \quad 0 < \gamma < 1 \tag{3.15}$$

where η and ρ are used to track the previous step size estimate, κ is a scaling factor, γ is a weight that controls the quality of estimations, and ε is a constant used to avoid numerical issues. In the overall adaptive scheme, this method substitutes the manual selection of step size μ with the parameter κ, which provides a more intuitive choice as it is used to scale the adaptive step size to a suitable range of values. The parameter γ determines the excess mean-square error, but it can be safely set to a value close to 1 as the damping method is not very sensitive with respect to variations in γ. With the benefits of additional adaptability, the variable step size modification only adds a small number of addition and multiplication operations and utilizes available CANF signals.

The overall adaptive damping scheme is summarized in Figure 3.9. The CANF obtains k modal frequency estimates from the response of a collocated plant. The update algorithm uses the CANF output signals to adapt the notch coefficients and the variable step size. The estimates are then extracted from the notch coefficients and used to tune a PPF controller for damping k modes of the structure.

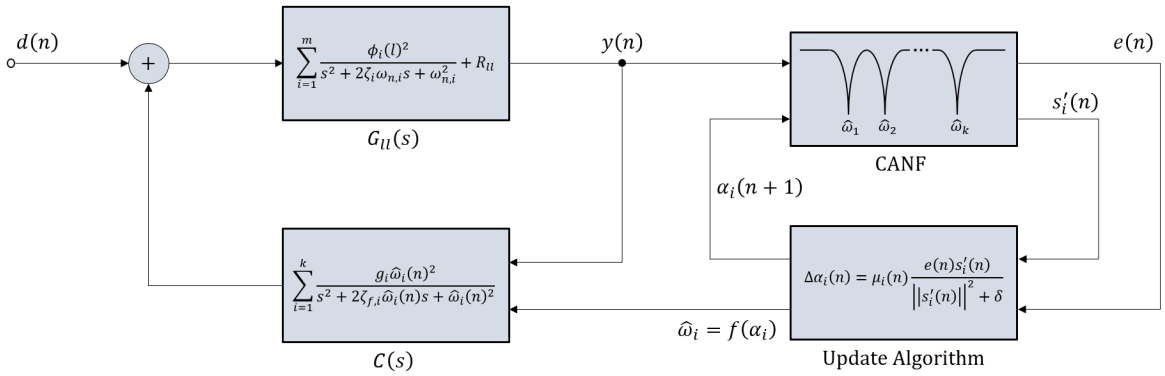

Figure 3.9: Overall adaptive damping scheme.

3.4 Simulations

Simulations of the adaptive scheme were carried out in MATLAB Simulink to analyze its performance. A time-varying structure was implemented using the transfer function given by Equation 3.2 with variable natural frequencies. Table 3.1 lists the control and estimator parameter values used throughout this section. Note that these tuning parameters are mostly fixed at suitable values that, as will be shown, work for various operating conditions and situations. The frequency estimates are obtained from the adapted parameters α_i at each step using Equation 3.11.

Table 3.1: Controller and estimator simulation parameters for single mode and multimodal simulations.

Parameter	Symbol	Single Mode	Multiple Modes		
			Mode 1	Mode 2	Mode 3
PPF gain	g	0.6	1	0.5	0.5
PPF damping ratio	ζ_f	0.3	0.3	0.3	0.3
ANF pole radius	r	0.99	0.99	0.99	0.99
Normalization division constant	δ	0.1	0.1	0.1	0.1
VSS weighting factor	γ	0.97	0.97	0.97	0.97
VSS division constant	ε	0.1	0.1	0.1	0.1
VSS scaling factor	κ	5000	5000	5000	5000

The first set of results are used to showcase different characteristics of the ANF when used to estimate the modal frequency of a single DOF system. Figure 3.10 shows the convergence behavior of the frequency estimate when the open loop system is excited sinusoidally from rest at the frequency of the mode (50 Hz). Starting from an initial estimate of 25 Hz, the estimates quickly converge to the correct frequency of the mode. This result mainly serves as a simple validation of the ANF since it was originally developed to isolate and enhance sinusoids in particular. The figure also shows the effect of changing the step size value, which clearly provides a trade-off between the estimation speed and the overshoot and settling time of the estimate.

Figure 3.11 shows the estimation results using the transient response of the same 1 DOF system, obtained by exciting it with pulse disturbances. The ANF effectively estimates the mode frequency despite the decaying response. Although a spike in the estimate occurs with each pulse excitation due to the initial lack of sufficient signal information, it quickly converges back to the mode frequency.

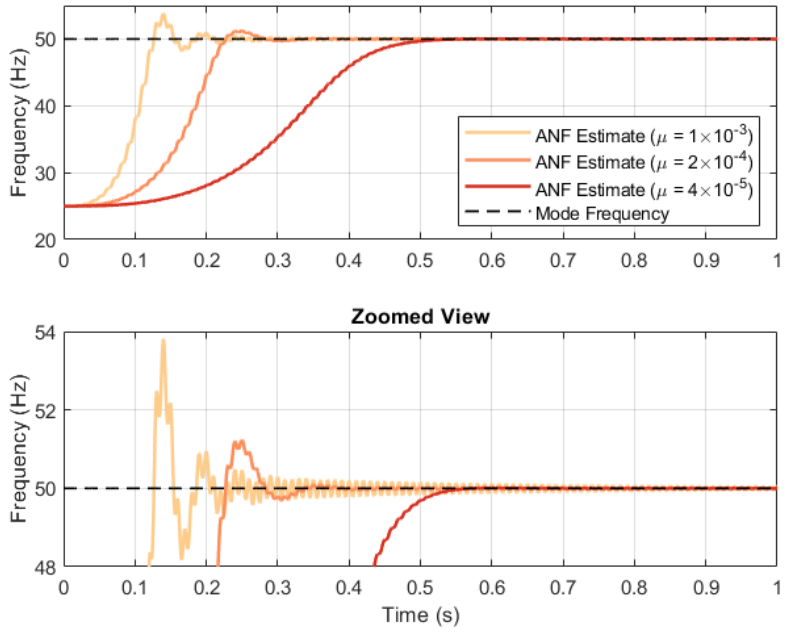

Figure 3.10: Frequency estimation simulation results using the position output of a sinusoidally excited 1 DOF structure.

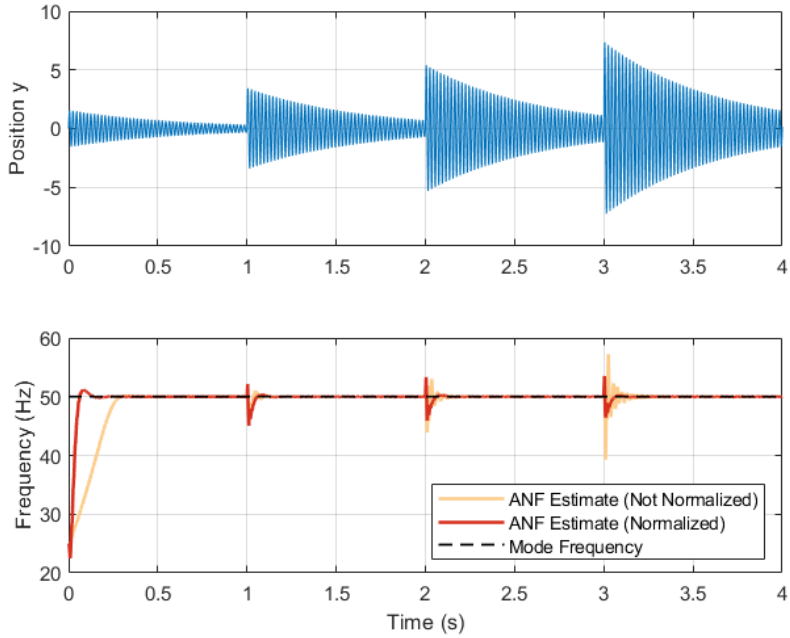

Figure 3.11: Frequency estimation simulation results using the transient position output of a 1 DOF structure.

Figure 3.11 also compares between ANF estimates using the regular and normalized update equations given by Equations 3.12 and 3.13. To carry out the comparison, the pulse disturbance amplitude is increased throughout the simulation. The results show that unlike the regular update, the normalized update provides robustness against variations in the magnitude of vibrations, allowing the ANF to obtain faster estimates from small disturbances and maintain its convergence behavior given large disturbances.

Figure 3.12 shows the benefits of using a variable step size. Similar to the normalized update equation with a fixed step size, the variable step size provides insensitivity against the vibration magnitude. On top of that, the variable step size sufficiently adapts the ANF to different frequency estimation scenarios. In this case, the mode of the 1 DOF structure has a sharp increase in frequency at the 1 s mark. It is shown that using fixed values of μ at the boundaries of the variable case degrades the performance when compared to the variable case. A large, fixed value of μ causes large oscillations and a small value increases convergence time. On the other hand, the variable case adapts μ to achieve reliable estimates in situations with different disturbances and frequency variations.

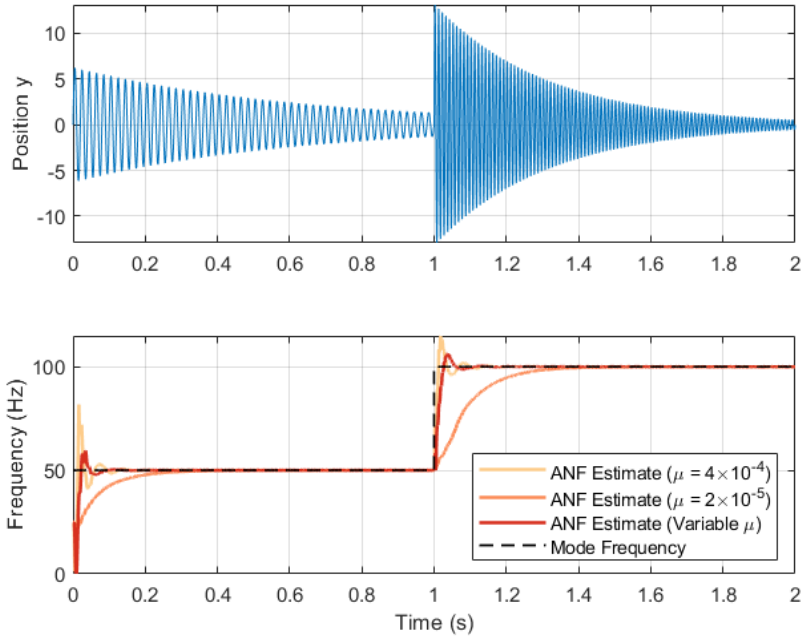

Figure 3.12: Frequency estimation simulation results with a time-varying mode frequency showing the benefits of using a variable step size.

Although a suitable parameter value must be selected for the two types of update equations (μ for the fixed step size update and κ for the variable step size update), the variable step size provides the advantage that κ is tuned to scale μ to a certain range within which it can vary.

In contrast, fixing the value of μ might limit the performance in situations like those shown in Figure 3.12. Either method can thus be used depending on how the structure's parameters vary.

Figure 3.13 provides more insight into the adaptation of the variable step size. The system is excited by the same pulse disturbance every second, and the modal frequency changes both gradually and sharply. The ANF is able to quickly and accurately track the frequency at all times as it is adapted based on the ANF error and sensitivity signals. A large error signal, for example caused by an incorrect initial estimate (0 s) or a change in the mode frequency (1.33 s), leads to an increase in the step size to eliminate the error quickly. Conversely, a large sensitivity signal (2 s) decreases the step size to prevent large fluctuations in the estimate. Once the estimate has settled on a slowly changing (0.5 s) or a fixed (1.5 s) frequency value, a larger step size is tolerated as the sensitivity decreases.

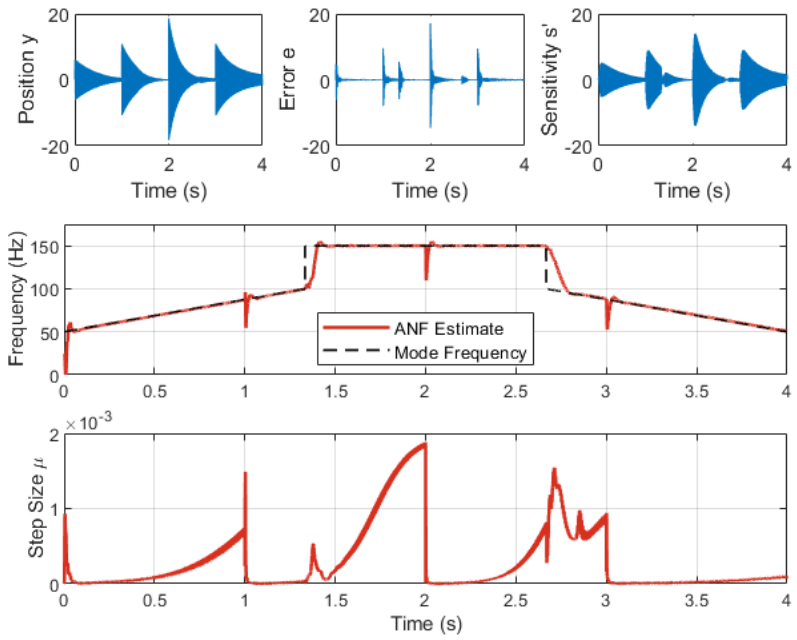

Figure 3.13: Frequency estimation simulation results showing the effect of ANF signals on step size adaptation.

The next result in Figure 3.14 compares between a fixed PPF tuned to damp a mode at 50 Hz and an adaptive PPF tuned using the frequency estimates obtained by an ANF with a variable step size. Starting with an incorrect initial frequency of 25 Hz, the adaptive PPF is quickly tuned to 50 Hz and its performance is identical to that of an exactly tuned fixed PPF. As the mode frequency gradually increases above 50 Hz, one can clearly see the degradation in the damping performance of the fixed PPF compared to the adaptive PPF,

which sufficiently suppresses the vibrations and maintains a lower settling time with each disturbance. Given a large enough difference between the mode and filter frequencies (6 s and later), the fixed PPF ceases to provide any vibration suppression.

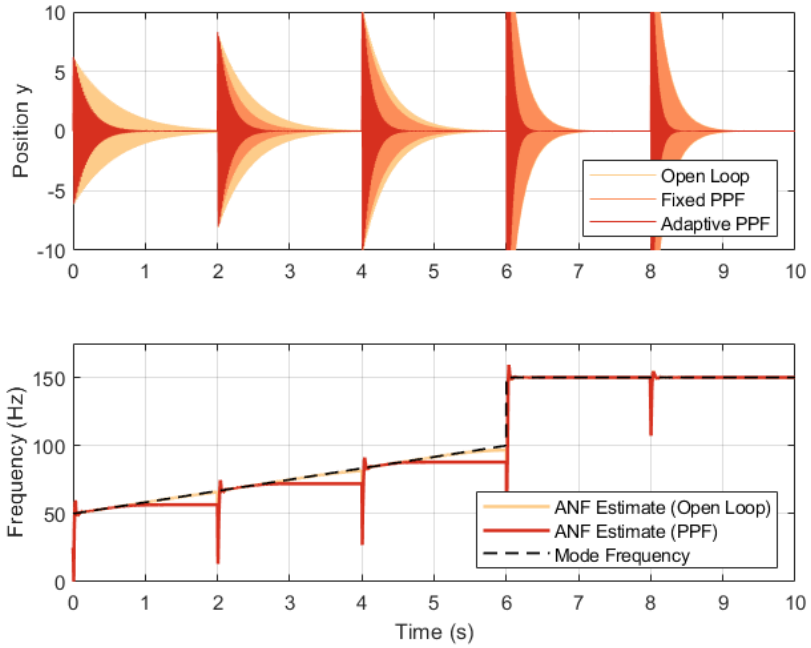

Figure 3.14: Single mode damping performance of adaptive PPF tuned using ANF estimation.

Note that while spikes occur in the estimate when the structure is first excited, quick convergence to the mode frequency and the properties of PPF as discussed in Section 3.2 prevent this from deteriorating the damping performance. It is also shown that the frequency estimate obtained from the damped closed loop system is nearly identical to the estimate obtained from the open loop system, but it stops tracking earlier. This is to be expected as the damped response decays faster and the ANF is no longer provided with a sufficient input signal. Regardless, the estimate quickly converges to the mode frequency at the next excitation of the structure.

Figure 3.15 shows the performance of the adaptive damping scheme applied to simultaneously estimate 3 modes of a time-varying structure and damp them. It is clear that the previously discussed advantages of the method extend to the multimodal damping case. In this example, using the frequency estimates once they have settled at t = 9 s, the first mode is tracked with 0.84% error, the second mode with 0.22% error, and the third mode with 1.56% error.

In addition, Figure 3.16 shows the active damping performance in the frequency domain. At first (t = 0 s), the adaptive PPF initially tuned to 15 Hz lower than the mode frequencies

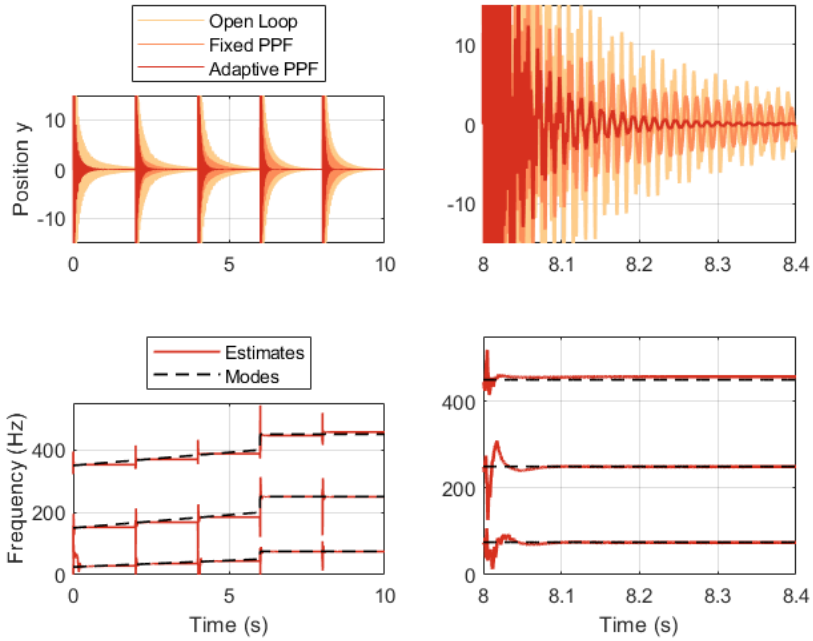

Figure 3.15: Performance of adaptive multimodal PPF in the time domain.

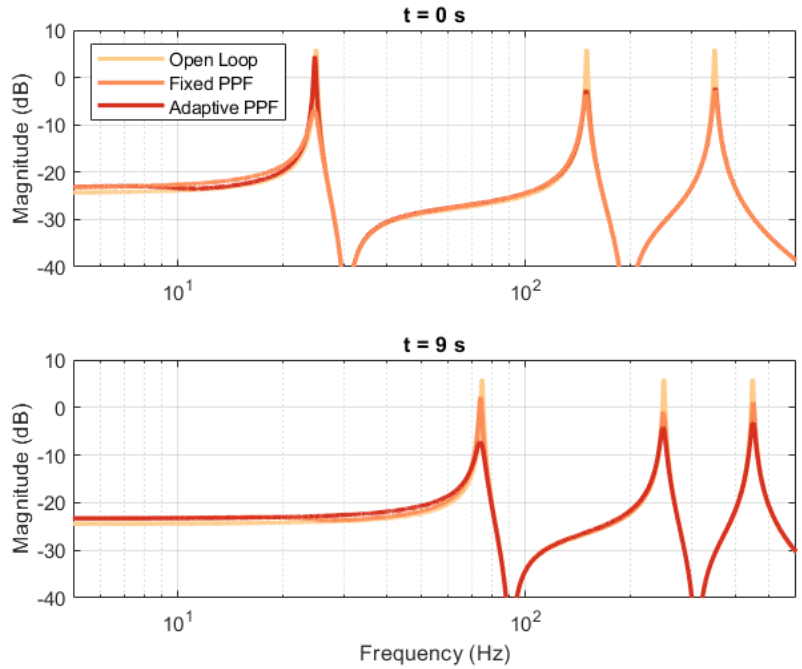

Figure 3.16: Performance of adaptive multimodal PPF in the frequency domain before and after the convergence of estimates.

does not damp the first mode and only slightly damps the higher frequency modes. Towards the end of the simulation (t = 9 s), the adaptive controller effectively attenuates 12 dB of the first mode, 8 dB of the second mode, and 7 dB of the third mode, whereas the detuned fixed PPF provides significantly less damping.

Figure 3.17 shows the method's performance when damping three closely spaced modes separated by 5 Hz. Frequency tracking is shown to be effective even in this extreme case, although there is a loss in the accuracy of the estimates (e.g., after t = 9 s). The smaller the difference between the modal frequencies, the more difficult and less reliable the estimates become. However, the pole radius r may be increased to achieve better mode separation as it controls the bandwidth of the adaptive notch filters. The estimates also exhibit interchanging behavior as two notches swap estimates (t = 8.2 s), but this does not affect the damping performance as all frequencies continue to be detected and tracked.

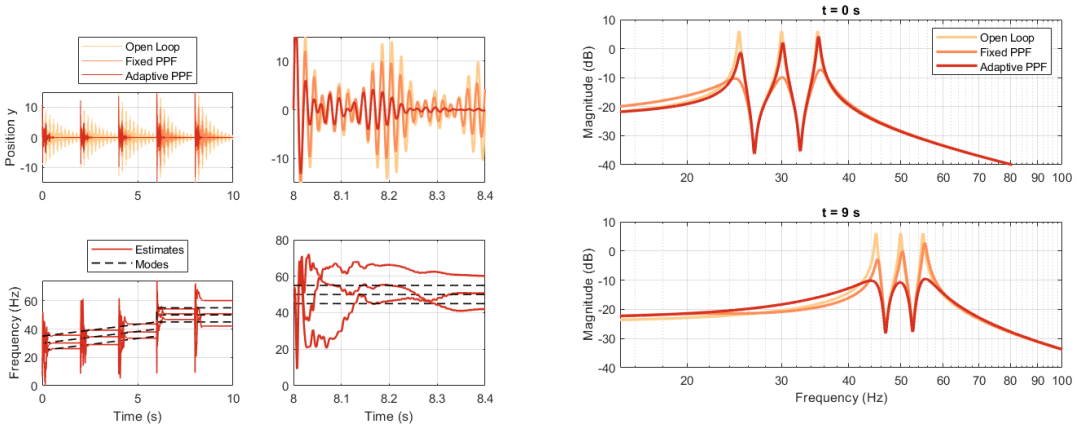

(a) Time domain performance.

(b) Frequency domain performance before and after convergence.

Figure 3.17: Performance of adaptive multimodal PPF with closely spaced structural modes.

Figure 3.18 shows a repetition of the previous tests but with modes having different magnitudes. From the lower to the higher frequency modes these magnitudes are 6 dB, 0 dB, and -6 dB. The adaptive scheme is able to estimate the frequencies and maintain sufficient damping with all three modes. Note that none of the estimator parameters were changed from those used in previous examples, but if the difference between the mode magnitudes becomes too large then either the scaling factor κ or – if using a fixed step size – the step size μ must be tuned according to the magnitudes of each estimated mode.

When estimating multiple frequencies simultaneously and the estimates are initially far from convergence, the coupling between the notch filters can create complications as the approximated Gauss-Newton update assumes orthogonal notch sensitivities (i.e., decoupled notches). This is tested in Figure 3.19 by varying the difference Δf_i between the initial

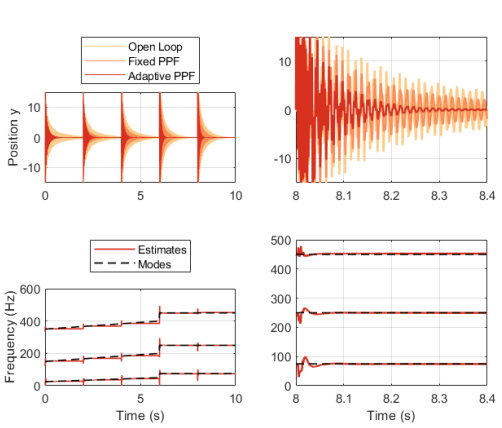

(a) Time domain performance.

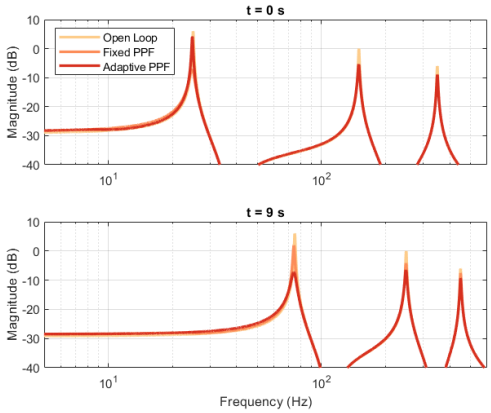

(b) Frequency domain performance before and after convergence.

Figure 3.18: Performance of adaptive multimodal PPF with structural modes of different magnitudes.

estimates and the constant mode frequencies. It is shown that the larger the difference, the longer it takes to estimate the corresponding frequency. In this particular case, the estimator requires two pulse excitations before it can track the three modes when the initial estimate for each mode is offset by 99 Hz from the modal frequency.

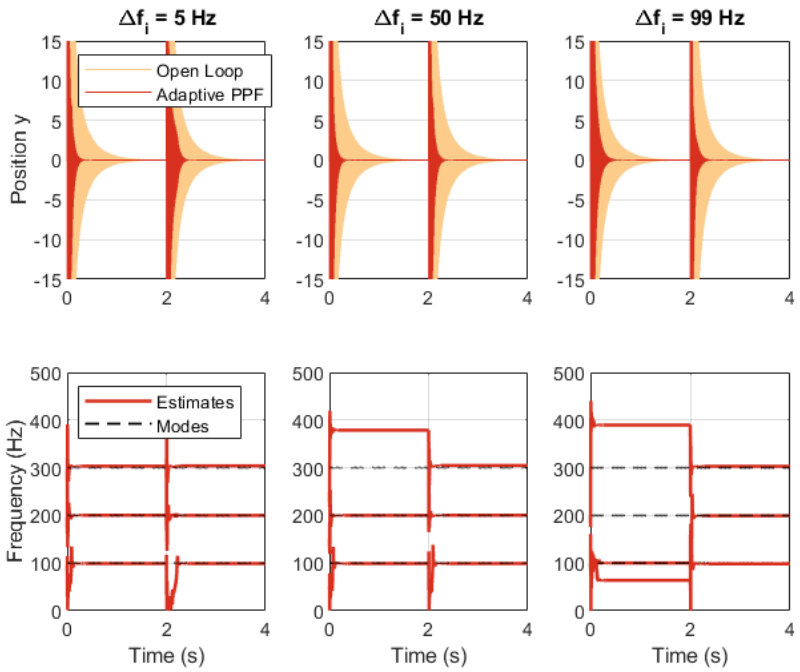

Figure 3.19: Adaptive multimodal PPF performance with different estimate initialization.

Finally, Figure 3.20 shows the effects of noise on the CANF performance. Band-limited white noise with power P_n is added to the structure's output signal and this summation is used as the CANF input. It is shown that for different magnitudes of noise power, the estimator performance remains largely the same. In the case when $P_n = 1 \times 10^{-3}$, the CANF input signal is effectively buried in noise, but the estimates remain accurate. This constitutes a major advantage of using CANF for real time frequency tracking and adaptive damping.

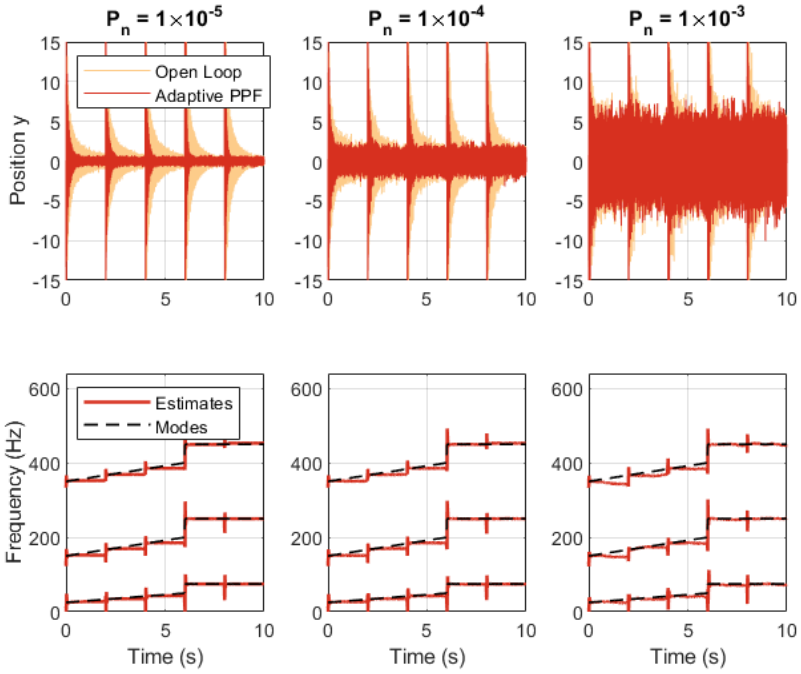

Figure 3.20: Adaptive multimodal PPF performance in the presence of varying levels of noise in the input signal.

3.5 Experimental Validation

An experimental test was used to validate the performance of the adaptive damping method in a real active damping implementation. The test structure is a vertically-oriented cantilever beam made from aluminium. The beam is shown in Figure 3.21 and its properties are given by Table 3.2.

A piezoelectric stack actuator (PiezoDrive SA050520) is attached to the base of the beam and used to generate disturbances. For AVC using PPF, piezoelectric patch transducers (PI P-876 DuraAct) are used for both actuation and sensing. Piezoelectric transducers add little mass, operate in a wide frequency band, and can be easily integrated into structural elements,

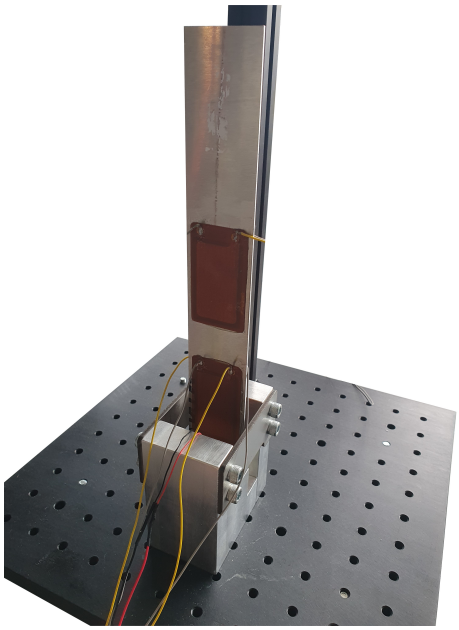

Figure 3.21: Cantilever aluminium beam with piezoelectric stack and patch transducers.

Table 3.2: Experimental beam parameters.

Parameter	Value
Length (cm)	27
Length from clamping point (cm)	25.1
Width (cm)	4
Thickness (mm)	1.5
Elastic modulus (GPa)	70
Density (kg/m^3)	2700

making them suitable for precise active damping applications [25]. Piezoelectric sensors are usually used for PPF control as they output a signal proportional to the strain of the patch, which is used as the generalized position measurement. The patch actuators and sensors are attached as pairs to the same DOFs but at opposite sides of the beam, thus providing the collocated system described in Section 3.2. The following experiments make use of the pair of patches attached close to the base of the beam as it is a high strain location suitable for measuring multiple bending modes.

The overall experimental setup is shown in Figure 3.22. A TI LAUNCHXL-F28379D development kit with the TMS320F28379D microcontroller (MCU) is used to implement the adaptive control algorithm. A charge amplifier circuit is used to convert the charge signal of the piezoelectric sensor into a voltage signal and condition the input to the analog-to-digital converter (ADC). The disturbance and control signals generated by the controller are

amplified by BD300 amplifiers before being sent to their respective actuators. Discretized models of a CANF and an adaptive PPF controller are implemented in MATLAB Simulink, which is then used for code generation, MCU monitoring, and data logging. Figure 3.23 shows a block diagram with the various elements and connections within the control system.

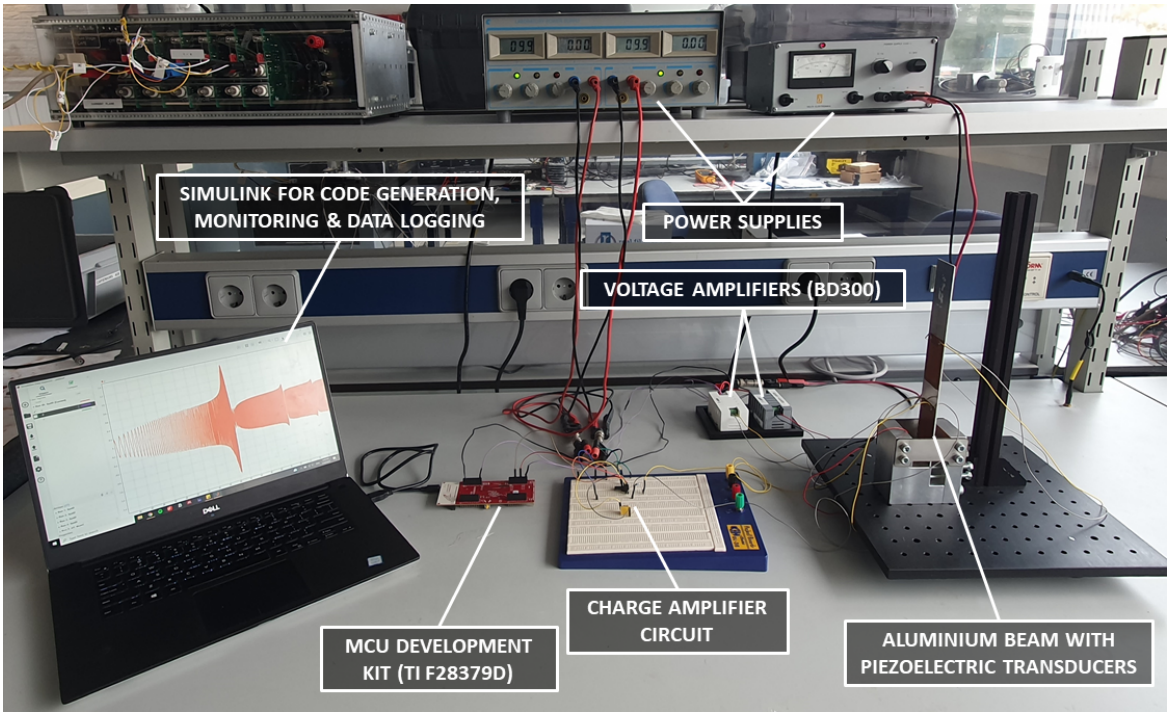

Figure 3.22: Experimental setup.

The beam was identified to determine its resonance modes for testing purposes. This was done using a chirp signal ranging from 1 Hz to 500 Hz. Figure 3.24 shows the collocated transfer function between the control force u and the strain measurement y, and Table 3.3 shows the magnitude and frequency values of the three identified bending modes.

Table 3.3: Experimentally identified mode frequencies and magnitudes.

Mode	Frequency (Hz)	Magnitude (dB)
1	23.5	18.3
2	127.2	9.3
3	328.9	8.3

Three different controllers were used to damp the three identified modes of the beam: a PPF controller with incorrect fixed tuning, a PPF controller tuned to the modal frequencies, and an adaptive PPF controller with incorrect initial estimates. Table 3.4 lists the estimation

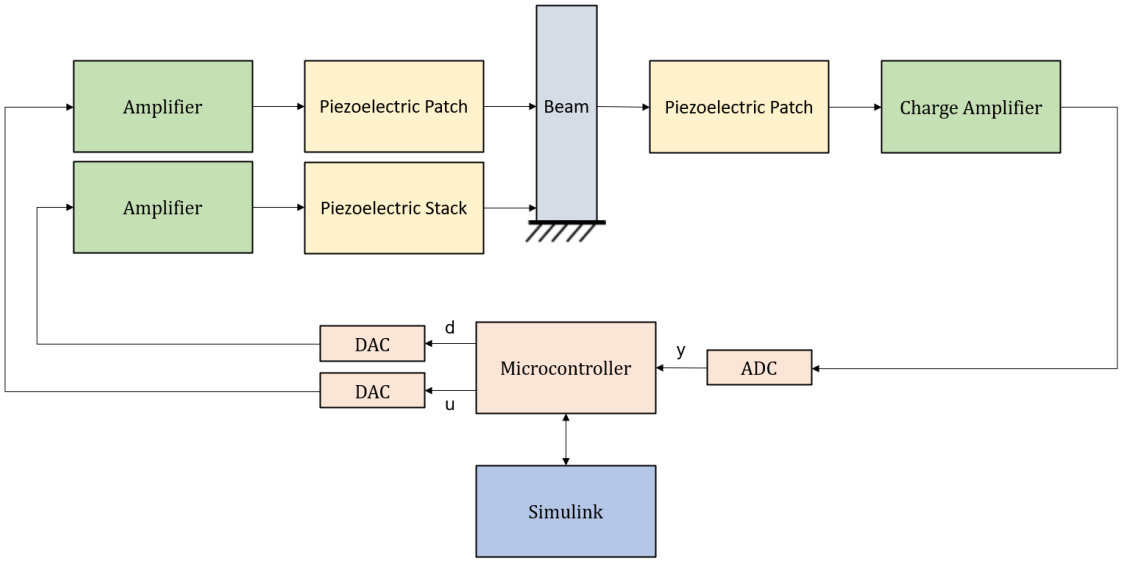

Figure 3.23: Block diagram of the control system used for experimental validation.

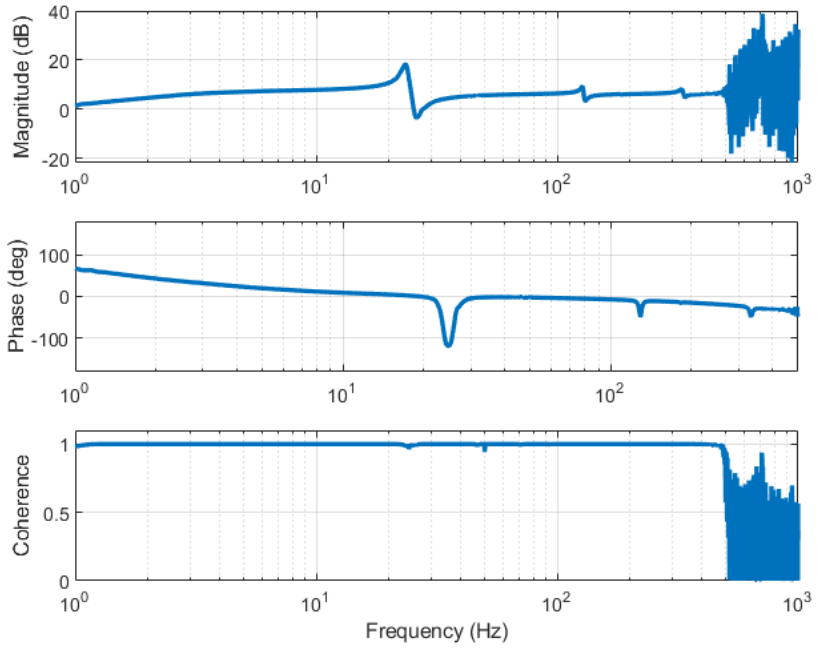

Figure 3.24: Frequency response of the beam with collocated piezoelectric transducers.

and control parameters used in the experiment. The PPF gains were selected for suitable multimodal damping of the modes given in Table 3.3. Most parameters are kept the same as the simulations, with the exception of κ which was set to provide a suitable step size

range for each estimate. This was necessary to increase the estimation sensitivity of higher frequency modes because of the relatively low magnitude of the modes.

Table 3.4: Controller and estimator experimental parameters.

Parameter	Symbol	Modes		
		Mode 1	Mode 2	Mode 3
PPF gain	g	0.1	0.08	0.02
PPF damping ratio	ζ_f	0.3	0.3	0.3
ANF pole radius	r	0.99	0.99	0.99
Normalization division constant	δ	0.1	0.1	0.1
VSS weighting factor	γ	0.97	0.97	0.97
VSS division constant	ε	0.1	0.1	0.1
VSS scaling factor	κ	500	5	5

Figure 3.25 shows the experimental results of the adaptive PPF scheme. The stack actuator is used to disturb the beam with pulses at regular intervals starting at 15 s, and the resulting vibrations are effectively suppressed by the adaptive PPF.

The frequency estimation plots show that by the time the beam settles from its first excitation, estimates for the first two modes have already converged within 1 Hz of error. However, estimation of the third mode is slow and requires multiple excitations for convergence. This can be attributed to a combination of the mode's relatively small magnitude in the collocated transfer function, as well as the significant high-frequency roll-off in the non-collocated transfer function between the stack disturbance at the base and the patch sensor. In the experimental case, the final errors between the estimates and the identified modes result from a combination of factors:

- Estimator bias. This is the true error between the CANF input signal frequencies and the provided estimates. CANF bias is usually extremely low and can be improved by further reducing the notch bandwidth through increasing the pole radius r.

- Spillover. As explained in Section 3.2, actively damping one mode with PPF can cause another mode to shift in frequency. The adaptive PPF accounts for the effects of spillover, which can partially explain a slight discrepancy between the identified open loop modes and the estimated frequencies in the closed loop, particularly for lower frequency modes.

- System variations. Modes shifting in frequency were observed between experiments. This might occur for a variety of reasons, including the clamping conditions and

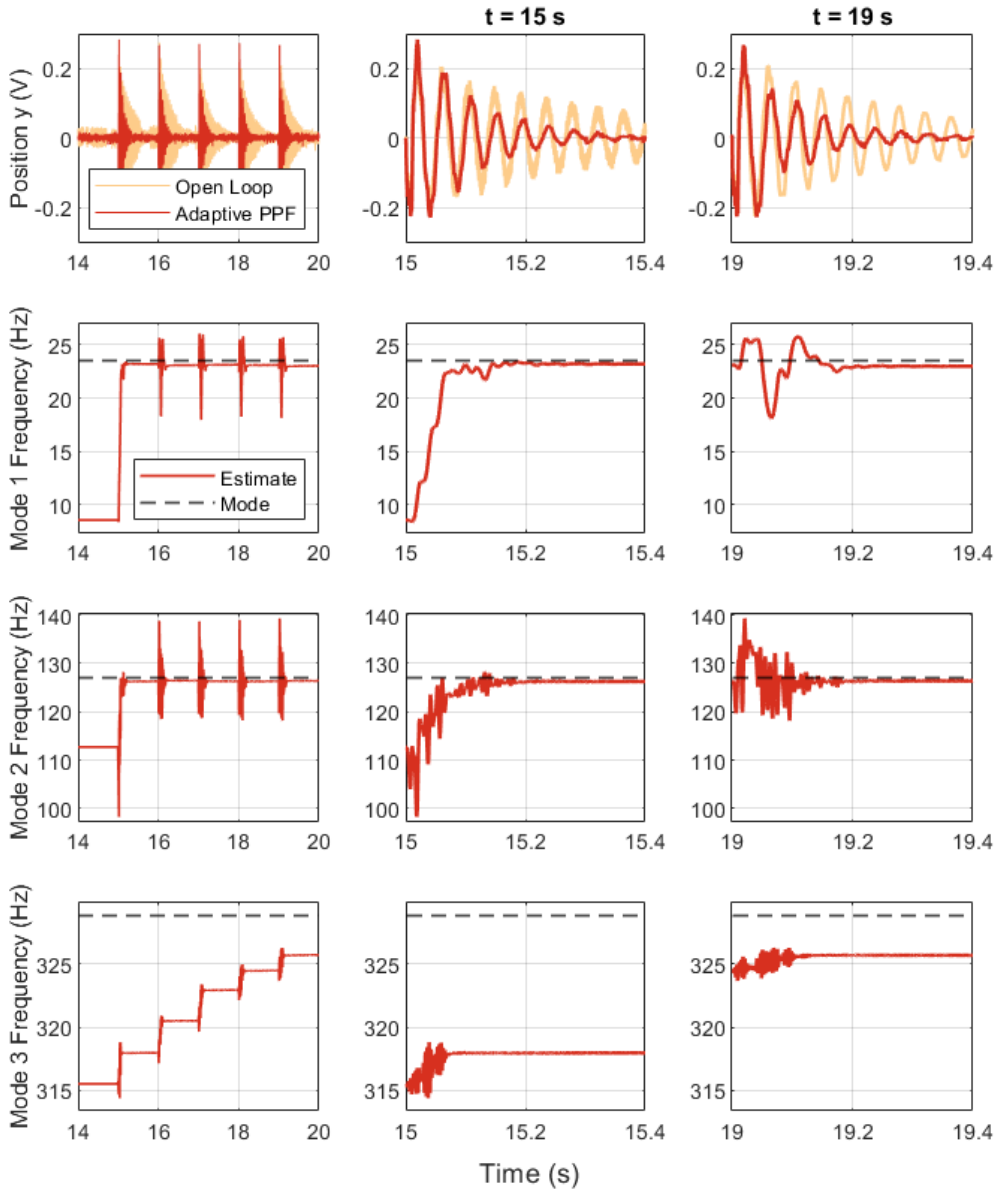

Figure 3.25: Experimental results showing the adaptive damping and modal frequency estimation performance of the method on a vibrating flexible beam.

variations in the screw used to pre-tension the stack actuator. Several experiments in succession might also cause system variation, which is more prominent at higher frequencies. The estimator accounts for these variations as intended, contributing to the difference between the estimates and the identified modes.

The damping performance of the adaptive PPF controller is also compared to tuned and de-tuned PPF controllers with fixed parameters in Figure 3.26. The adaptive PPF quickly surpasses the detuned PPF in vibration suppression performance despite starting with the same tuning frequencies. This is because the first two modes are quickly and accurately estimated by the CANF within 0.2 s of the first excitation as shown in Figure 3.25. As for the tuned fixed PPF, it initially outperforms the adaptive PPF as seen by the comparing the vibration signals at 15 s, but their damping action matches once the estimates for the first two modes have converged. The following excitations of the beam are then damped with similar results between the two controllers, showing the effectiveness of the adaptive method and its behavior as a well-designed PPF controller regardless of a priori knowledge about the modes and their variation.

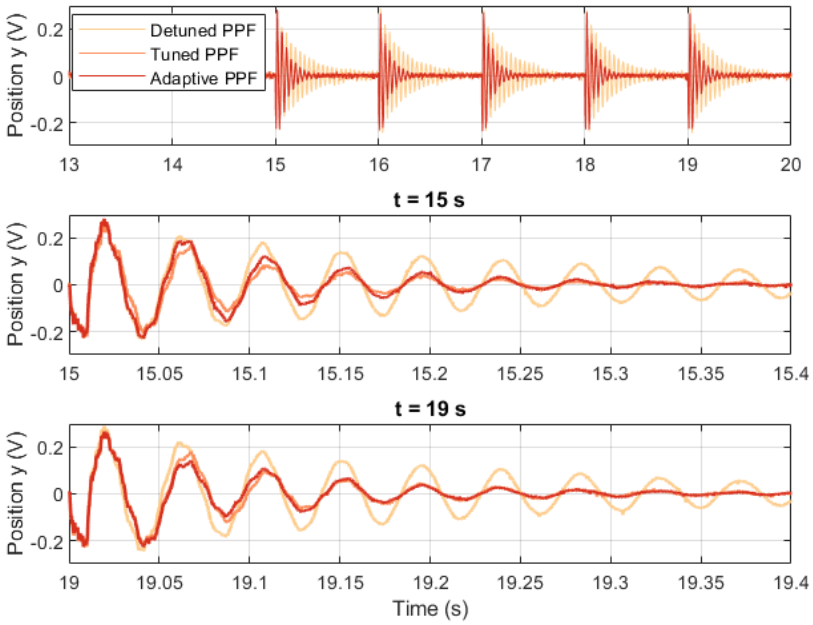

Figure 3.26: Experimental results comparing the performance of the adaptive PPF controller to non-adaptive controllers.

3.6 Conclusion

This paper presented a simple yet effective adaptive method for actively damping multiple modes of an uncertain or time-varying structure. Adaptive notch filters in a cascade structure (CANF) are used to provide quick and accurate frequency estimates of multiple modes simultaneously and in real time. The frequency estimates are then used to tune an adaptive positive

position feedback (PPF) controller for multimodal damping with a simple adjustment rule. The estimator only requires available position measurements used in the PPF control loop and can estimate modal frequencies using transient structural vibrations, allowing the method to be used in applications like precision motion systems where any additional disturbance or noise injection for identification purposes would degrade the motion performance. Furthermore, the method is computationally efficient, requiring fewer operations than alternative estimation methods and avoiding the need for additional prefiltering or root-finding. The method also showcases consistently effective performance with noisy signals. A variable update step size is used to further improve the frequency tracking performance and allow the estimation to adapt to different vibration amplitudes as well as different scenarios of modal frequency variation. Simulations and an experimental test using a flexible beam were used to investigate and validate the method's effectiveness, showing its applicability in practical implementations.

For future work, the use of adaptive notch filters can be explored further to achieve effective tracking. This may be done by using different adaptive filter structures, notch structures, and update algorithms. Different estimator parameters may also be adapted, for example by updating the notch pole radius (i.e., notch bandwidth) depending on the distance to convergence and the spacing between the modes to obtain better estimates. The proposed method utilizes a single parameter κ to scale the range of the step size, but an improved variable step size algorithm that eliminates the need to manually select any parameters would further simplify the method. In addition, the CANF can be easily extended for use with other modal AVC methods where tuning is largely dependent on accurate knowledge of the modal frequencies. Implementation in PPF and other AVC methods can also be extended using real-time optimization-based design to maximize the damping performance at each time step. Finally, the strengths of the method can be further highlighted in smart structures with distributed or networked actuation and sensing, as the slow convergence of the 3rd mode encountered in Figure 3.25 can be alleviated using sensors at high strain locations for each mode. Estimates from different measurements can be used to enhance the overall adaptive damping scheme without adding much complexity due to the method's high efficiency.

Chapter 4

Discussion

The following sections discuss additional aspects of the adaptive damping scheme with the aim of providing further insights into the method and motivating future developments.

4.1 Sensitivity Analysis and Parameter Selection

In Section 2.3, one of the desired properties of the method was to minimize the complexity of parameter tuning. Although many parameters are used in the overall adaptive damping scheme, steps were taken to significantly reduce the design burden by simplifying the estimation problem to 1 estimated value per damped mode and implementing a variable step size in the update equations to compensate for different tracking scenarios. The results obtained in Sections 3.4 and 3.5 have shown that fixed values can be chosen for most parameters in vastly different situations without a loss in performance.

Figure 4.1 shows the effects of different method parameters on the frequency estimates. The following can be inferred from the figure:

- It is clear that the PPF parameters – the feedback gain and filter damping ratio used to damp each mode – have negligible effects on the estimates. As a result, PPF filters may be designed as usual without having to take the estimator into consideration.
- The estimates are slightly more sensitive to the pole radius r of the ANF as it defines the notch bandwidth, leading to larger steady-state estimation bias at lower values of r due to the wider notch. It was shown that a fixed value of $r = 0.99$ was sufficient for many situations. An exception is the estimation of closely-spaced structural modes, since choosing a suitable value of r can adjust the notch bandwidth to resolve closer frequencies.

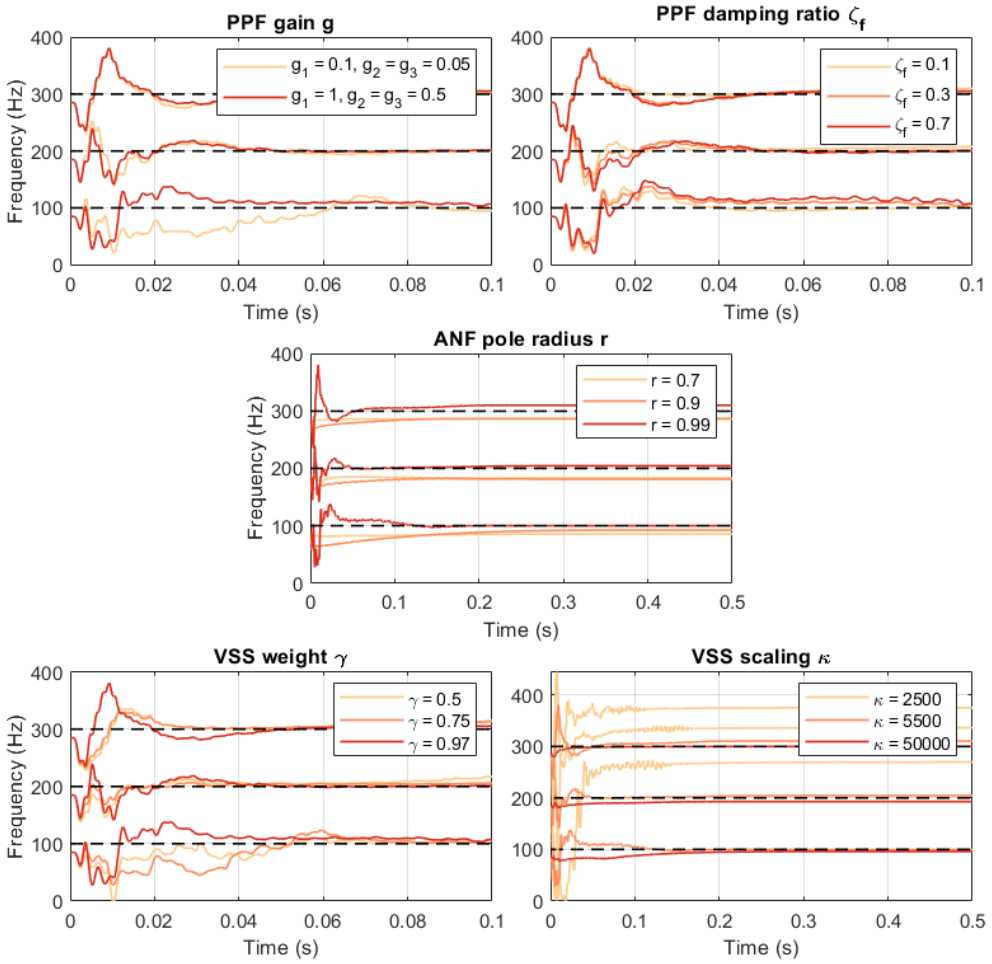

Figure 4.1: Sensitivity analysis of the parameters used in the overall adaptive damping scheme.

- Estimation sensitivity with respect to the parameter γ is almost negligible, but lower values will cause larger steady-state estimation errors. A fixed value of $\gamma = 0.97$ was sufficient for many situations. This value can be adjusted in cases where a particular maximum steady-state error is desired [86], although r also influences this behavior and its effects should be considered in tandem.

- The estimates are shown to be quite sensitive to the scaling factor κ, which is used to scale the range of the variable step size. The estimation becomes slower with large values of κ, and diverges with smaller values. This parameter effectively replaces the fixed step size as the principal tuning parameter of the method. An update equation

with normalization (Equation 3.13) can be used in cases where the nature of system variations is known by setting a suitable value for the fixed step size. In more general cases, the variable step size should be used but scaled to an appropriate range of values using κ. Section 3.5 has shown that when modes of significantly different magnitudes are adaptively damped, different scaling values should be used for each mode. Otherwise, the estimates will converge at different rates. However, this is not a significant issue in active damping applications since the controlled modes at a given DOF are usually higher magnitude modes with a stronger influence on structural vibrations. For example, Figure 3.25 shows that using the estimates of the first 2 modes to damp a flexible beam significantly improves the settling time, despite having not yet converged to the frequency of the 3rd mode which has a much lower magnitude. In applications where damping lower magnitude modes is desired, rough knowledge of the relative mode magnitudes can be used to tune the values of κ.

To summarize, the estimation behavior is robust to PPF tuning parameters, and the parameters can be simply fixed at certain values without a loss in generality. One exception is the scaling factor κ, which is the main tuning parameter of the method and must be chosen appropriately.

4.2 Comparison with AR Estimation

A commonly used method to obtain system parameters for adaptive AVC applications is parametric system identification using recursive estimation of an AR model (see Section 2.2.2). This method has been successfully used to estimate multiple structural mode frequencies and damp the modes using PPF [48], and thus serves as a suitable point of reference for the method developed in this thesis.

Figure 4.2 shows the estimation performance of both methods using a 3 DOF structure damped with PPF and forced sinusoidally at the frequencies of its modes. This is an ideal yet impractical case, and is only used for the purpose of comparison. Similarly to [48], the forgetting factor of the recursive estimator is set to be 0.995, a value suitable for structural identification. The main benefit of the recursive AR estimation method is its fast convergence regardless of the initial conditions. In contrast, the rate of CANF convergence depends on the initial guess provided, but this can be adjusted by tuning the update step size or κ if using a variable step size.

Figure 4.3 compares the two methods when the same structure is excited by an impulse disturbance to obtain its transient response. The performance of the AR estimation method is significantly deteriorated in this case, with two slowly converging mode estimates, a

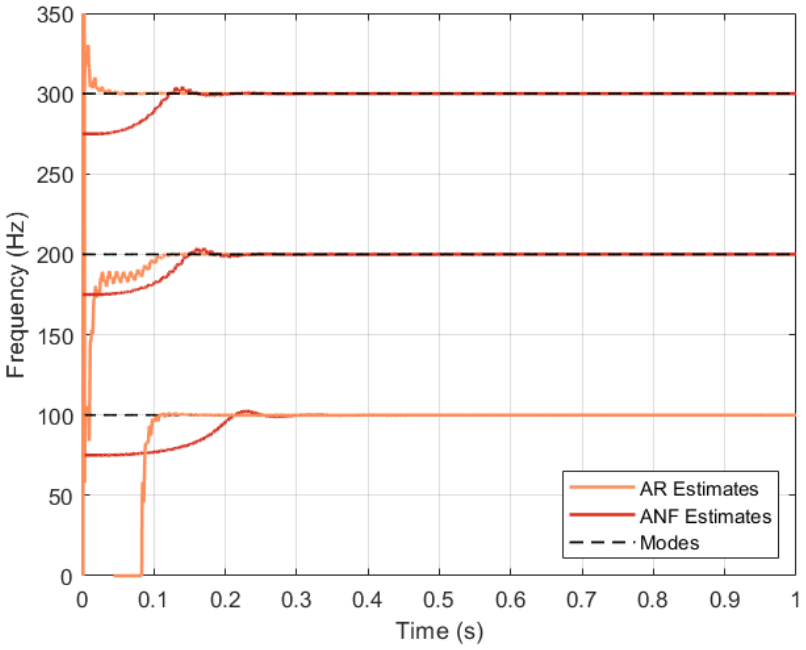

Figure 4.2: Frequency estimation results comparing CANF to AR estimation using the response of a damped structure with sinusoidal excitation of its modes.

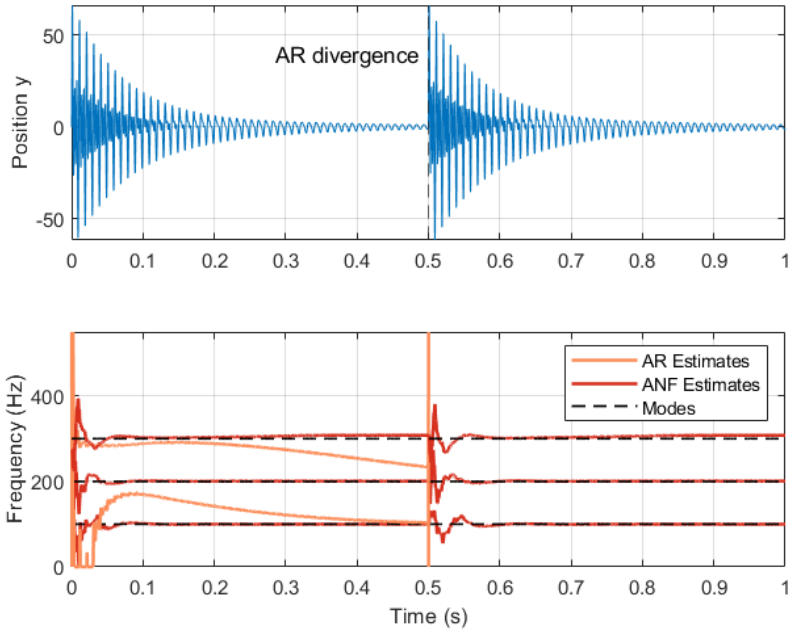

Figure 4.3: Frequency estimation results comparing CANF to AR estimation using the response of a damped structure excited with an impulse disturbance.

diverging 3rd estimate, and overall divergence at the moment of the impulse disturbance. This can possibly be improved by using a certain amplitude threshold for tuning the PPF controller with the estimates, but convergence remains poor even after the initial period of divergence. In the figure, the AR estimates begin to converge towards the 2nd and 3rd mode frequencies at 200 Hz and 300 Hz, but as the response becomes mainly dominated by the frequency of the first mode at 100 Hz, both estimates start decreasing. A main advantage of using CANF is that once a mode is tracked by one ANF, it becomes decoupled from the other ANFs which efficiently start to estimate other modes.

Another disadvantage of AR estimation compared to CANF is its poor performance when using noisy measurements for estimation. Figure 4.4 compares between the two methods when white noise is present in the measurement. The noise power used is 1×10^{-8}, which is significantly lower than the noise power tolerated by CANF (see Figure 3.20). Note that despite directly exciting the modes with sinusoidal disturbances and the added noise, the AR method fails to estimate the frequencies.

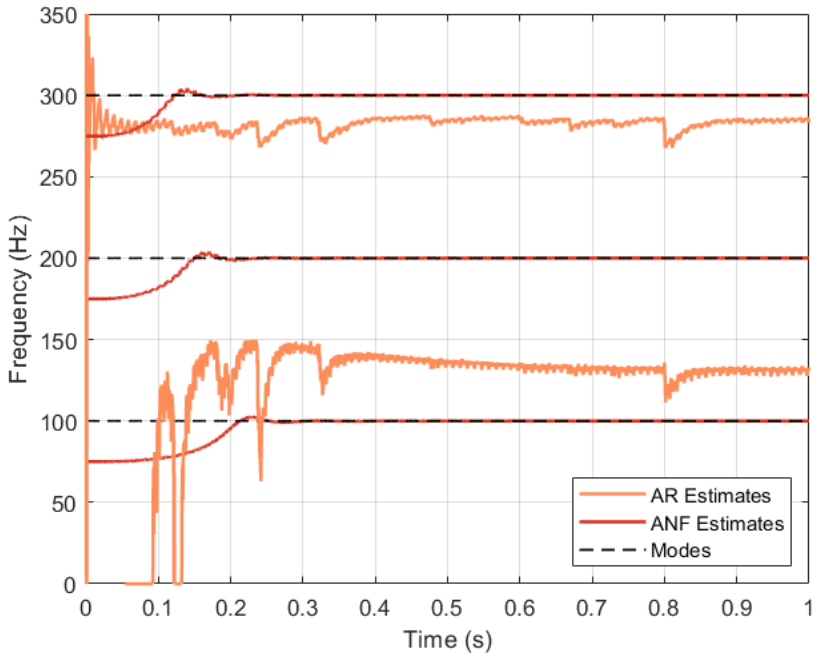

Figure 4.4: Frequency estimation results comparing CANF to AR in the presence of low power measurement noise.

In addition, recursive AR estimation is computationally more complex and requires pre-filtering or root-finding in order to decouple the poles of the estimated system and extract the modal frequencies [66]. When it comes to modal frequency estimation, CANFs therefore provide many advantages over conventional real time system identification.

4.3 Extension to Other AVC Methods

The generality of the developed method allows it to be applied in combination with other AVC methods that require accurate modal frequency estimates to provide sufficient damping. Here, negative derivative feedback (NDF) is used for validation. NDF feeds back a structural velocity signal through a bandpass filter tuned to the frequency of the mode to be damped [38]. It can also be extended to the multimodal damping case by using multiple bandpass filters in parallel, each tuned to a target mode.

The following figures show the time and frequency domain damping performance when using CANF estimates to tune an NDF controller with the same estimator parameters as those used in the PPF case. The results show that the CANF estimates are successfully used to damp the modes of the structure, but with substantial steady state estimation errors of the higher frequency modes. The reason for this is that the damping performance of NDF is quite robust and can sufficiently damp modes with inexactly tuned filters, leading to a quickly decaying response even when the estimates have not yet accurately converged. As a result, the estimates do not converge by the time the response has mostly settled. Nevertheless, there is a need for tracking frequency variations in which the controller loses robustness, as shown by the figure. All 3 modes are generally tracked and active damping is maintained.

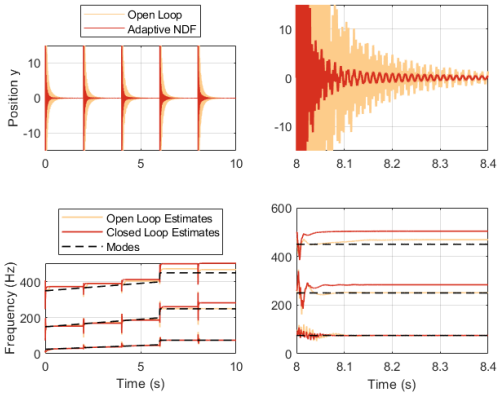

(a) Time domain performance.

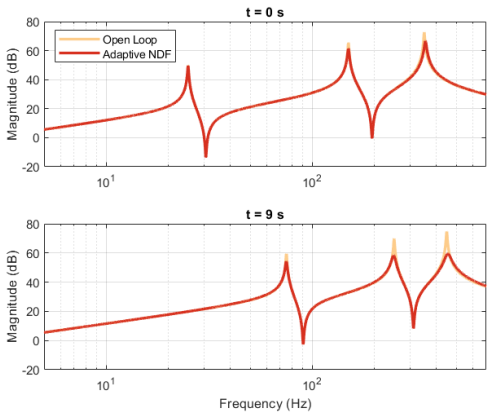

(b) Frequency domain performance before and after convergence.

Figure 4.5: Adaptive damping results using CANF with NDF.

Chapter 5

Conclusion and Recommendations

In this thesis, an adaptive damping scheme was developed to suppress multiple structural modes. A clear motivation was first established for active damping in general and adaptive damping in particular. The underlying issue of concern was the suppression of undesired vibrations to achieve the desired system performance. An adaptive approach was considered to ensure that the vibration controller achieves sufficient damping regardless of system variations and uncertainties.

A comprehensive background and literature review was conducted to identify different vibration suppression methods with a focus on active damping. Collocated PPF control was chosen as the basis of this research due to its properties. Mainly, the simple filter adjustment law, the reliance on only one estimation parameter per damped mode, its robust stability, and its effective performance all make PPF a method that complements adaptive schemes well. Adaptive methods used in AVC were also investigated, and their strengths and weaknesses were discussed. This led to the identification of a research gap in the use of ANFs for AVC applications, which provide direct modal frequency estimates without requiring extraneous parameter estimation or excessive computations.

An overall adaptive scheme was then developed using PPFs in parallel for multimodal damping and ANFs in a cascade structure for multimodal frequency estimation. A variable step size was also used in the ANF update equation to account for different mode and disturbance magnitudes, and ensure quick convergence of estimates regardless of the rate of change of modal frequencies. The method was then validated using simulations and experimental results. It was able to provide the desired estimation and damping performance quickly and accurately for up to 3 modes. This was shown for a number of scenarios, including the adjustment of incorrectly tuned filters from various initial estimates and tracking different variations in frequency. The method was also able to provide quick and accurate estimates and damp prominent modes given extremely brief transient signals from pulse

excitations of a flexible beam. Additional benefits of the method include its insensitivity to noise and computational efficiency.

A cascade structure of adaptive notch filter was used in this thesis to achieve effective multimodal tracking for adaptive damping purposes. The ANF concept can be explored further through various structures (e.g., parallel and lattice layouts) and update algorithms (e.g., RLS) if potential improvements can be made. In addition to the use of a variable step size, different estimator parameters may also be adapted to achieve better performance. An example of this is to adapt the notch pole radius r, starting with a large notch bandwidth for quick initial convergence, and decreasing the bandwidth as the estimate converges to minimize steady-state error. Similarly, adapting the notch bandwidth according to the estimated frequency distance between the modes can be used to obtain higher resolution estimates of closely-spaced modes. The proposed method has one tuning parameter (κ) used to achieve effective estimation by scaling the range of the variable step size used in the notch update. An improved variable step size algorithm that also takes the relative mode magnitudes into account would serve to further automate the method by effectively eliminating the need for manual parameter selection.

There is potential in using CANF with other modal vibration control methods such as negative position feedback and acceleration feedback. This was shown in Section 4.3 using NDF. Different methods may be used depending on the application, required robustness, tolerated spillover, and the types of actuators and sensors used. Implementation in PPF and other AVC methods can also be extended by using the estimates in real-time control optimization algorithms to maximize the performance at each time step. In addition, the method can be implemented in smart structures using distributed and networked actuation and sensing [87]. Doing so can improve the estimates by measuring the structural response at the locations of highest strain energy for each mode. This could avoid the issue encountered in Figure 3.25, where only one collocated actuator-sensor pair was used and estimation of the 3rd mode was relatively slow due to its low magnitude at that particular location. A single ANF or a cascade of several ANFs can be used per sensor signal, and the distributed estimates can be processed to obtain more reliable estimation and better adaptive damping performance. For further validation, additional experimental testing is required using structures with distributed actuation and sensing as well as time-varying parameters.

There are also numerous estimation methods that are potentially applicable for adaptive damping and may be explored in future research on the topic. For example, certain modal parameter identification methods can algebraically estimate natural frequencies and damping ratios of a mechanical system with multiple DOFs using a position measurement [88, 89]. Another example is the Hilbert-Huang transform, a non-parametric method that can be used

to identify time-varying vibrating systems and obtain instantaneous frequencies [90]. It is also capable of analyzing nonlinear data, and its performance has been investigated in analyzing seismic dynamics [91] and monitoring structural health [92]. The method could be promising for analyzing nonlinearities in structures and piezoelectric materials, building on the use of the Hilbert transform for modal analysis and detecting nonlinearities [93, 89]. Two frequency estimation methods not discussed in the main contents of the report, the wavelet transform and the phase locked loop, are discussed in Appendix A.

Overall, the adaptive damping scheme meets the criteria and desired properties listed in Section 2.3. There is great potential for implementing the developed method in practical applications, particularly in motion control systems with flexible elements and smart structures.

References

[1] M. F. Heertjes, H. Butler, N. J. Dirkx, S. H. Van Der Meulen, R. Ahlawat, K. O'Brien, J. Simonelli, K. T. Teng, and Y. Zhao, "Control of Wafer Scanners: Methods and Developments," *Proceedings of the American Control Conference*, vol. 2020-July, pp. 3686–3703, 2020.

[2] J. B. Hopkins and M. L. Culpepper, "Synthesis of multi-degree of freedom, parallel flexure system concepts via Freedom and Constraint Topology (FACT) - Part I: Principles," *Precision Engineering*, vol. 34, no. 2, pp. 259–270, 2010.

[3] L. L. Howell, "Compliant Mechanisms," in *21st Century Kinematics*. London: Springer London, 2013, pp. 189–216.

[4] Georgia Tech Intelligent Machine Dynamics Lab, "Flexible Motion System Control." [Online].

[5] J. L. Fanson and T. K. Caughey, "Positive position feedback control for large space structures," *AIAA Journal*, vol. 28, no. 4, pp. 717–724, 1990.

[6] N. Kodera, H. Yamashita, and T. Ando, "Active damping of the scanner for high-speed atomic force microscopy," *Review of Scientific Instruments*, vol. 76, no. 5, pp. 1–6, 2005.

[7] M. A. Creasy, D. J. Leo, and K. M. Farinholt, "Adaptive collocated feedback for noise absorption in payload fairings," *Journal of Spacecraft and Rockets*, vol. 45, no. 3, pp. 592–599, 2008.

[8] A. Preumont, *Vibration Control of Active Structures*, 3rd ed. Berlin: Springer, 2011, vol. 46, no. 09.

[9] S. J. Elliott, I. M. Stothers, and P. A. Nelson, "A multiple error lms algorithm and its application to the active control of sound and vibration," *IEEE Transactions on Acoustics, Speech, and Signal Processing*, vol. 35, no. 10, pp. 1423–1434, 1987.

[10] J. Holterman and T. J. de Vries, "Active damping based on decoupled collocated control," *IEEE/ASME Transactions on Mechatronics*, vol. 10, no. 2, pp. 135–145, 2005.

[11] C. D. Johnson, "Design of Passive Damping Systems," *Journal of Vibration and Acoustics, Transactions of the ASME*, vol. 117, no. B, pp. 171–176, 1995.

[12] V. Gupta, M. Sharma, and N. Thakur, "Optimization criteria for optimal placement of piezoelectric sensors and actuators on a smart structure: A technical review," *Journal of Intelligent Material Systems and Structures*, vol. 21, no. 12, pp. 1227–1243, 2010.

[13] A. J. Fleming, S. S. Aphale, and S. O. Moheimani, "A new method for robust damping and tracking control of scanning probe microscope positioning stages," *IEEE Transactions on Nanotechnology*, vol. 9, no. 4, pp. 438–448, 2010.

[14] E. Pereira, S. S. Aphale, V. Feliu, and S. O. Moheimani, "Integral resonant control for vibration damping and precise tip-positioning of a single-link flexible manipulator," *IEEE/ASME Transactions on Mechatronics*, vol. 16, no. 2, pp. 232–240, 2011.

[15] D. Farruggio and L. Menini, "Two degrees of freedom H∞ control of a flexible link," *Proceedings of the American Control Conference*, vol. 4, no. June, pp. 2280–2284, 2000.

[16] I. Golovin and S. Palis, "Robust control for active damping of elastic gantry crane vibrations," *Mechanical Systems and Signal Processing*, vol. 121, pp. 264–278, 2019.

[17] M. Karkoub and K. Tamma, "Modelling and μ-synthesis control of flexible manipulators," *Computers and Structures*, vol. 79, no. 5, pp. 543–551, 2001.

[18] K. J. Åström, L. Neumann, and P. O. Gutman, "A Comparison Between Robust and Adaptive Control of Uncertain Systems," in *IFAC Adaptive Systems in Control and Signal Processing*, vol. 20, no. 2, 1986, pp. 43–48.

[19] Y.-p. Chen and H.-t. Hsu, "Regulation and Vibration Control of an FEM-Based Single-Link Flexible Arm Using Sliding-Mode Theory," *Journal of Vibration and Control*, vol. 7, 2001.

[20] Z. C. Qiu, J. D. Han, X. M. Zhang, Y. C. Wang, and Z. W. Wu, "Active vibration control of a flexible beam using a non-collocated acceleration sensor and piezoelectric patch actuator," *Journal of Sound and Vibration*, vol. 326, no. 3-5, pp. 438–455, 2009.

[21] J. Y. Hung, W. Gao, and J. C. Hung, "Variable Structure Control: A Survey," *IEEE Transactions on Industrial Electronics*, vol. 40, no. 1, pp. 2–22, 1993.

[22] H. Gu, G. Song, and H. Malki, "Chattering-free fuzzy adaptive robust sliding-mode vibration control of a smart flexible beam," *Smart Materials and Structures*, vol. 17, no. 3, 2008.

[23] P. Avitabile, "Experimental Modal Analysis," *Sound and Vibration*, 2001.

[24] J. J. Dosch, D. J. Inman, and E. Garcia, "A Self-Sensing Piezoelectric Actuator for Collocated Control," *Journal of Intelligent Material Systems and Structures*, vol. 3, no. 1, pp. 166–185, jan 1992.

[25] S. Poh and A. Baz, "Active Control of a Flexible Structure Using a Modal Positive Position Feedback Controller," *Journal of Intelligent Material Systems and Structures*, vol. 1, no. 3, pp. 273–288, jul 1990.

[26] B. Babakhani, "Active Damping of Vibrations in High-Precision Motion Systems," Ph.D. dissertation, University of Twente, 2012.

[27] M. J. Balas, "Direct Velocity Feedback Control of Large Space Structures," *Journal of Guidance and Control*, vol. 2, no. 3, pp. 252–253, 1979.

[28] C. Goh and T. K. Caughey, "On the stability problem caused by finite actuator dynamics in the collocated control of large space structures," *International Journal of Control*, vol. 41, no. 3, pp. 787–802, 1985.

[29] M. A. Creasy, D. J. Leo, and K. M. Farinholt, "Adaptive positive position feedback for actively absorbing energy in acoustic cavities," *Journal of Sound and Vibration*, vol. 311, no. 1-2, pp. 461–472, 2008.

[30] A. K. Smith, "Adaptive Resonant Mode Active Noise Control," University of Pittsburgh, Tech. Rep., 2005.

[31] L. Marinangeli, "Active Vibration Control of Smart Structures using Fractional-order Control," Delft University of Technology, Tech. Rep., 2016.

[32] D. J. Leo and S. Griffin, "Microcontroller-Based Implementation of Adaptive Structural Control," in *SPIE Conference on Smart Structures and Integrated Systems*, vol. 3329, 1998, pp. 115–127.

[33] S. M. Kim, S. Pietrzko, and M. J. Brennan, "Active vibration isolation using an electrical damper or an electrical dynamic absorber," *IEEE Transactions on Control Systems Technology*, vol. 16, no. 2, pp. 245–254, 2008.

[34] S. M. Kim, S. Wang, and M. J. Brennan, "Comparison of negative and positive position feedback control of a flexible structure," *Smart Materials and Structures*, vol. 20, no. 1, 2011.

[35] S. S. Aphale, A. J. Fleming, and S. O. Reza Moheimani, "Integral resonant control of collocated smart structures," *Smart Materials and Structures*, vol. 16, no. 2, pp. 439–446, 2007.

[36] Y. K. Yong, S. S. Aphale, and S. O. R. Moheimani, "Design, Identification, and Control of a Flexure-Based XY Stage for Fast Nanoscale Positioning," *IEEE Transactions on Nanotechnology*, vol. 8, no. 1, pp. 46–54, 2009.

[37] M. Namavar, A. J. Fleming, M. Aleyaasin, K. Nakkeeran, and S. S. Aphale, "An analytical approach to integral resonant control of second-order systems," *IEEE/ASME Transactions on Mechatronics*, vol. 19, no. 2, pp. 651–659, 2014.

[38] G. Cazzulani, F. Resta, F. Ripamonti, and R. Zanzi, "Negative derivative feedback for vibration control of flexible structures," *Smart Materials and Structures*, vol. 21, no. 7, 2012.

[39] H. H. Syed, "Comparative study between positive position feedback and negative derivative feedback for vibration control of a flexible arm featuring piezoelectric actuator," *International Journal of Advanced Robotic Systems*, vol. 14, no. 4, pp. 1–9, 2017.

[40] K. J. Åström and B. Wittenmark, *Adaptive Control*, 2nd ed. Mineola, New York: Dover Publications, 2008.

[41] X. Shu, P. Ballesteros, and C. Bohn, "Active vibration control for harmonic disturbances with time-varying frequencies through LPV gain scheduling," *Proceedings of the 2011 Chinese Control and Decision Conference, CCDC 2011*, pp. 728–733, 2011.

[42] W. Black, P. Haghi, and K. Ariyur, "Adaptive Systems: History, Techniques, Problems, and Perspectives," *Systems*, vol. 2, no. 4, pp. 606–660, 2014.

[43] A. Baz and J.-T. Hong, "Adaptive Control of Flexible Structures Using Modal Positive Position Feedback," *International Journal of Adaptive Control and Signal Processing*, vol. 11, pp. 231–253, 1997.

[44] M. O. Tokhi and M. A. Hossain, "Self-tuning active vibration control in flexible beam structures," *Proceedings of the Institution of Mechanical Engineers. Part I, Journal of systems and control engineering*, vol. 208, no. 14, pp. 263–278, 1994.

[45] C. Manu, "Dynamic analysis of structures with closely spaced modes using the response spectrum method," *Computers and Structures*, vol. 22, no. 3, pp. 405–412, 1986.

[46] J. Enríquez-Zárate, G. Valencia-Palomo, F. R. López-Estrada, G. Silva-Navarro, and J. A. Hoyo-Montaño, "Efficient predictive vibration control of a building-like structure," *Asian Journal of Control*, vol. 22, no. 4, pp. 1411–1421, 2020.

[47] K. B. Choi, J. J. Lee, and S. Hata, "A piezo-driven compliant stage with double mechanical amplification mechanisms arranged in parallel," *Sensors and Actuators A: Physical*, vol. 161, no. 1-2, pp. 173–181, 2010.

[48] K. H. Rew, J. H. Han, and I. Lee, "Multi-modal vibration control using adaptive positive position feedback," *Journal of Intelligent Material Systems and Structures*, vol. 13, no. 1, pp. 13–22, 2002.

[49] S. N. Mahmoodi, M. Ahmadian, and D. J. Inman, "Adaptive modified positive position feedback for active vibration control of structures," *Journal of Intelligent Material Systems and Structures*, vol. 21, no. 6, pp. 571–580, 2010.

[50] N. Malik, S. Neild, and D. Wagg, "Vibration control of composite beams using adaptive positive position feedback," in *ASME 2007 International Design Engineering Technical Conferences and Computers and Information in Engineering Conference*, vol. 5, 2007, pp. 863–871.

[51] Z. S. Ma and Q. Ding, "Short data-based output-only identification for time-varying systems with fast dynamic evolution," *Shock and Vibration*, vol. 2019, 2019.

[52] B. Widrow, C. S. Williams, J. R. Glover, J. M. McCool, R. H. Hearn, J. R. Zeidler, J. Kaunitz, E. Dong, and R. C. Goodlin, "Adaptive Noise Cancelling: Principles and Applications," *Proceedings of the IEEE*, vol. 63, no. 12, pp. 1692–1716, 1975.

[53] L. J. Griffiths, "Rapid Measurement of Digital Instantaneous Frequency," *IEEE Transactions on Acoustics, Speech, and Signal Processing*, vol. ASSP-23, no. 2, pp. 207–222, 1975.

[54] R. M. Ramli, A. O. Noor, and S. A. Samad, "A review of adaptive line enhancers for noise cancellation," *Australian Journal of Basic and Applied Sciences*, vol. 6, no. 6, pp. 337–352, 2012.

[55] L. Hsu, R. Ortega, and G. Damm, "A globally convergent frequency estimator," *IEEE Transactions on Automatic Control*, vol. 44, no. 4, pp. 698–713, 1999.

[56] D. Hush and N. Ahmed, "Detection and Identification of Sinusoids in Broadband Noise Via a Parallel Recursive Ale." *ICASSP, IEEE International Conference on Acoustics, Speech and Signal Processing - Proceedings*, pp. 1193–1196, 1985.

[57] N. Ahmed, D. Hush, G. R. Elliott, and R. J. Fogler, "Detection of Mutliple Sinusoids Using an Adaptive Cascaded Structure." *ICASSP, IEEE International Conference on Acoustics, Speech and Signal Processing - Proceedings*, vol. 2, no. 7, pp. 7–10, 1984.

[58] N. I. Cho, C. H. Choi, and S. U. Lee, "Adaptive Line Enhancement By Using An IIR Lattice Notch Filter," *IEEE Transactions on Acoustics, Speech, and Signal Processing*, vol. 37, no. 4, pp. 585–589, 1989.

[59] S. N. Mahmoodi, M. J. Craft, S. C. Southward, and M. Ahmadian, "Active vibration control using optimized modified acceleration feedback with Adaptive Line Enhancer for frequency tracking," *Journal of Sound and Vibration*, vol. 330, no. 7, pp. 1300–1311, 2011.

[60] K. Ohno and T. Hara, "Adaptive Resonant Mode Compensation for Hard Disk Drives," *IEEE Transactions on Industrial Electronics*, vol. 53, no. 2, pp. 624–630, 2006.

[61] H. Wang, D. H. Lee, Z. G. Lee, and J. W. Ahn, "Vibration rejection scheme of servo drive system with adaptive notch filter," *PESC Record - IEEE Annual Power Electronics Specialists Conference*, 2006.

[62] S. C. Fu and S. Cheng, "Analysis and suppression of torsional vibrations for the permanent magnet synchronous motor-load system," *Conference Proceedings - IEEE International Conference on Systems, Man and Cybernetics*, no. October, pp. 3359–3364, 2009.

[63] J. Levin, N. O. Pérez-Arancibia, and P. A. Ioannou, "Adaptive notch filter using real-time parameter estimation," *IEEE Transactions on Control Systems Technology*, vol. 19, no. 3, pp. 673–681, 2011.

[64] S. M. Yang and S. C. Wang, "The detection of Resonance frequency in motion control systems," *IEEE Transactions on Industry Applications*, vol. 50, no. 5, pp. 3423–3427, 2014.

[65] S. T. Wu, S. H. Lian, and S. H. Chen, "Vibration control of a flexible beam driven by a ball-screw stage with adaptive notch filters and a line enhancer," *Journal of Sound and Vibration*, vol. 348, pp. 71–87, 2015.

[66] K. H. Rew, S. Kim, I. Lee, and Y. Park, "Real-time estimations of multi-modal frequencies for smart structures," *Smart Materials and Structures*, vol. 11, no. 1, pp. 36–47, 2002.

[67] G. W. Colman and J. W. Wells, "On the use of RLS with covariance reset in tracking scenarios with discontinuities," *Canadian Conference on Electrical and Computer Engineering*, no. May, pp. 693–696, 2006.

[68] M. A. Hossain and M. O. Tokhi, "Evolutionary adaptive active vibration control," *Proceedings of the Institution of Mechanical Engineers. Part I: Journal of Systems and Control Engineering*, vol. 211, no. 3, pp. 183–193, 1997.

[69] M. K. Kwak and S. Heo, "Real-time multiple-parameter tuning of PPF controllers for smart structures by genetic algorithms," *Smart Structures and Materials 2000: Mathematics and Control in Smart Structures*, vol. 3984, no. June 2000, pp. 279–290, 2000.

[70] M. K. Kwak, S. Heo, and G.-J. Jin, "Adaptive positive-position feedback controller design for the vibration suppression of smart structures," *Smart Structures and Materials 2002: Modeling, Signal Processing, and Control*, vol. 4693, no. July 2002, pp. 246–255, 2002.

[71] R. Orszulik and J. Shan, "Multi-mode adaptive positive position feedback: An experimental study," *Proceedings of the American Control Conference*, pp. 3315–3319, 2011.

[72] R. R. Orszulik and J. Shan, "Active vibration control using genetic algorithm-based system identification and positive position feedback," *Smart Materials and Structures*, vol. 21, no. 5, 2012.

[73] X. Wang and B. Yang, "Transient vibration control using nonlinear convergence active vibration absorber for impulse excitation," *Mechanical Systems and Signal Processing*, vol. 117, pp. 425–436, 2019.

[74] T. Lobos and J. Rezmer, "Real-time determination of power system frequency," *IEEE Transactions on Instrumentation and Measurement*, vol. 46, no. 4, pp. 877–881, 1997.

[75] M. Blödt, M. Chabert, J. Regnier, and J. Faucher, "Mechanical load fault detection in induction motors by stator current time-frequency analysis," *IEEE Transactions on Industry Applications*, vol. 42, no. 6, pp. 1454–1463, 2006.

[76] F. Engels, P. Heidenreich, A. M. Zoubir, F. K. Jondral, and M. Wintermantel, "Advances in Automotive Radar: A framework on computationally efficient high-resolution frequency estimation," *IEEE Signal Processing Magazine*, vol. 34, no. 2, pp. 36–46, 2017.

[77] Q. Zhu, J.-Z. Yue, W.-Q. Liu, X.-D. Wang, and J. Chen, "Active vibration control for piezoelectricity cantilever beam: an adaptive feedforward control method," *Smart Materials and Structures*, vol. 26, no. 4, p. 47003, 2017.

[78] I. Santamaría, C. Pantaleón, and J. Ibañez, "Comparative study of high-accuracy frequency estimation methods," *Mechanical Systems and Signal Processing*, vol. 14, no. 5, pp. 819–834, 2000.

[79] H. Tjahyadi, F. He, and K. Sammut, "M4ARC: Multi-model-multi-mode adaptive resonant control for dynamically loaded flexible beam structures," *Smart Materials and Structures*, vol. 17, no. 4, 2008.

[80] M. I. Friswell and D. J. Inman, "Relationship between positive position feedback and output feedback controllers," *Smart Materials and Structures*, vol. 8, no. 3, pp. 285–291, 1999.

[81] G. Song, S. P. Schmidt, and B. N. Agrawal, "Experimental robustness study of positive position feedback control for active vibration suppression," *Journal of Guidance, Control, and Dynamics*, vol. 25, no. 1, pp. 179–182, 2002.

[82] D. V. B. Rao and S. Y. Kung, "Adaptive Notch Filtering for the Retrieval of Sinusoids in Noise," *IEEE Transactions on Acoustics, Speech, and Signal Processing*, vol. 32, no. 4, pp. 791–802, 1984.

[83] D. R. Hush, N. Ahmed, R. David, and S. D. Stearns, "An Adaptive IIR Structure for Sinusoidal Enhancement, Frequency Estimation, and Detection," *IEEE Transactions on Acoustics, Speech, and Signal Processing*, vol. ASSP-34, no. 6, pp. 1380–1390, 1986.

[84] T. Kwan and K. Martin, "Adaptive Detection and Enhancement of Multiple Sinusoids Using a Cascade IIR Filter," *IEEE Transactions on Circuits and Systems*, vol. 36, no. 7, pp. 937–947, 1989.

[85] A. Nehorai, "Minimal Parameter Adaptive Notch Filter With Constrained Poles and Zeros." *ICASSP, IEEE International Conference on Acoustics, Speech and Signal Processing - Proceedings*, p. 1185, 1985.

[86] K. Mayyas and F. Momani, "An LMS adaptive algorithm with a new step-size control equation," *Journal of the Franklin Institute*, vol. 348, no. 4, pp. 589–605, 2011.

[87] E. Omidi and S. N. Mahmoodi, "Multiple mode spatial vibration reduction in flexible beams using H2- and H∞ - Modified positive position feedback," *Journal of Vibration and Acoustics, Transactions of the ASME*, vol. 137, no. 1, pp. 1–7, 2015.

[88] F. Beltrán-Carbajal, G. Silva-Navarro, and L. G. Trujillo-Franco, "Evaluation of on-line algebraic modal parameter identification methods," in *Conference Proceedings of the Society for Experimental Mechanics Series*, vol. 8, no. 2508, 2014, pp. 145–152.

[89] L. G. Trujillo-Franco, G. Silva-Navarro, and F. Beltran-Carbajal, "On the modal parameters estimation in mechanical structures: A case study," in *14th International Conference on Electrical Engineering, Computing Science and Automatic Control (CCE)*, 2017.

[90] L. Garibaldi and S. Fassois, "MSSP special issue on the identification of time varying structures and systems," *Mechanical Systems and Signal Processing*, vol. 47, no. 1-2, pp. 1–2, 2014.

[91] R. R. Zhang, S. Ma, E. Safak, and S. Hartzell, "Hilbert-Huang Transform Analysis of Dynamic and Earthquake Motion Recordings," *Journal of Engineering Mechanics*, vol. 129, no. 8, pp. 861–875, 2003.

[92] D. Pines and L. Salvino, "Structural health monitoring using empirical mode decomposition and the Hilbert phase," *Journal of Sound and Vibration*, vol. 294, no. 1-2, pp. 97–124, 2006.

[93] M. Simon and G. R. Tomlinson, "Use of the Hilbert transform in modal analysis of linear and non-linear structures," *Journal of Sound and Vibration*, vol. 96, no. 4, pp. 421–436, 1984.

[94] I. Collins, "Phase-Locked Loop (PLL) Fundamentals," *Analog Dialogue*, vol. 52, 2018.

[95] M. Algrain, S. Hardt, and D. Ehlers, "A phase-lock-loop-based control system for suppressing periodic vibration in smart structural systems," *Smart Materials and Structures*, vol. 6, no. 1, pp. 10–22, 1997.

[96] M. A. McEver and D. J. Leo, "Adaptive low-authority control algorithms for precision space structures," in *AIAA Space Technology Conference & Exposition*, 1999.

[97] J. B. Tan, Y. Liu, L. Wang, and W. G. Yang, "Identification of modal parameters of a system with high damping and closely spaced modes by combining continuous wavelet transform with pattern search," *Mechanical Systems and Signal Processing*, vol. 22, no. 5, pp. 1055–1060, 2008.

[98] A. Klepka and T. Uhl, "Identification of modal parameters of non-stationary systems with the use of wavelet based adaptive filtering," *Mechanical Systems and Signal Processing*, vol. 47, no. 1-2, pp. 21–34, 2014.

[99] T. M. Adami, R. Sabala, and J. J. Zhu, "Time-varying notch filters for control of flexible structures and vehicles," *AIAA/IEEE Digital Avionics Systems Conference - Proceedings*, vol. 2, pp. 3–8, 2003.

[100] Z. Qiu, C. M. Lee, Z. H. Xu, and L. N. Sui, "A multi-resolution filtered-x LMS algorithm based on discrete wavelet transform for active noise control," *Mechanical Systems and Signal Processing*, vol. 66-67, pp. 458–469, 2016.

[101] PiezoDrive, "Dual Channel Drivers for Piezo Bender Actuators," pp. 1–12, 2021. [Online].

[102] J. Karki, "Signal Conditioning Piezoelectric Sensors," Tech. Rep., 2000. [Online].

Appendix A

Frequency Estimation Methods

A.1 Parametric System Identification

The least-squares regression analysis method can be used effectively for parameter estimation if the system model is linear in its parameters. The regression model is:

$$\hat{y}(i) = \phi_1(i)\theta_1 + \phi_2(i)\theta_2 + ... + \phi_n(i)\theta_n = \phi^T(i)\theta \tag{A.1}$$

where y is the measured variable, θ are the model parameters to be determined, and ϕ are regressors, which are known functions that may depend on other known variables. Note that the regressors used in the model should be appropriately chosen to prevent underfitting or overfitting of data. The model is indexed by i which represents discrete time. Parameters are estimated by determining the values that minimize the difference between the measured output and the estimated output (computed using Equation A.1). The cost function to be minimized is:

$$V(\theta,t) = \frac{1}{2}\sum_{i=1}^{t}(y(i) - \phi^T(i)\theta)^2 = \frac{1}{2}E^T E \tag{A.2}$$

where the term inside the brackets is the squared residual (error) between the estimated and the measured output. If $\Phi^T\Phi$ is nonsingular, the solution to the least squares problem is given by:

$$\hat{\theta} = (\Phi^T\Phi)^{-1}\Phi^T Y = P(t)\Phi^T Y \tag{A.3}$$

where $\Phi = \begin{bmatrix}\phi^T(1) & \phi^T(2) & ... & \phi^T(t)\end{bmatrix}^T$ and $Y = \begin{bmatrix}y(1) & y(2) & ... & y(t)\end{bmatrix}^T$.

For adaptive control purposes, the estimation can be done recursively (RLS) by using the estimate at the previous time step to predict the next estimate:

$$\hat{\theta}(t) = \hat{\theta}(t-1) + K(t)\varepsilon(t) \tag{A.4}$$

where $K(t)$ is related to the regressors and $\varepsilon(t) = y(t) - \phi^T(t)\hat{\theta}(t-1)$ is the error in predicting the signal $y(t)$ one step ahead based on the estimate $\hat{\theta}(t-1)$. This gives an intuitive estimate update as it depends on the previous estimate plus a correction term related to the error.

If the parameters are time-varying, several methods can be used to enhance estimation depending on the nature of the variation. If the parameters change suddenly, $P(t)$ from Equation A.3 can be periodically reset to αI where α is a large multiplier and I is the identity matrix. This causes $K(t)$, which describes the step size in Equation A.4, to become large in order to adapt to abrupt changes in the system. If the parameters change slowly over time, a forgetting factor λ may be used to weigh the relative importance between past and present errors. The cost function in this case is:

$$V(\theta,t) = \frac{1}{2}\sum_{i=1}^{t} \lambda^{t-i} e^2(i)(y(i) - \phi^T(i)\theta)^2 \tag{A.5}$$

where λ is between 0 and 1. When λ is 1, all previous errors are equally considered. As λ approaches 0, past errors play a smaller role. A smaller value makes the algorithm more adaptable to changes, but more sensitive to noise as well.

To summarize, RLS is an adaptive filter algorithm used to recursively determine the filter coefficients that minimize a cost function such as the one given in Equation A.5. This concept can be used to identify systems in real time. A linear dynamical system can be represented as an auto regressive moving average (ARMA) model:

$$H(z^{-1}) = \frac{B(z^{-1})}{A(z^{-1})} = \frac{b_1 z^{-1} + b_2 z^{-2} + ... b_{2p} z^{-2p}}{1 + a_1 z^{-1} + a_2 z^{-2} + ... + a_{2p} z^{-2p}} \tag{A.6}$$

where $A(z^{-1})$ describes the AR part, $B(z^{-1})$ describes the MA part, and p is the number of modes to be estimated. Since the denominator contains information about the natural frequencies, estimation of only the AR part is required. This can be restructured into the form given by Equation A.1 by defining the regressor $\phi(i)$ and estimated parameter vector $\theta(i)$ as:

$$\phi(i) = \begin{bmatrix} -y(i-1) & -y(i-2) & ... & -y(i-2p) \end{bmatrix}^T \tag{A.7}$$

$$\theta(i) = \begin{bmatrix} a_1(i) & a_2(i) & ... & a_{2p}(i) \end{bmatrix}^T \tag{A.8}$$

Then an RLS adaptive filter is implemented to find the parameters that minimize Equation A.5. Note that this only utilizes the output measurement y, which is suitable for the active damping problem where no disturbance information is available. The model order must be set in advance, and simple inputs like step inputs may not be enough for accurate identification. In order to obtain the p natural frequencies from the resulting characteristic equation $A(z^{-1})$, it must be decoupled into second order equations. This can be done numerically with a root-finding algorithm.

$$A(z^{-1}) = 1 + a_1 z^{-1} + a_2 z^{-2} + ... + a_{2p} z^{-2p} = z^{-2p} \prod_{k=1}^{p} (z^2 + p_k z + q_k) \tag{A.9}$$

An alternative method to root-finding is to pre-filter the structure's output signal y to decouple it into different modal components before using it in the estimation block. Each component of the separated signal can then be used to estimate individual second-order models corresponding to different modes, and the mode frequencies can be obtained analytically instead of numerically [79]. Regardless of the approach used, the estimated natural frequencies can then be obtained from the decoupled characteristic equation coefficients:

$$\hat{\omega}(k) = \frac{1}{T_s} cos^{-1}(-p_k / 2\sqrt{q_k}) \tag{A.10}$$

A.2 Phase Locked Loop

A phase locked loop (PLL) generates an output signal with a frequency equal or related to the frequency of the input signal. More precisely, the PLL controls the phase of its output signal in such a way that the phase error between the signals reduces to a minimum. Keeping the input and output phase in lock results in equal input and output signal frequencies.

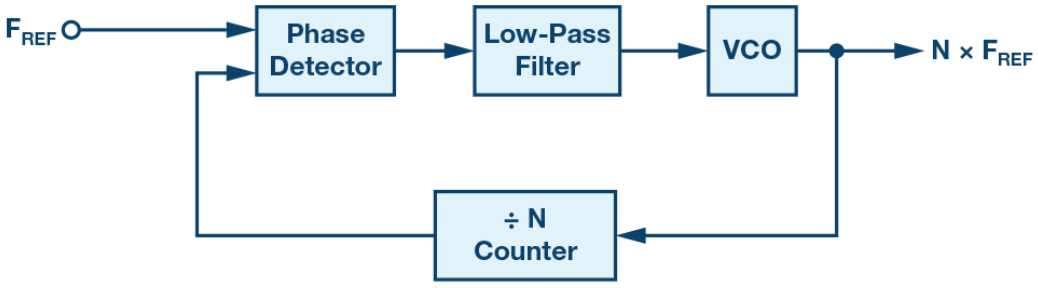

Figure A.1: Phase locked loop block diagram [94].

The components of a basic PLL are:

- **Phase detector.** Compares the output frequency with a reference frequency and generates an error signal. This is usually a multiplier which outputs two components:

$$V_i V_o = A_i sin(\omega_i t + \phi_i) \times A_o sin(\omega_o t + \phi_o) = \\ \frac{A_i A_o}{2} [cos((\omega_i - \omega_o)t + \phi_i - \phi_o) - cos((\omega_i + \omega_o)t + \phi_i + \phi_o)] \tag{A.11}$$

  The first component is a low frequency oscillating term proportional to the angular $(\omega t + \phi)$ difference between the signals, and the second component is a high frequency oscillating term. In digital implementations of the PLL, a phase frequency detector can be used for the same purpose [94].

- **Loop filter.** This is usually a low pass filter that eliminates the high frequency component generated by the phase detector in Equation A.11. This leaves the component proportional to the angular difference between the signals. In the case where $\omega_i = \omega_o$, this term becomes a DC offset proportional to the phase difference.

- **Voltage controlled oscillator (VCO).** The VCO produces an output whose instantaneous frequency depends on the input voltage (which is proportional to the angular difference). The VCO increases the output frequency if there is a positive angular difference and decreases the frequency if there is a negative angular difference between the signal. When the loop is just turned on, the VCO outputs a predetermined center frequency (called the free-running or quiescent frequency).

By feeding back the VCO output to the phase detector, the phase error tends to drive the PLL into a steady state locked condition with zero frequency error and finite phase error. The VCO eventually outputs a frequency that is equal to the reference frequency.

PLLs can be treated like any feedback loop, where different component parameters define the transient response, bandwidth, and steady-state error in the output. There are also two additional properties of importance:

- **Lock range.** This is the range of input frequencies over which the loop remains in the lock condition once it has captured the input signal. This depends on the VCO gain.

- **Capture range.** This is the range of input frequencies around the VCO center frequency onto which the loop can lock when starting from the unlocked condition. If the reference frequency is outside the capture range then the PLL can't lock to it. This range is usually smaller than the lock range and depends on the low pass filter's cut-off frequency.

With PLLs, some knowledge about the frequency content must be known a priori in order to set suitable values for the capture range and lock range, and the various components (loop filter, VCO) must be tuned accordingly.

PLL in AVC:

- Algrain et al. [95] track the frequencies of periodic disturbances with a PLL and use the estimates to tune an analog bandpass filter for disturbance attenuation. It is possible to extend this method for tracking multiple frequency components using multiple PLLs and bandpass filters, but some knowledge of each component's frequency range must be known beforehand.

- Leo and Griffin [32] use a PLL to identify the frequency of a single structural mode during transient vibrations. The PLL is able to track changes in the frequency of a mode within a small variation range. The estimate is then used to tune a PPF filter for controlling a flexible beam.

- McEver and Leo [96] further test the PLL and PPF combination in the case of broadband excitations, showing that the Signal to Noise Ratio (SNR) determines whether the PLL will lock onto the target frequency or not. Since the presence of higher frequency modes with large amplitudes reduces the SNR when tracking a single frequency, the PLL fails to lock onto the target mode.

In conclusion, the PLL is effective at tracking a signal's frequency and locking onto it as it varies, as long as the signal remains within the lock range and the SNR is not too low. This makes it a simple and recommended method for tracking a single dominant mode of a structure. However, it cannot be used to track multiple modes without additional PLLs and filtering (e.g., modal filters). In addition, there are many parameters to assign that demand partial knowledge of the frequency range of the signal, which might not always be available.

A.3 Short-Time Fourier Transform

The Fourier transform cannot be used for real-time frequency estimation of non-stationary signals because it does not provide temporal information about the frequency components. Time-frequency analysis methods were thus developed to overcome this issue. This class of methods constitute a non-parametric approach for identifying systems using their frequency spectra.

The short-time Fourier transform (STFT) considers small portions of the non-stationary signal as stationary. The fast Fourier transform (FFT) is then performed on each stationary

portion along the signal to obtain its frequency spectrum as a function of time. To do this, a window function of fixed length is moved along the signal from start to end and an FFT is taken at each stationary section. The window function is zero-valued outside its given interval. When the waveform is multiplied by the window function, the overlap between them is included while the rest of the signal is not considered.

The STFT equation is shown below. It includes the window function $w(t-\tau)$ and a translation parameter τ which translates the window through time. Compared to the regular Fourier transform, the only new component is the window function. This gives the desired time localization property and the transform becomes a function of both frequency and time.

$$F(\tau,\omega) = \int_{-\infty}^{+\infty} f(t)w(t-\tau)e^{-i\omega t}dt \tag{A.12}$$

Figure A.2a shows a periodic signal that changes in frequency from 10 Hz to 50 Hz then back to 10 Hz. The STFT method divides it into portions denoted by the red dashed lines, such that the frequency estimated from each portion is constant. Figure A.2b shows the STFT spectrogram of the signal, which gives the frequency spectrum as it varies with time. After obtaining the spectrum, an algorithm such as peak picking can be used to obtain the mode frequencies.

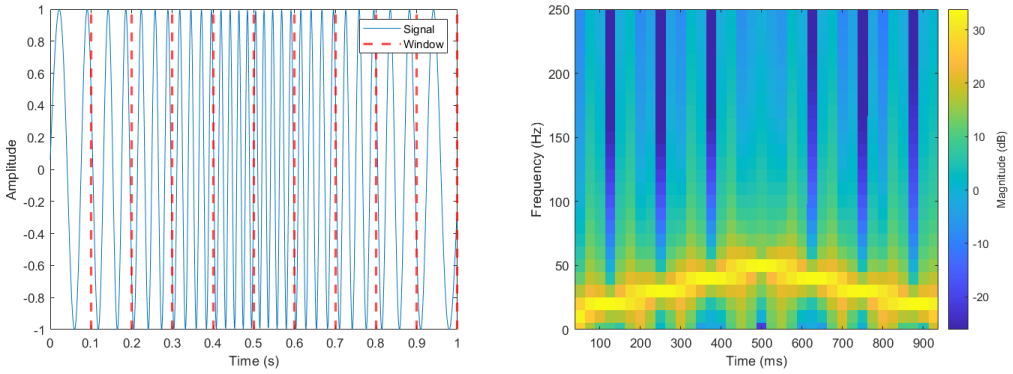

(a) Signal. (b) STFT spectrogram.

Figure A.2: STFT spectrogram of a periodic signal with time-varying frequency.

The Gabor limit, based on the Heisenberg uncertainty principle, shows that localization in both time and frequency cannot be achieved, and that one resolution comes at the cost of the other:

$$\Delta t \Delta f \geq \frac{1}{4\pi} \tag{A.13}$$

The choice of window function depends on the desired frequency resolution (ability to resolve similar frequencies), dynamic range (ability to resolve dissimilar amplitudes), and

sensitivity to noise. Windows that balance between these properties include the Hann and Hamming windows.

FFT methods have a computational complexity of the order $O(Nlog(N))$. There are several improvements on the FFT method that increase the accuracy of the estimate and can separate sinusoids more closely spaced than the resolution limit (superresolution), but these also increase the computational cost [78].

A.4 Wavelet Transform

It is not possible to know which frequencies exist at different time instances as shown by Equation A.13, but it is possible to know which frequency bands exist at different time intervals. Low frequency components have long time periods, so a good frequency resolution (poor time resolution) should be used. High frequency components appear as short bursts, necessitating a good time resolution (poor frequency resolution).

The wavelet transform (WT) uses this principle to overcome the limitations of STFT by analyzing a signal with different frequencies at different resolutions. This is known as multiresolution analysis. It offers simultaneous localization in the time and frequency domains. Figure A.3 compares between the temporal and spectral resolutions of STFT and WT. In STFT, the resolution is fixed in size, so it is not possible to enhance the estimation based on the signal frequencies. In WT, as the frequency increases, the time resolution is improved.

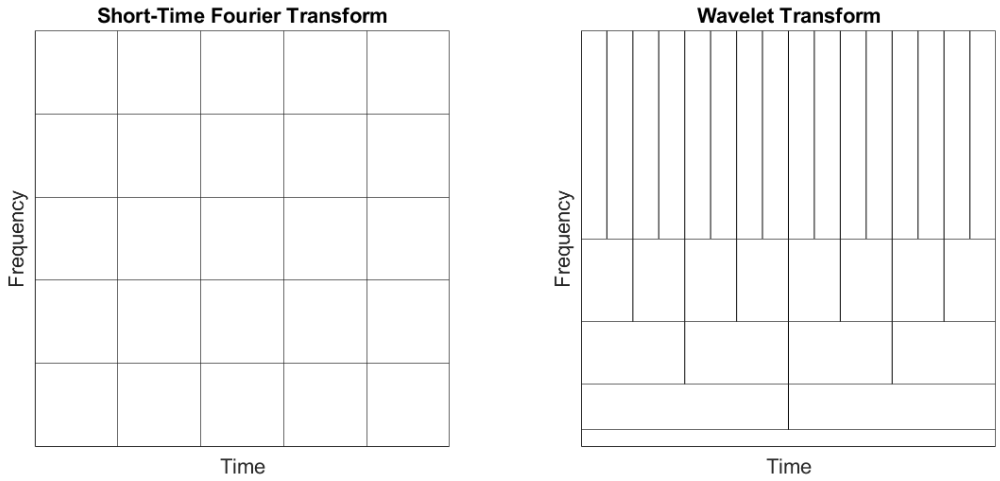

Figure A.3: STFT and WT resolution grids.

The basis functions used in the Fourier transform are sines and cosines. In WT, wavelets are used as both the basis functions and act as window functions. An example of a wavelet is the Morlet wavelet shown in Figure A.4.

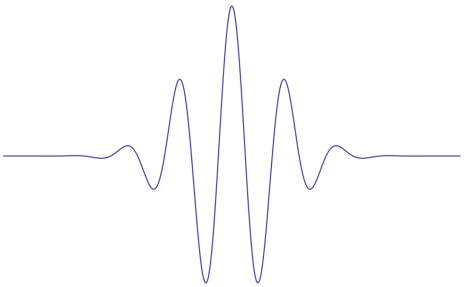

Figure A.4: Morlet wavelet.

The continuous wavelet transform (CWT) replaces the exponential term in FT by a wavelet $\psi(t)$.

$$F(\tau,s) = \frac{1}{\sqrt{|s|}} \int_{-\infty}^{+\infty} f(t)\psi^* \left(\frac{t-\tau}{s}\right) dt \tag{A.14}$$

where s is the inverse of frequency, and is used to change the width of the wavelet and its central frequency as it passes across a signal (scaling). This gives WT its multiresolution property as it is able to resolve both high and low frequency components with good resolution. Expanded wavelets can better resolve low frequency components, while shrunken wavelets are better for resolving high frequency components.

Figure A.5: Wavelet scaling.

All the windows used are thus dilated, compressed, shifted versions of the mother wavelet $\psi(t)$. The scaled wavelets are each multiplied by the signal to obtain a spectrogram relating frequency, time, and amplitude. Calculating wavelet coefficients at every possible scale produces a lot of data. If s and τ are chosen to be discrete then the WT will generate less data. If they are based on powers of 2 (dyadic), then analysis becomes much more efficient and accurate.

WT offers the following advantages over STFT:

- Faster computation than the Fourier transform. The computational complexity is $O(N)$.
- Simultaneous localization in time and frequency domains.
- Can separate finer details in a signal.

One disadvantage is that the choice of wavelet basis function affects the estimation performance, as it must closely match the data. In general, WT works very well when analyzing known non-sinusoidal shapes such as heartbeats.

Tan et al. [97] propose a method that improves the time period for modal identification with CWT. This is done by correcting the results with a pattern search error minimization algorithm. The resulting method can obtain accurate estimates of the frequency, damping ratio, amplitude, and phase of multiple highly damped and closely spaced modes, and requires shorter sampling periods than the classical CWT method. The proposed method was applied experimentally on an optical vibration isolation platform with 2 modes separated only by 1 Hz. The improved method reduces the sampling time by 70% while maintaining accurate estimates.

Klepka and Uhl [98] use CWT to separate signals into their components for easier system identification with RLS. The CWT bandwidth is updated according to the RLS frequency estimates. The decoupled second-order equations are then used to analytically determine the parameters (as opposed to [48], which uses RLS and a numerical root-finding algorithm to decouple the equations).

WT methods have seen little, if any, implementation in AVC. Relevant cases include the use of WT in simulations to estimate mode frequencies and tune adaptive notch filters [99], as well as implementation of WT in FxLMS-based ANC [100].

Appendix B

Experimental Setup

The experimental setup used to test the adaptive damping method consists of a flexible beam with piezoelectric transducers. The various components are shown and labeled in Figure 3.22, and a block diagram of the overall control system is shown in Figure 3.23.

B.1 Cantilever Beam

The structure used for damping is a cantilever aluminium beam that is oriented vertically and clamped at one end (see Figure 3.21). Due to its flexibility, the beam exhibits multiple lightly damped resonance modes in a suitable frequency range for testing the adaptive method. The parameters of the beam are given by Table 3.2.

B.2 Piezoelectric Transducers

For active damping control, P-876.A12 DuraAct patch transducers are used for both actuation and sensing, with actuator-sensor pairs situated in collocated layouts at opposite sides of the beam. For the experimental tests in this thesis, the collocated pair near the base of the beam was used. A patch consists of a piezoceramic plate, electrodes, and a polymer coating that provides electrical insulation and mechanical preload. The patches are attached to the beam using epoxy glue, and have soldering points for voltage connections. Table B.1 summarizes the specifications of the patch transducers.

In addition, a PiezoDrive SA050520 piezoelectric stack actuator, as shown in Figure B.1, is used to generate disturbances at the base of the beam, including pulse disturbances for generating transient structural responses. The specifications of the stack actuator are provided in Table B.2.

Table B.1: Piezoelectric patch transducer specifications.

Specification	Value
Dimensions (mm × mm × mm)	$61 \times 35 \times 0.5$
Operating voltage range (V)	-100 to 400
Min. lateral contraction (µm/m)	650
Rel. lateral contraction (µm/m/V)	1.3
Blocking force (N)	265
Min. bending radius (mm)	20
Capacitance (nF)	$90 \pm 20\%$
Piezoceramic height (µm)	200

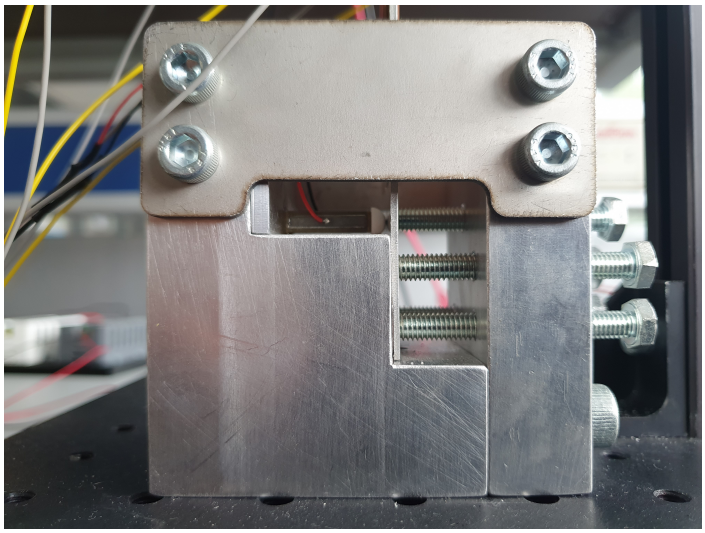

Figure B.1: Beam clamp and piezoelectric stack actuator.

Table B.2: Piezoelectric stack actuator specifications.

Specification	Value
Length (mm)	20
Cross section (mm × mm)	5×5
Operating voltage range (V)	-30 to 150
Range (µm)	$31 \pm 10\%$
Blocking force (N)	900
Capacitance (µF)	$1.8 \pm 20\%$
Resonance frequency (kHz)	74 kHz

Special care must be taken when using piezoelectric stack actuators. High tensile loads, unequally distributed and off-axis loads, bending moments, and torque should all be avoided.

In this setup, a ball end is attached to the end of the stack interfacing with the beam to improve the loading conditions. The stack actuator should also be preloaded, particularly if it is used in tensile operation. This is achieved in this case by tightening a screw against the stack.

B.3 Amplifiers

B.3.1 Actuator Drivers

PiezoDrive BD-300 amplifiers (shown in Figure B.2) were used to obtain the high voltage signals required to drive the piezoelectric patch and stack actuators. The specifications of the amplifier are shown in Table B.3.

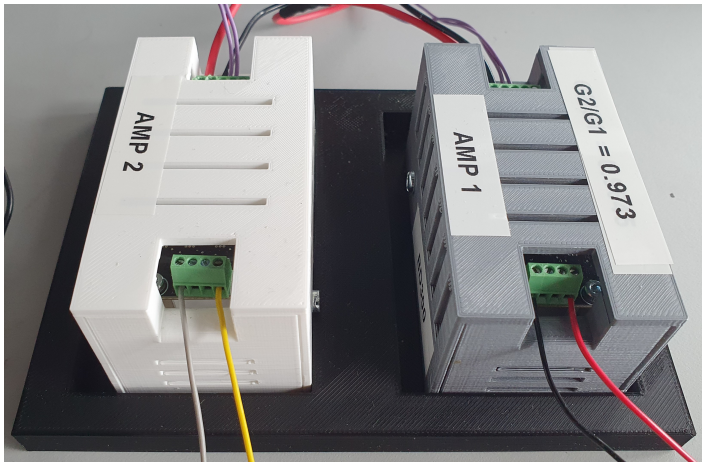

Figure B.2: BD-300 amplifiers.

Table B.3: BD-300 amplifier specifications.

Specification	Value
Supply voltage (V)	12-30
Input voltage range (V)	0-3
Input impedance (kΩ)	5-10
Output voltage (V)	300
Differential output (V)	± 300
Gain	101
Peak current (mA)	50
RMS current (mA)	11
Small signal bandwidth (kHz)	20

Figure B.3 shows the wiring diagram of the amplifier for driving a piezoelectric patch bender. The same configuration is used to drive the stack actuator as well. A 0-3 V input can be used to provide a ± 300 V output range, with a 1.5 V input corresponding to a 0 V output. Note that both actuators must be driven using their provided operating voltage ranges, which are both well within the amplifier output range.

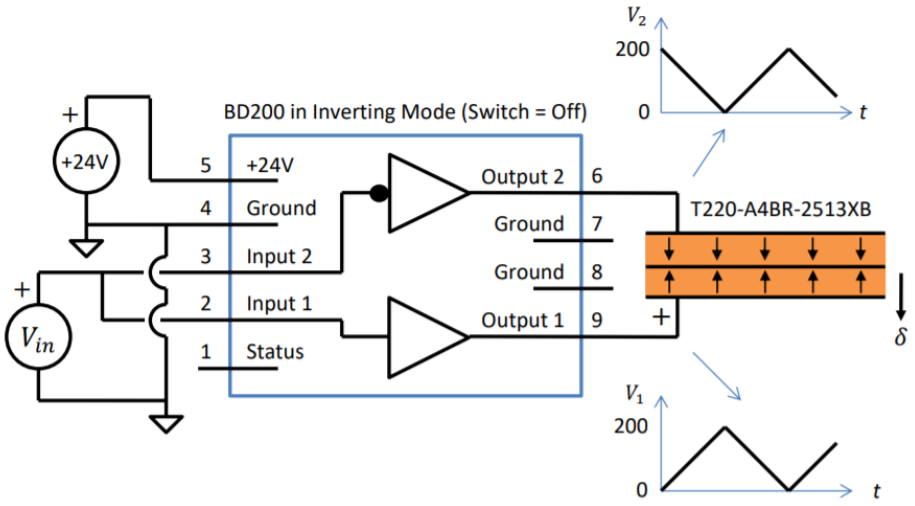

Figure B.3: BD-300 wiring diagram for a piezoelectric bender [101].

B.3.2 Charge Amplifier

A simple charge amplifier circuit was also used to condition the measurement signal of the piezoelectric patch sensor. The main function is to produce a suitable voltage output proportional to the charge of the sensor by integrating the generated current. The charge amplifier circuit is beneficial in this experimental setup for a variety of reasons:

- It enables quasi-static measurements and generally improves low frequency measurements.
- The amplifier gain is determined by a feedback capacitor. As a result, scaling the measurement is simplified for testing purposes, which is important for data acquisition purposes as discussed in Sections B.4 and B.6.
- Components with capacitance parallel to the sensor (e.g., cables) can introduce disturbances. The charge amplifier negates this effect.
- Measurement drift is prevented. In contrast, drift was observed in the absence of signal conditioning circuitry.

A circuit diagram of the charge amplifier is shown in Figure B.4. An operational amplifier (OP497) is used with a feedback capacitor (C_f) for integration. A feedback resistor (R_f) in parallel with the capacitor provides a discharge path to prevent saturation. In addition, an input resistor (R_i) is used to protect against electrostatic discharge. Table B.4 presents the circuit parameters used in this thesis.

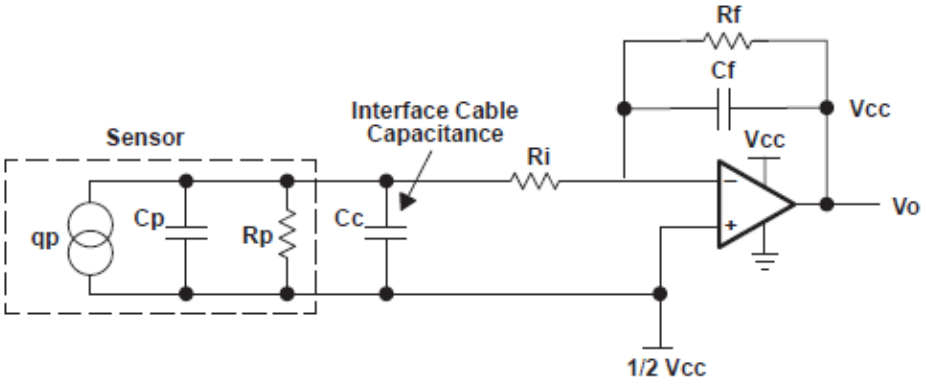

Figure B.4: Charge amplifier circuit [102].

Table B.4: Charge amplifier specifications.

Specification	Value
Supply voltage (V)	$\pm$ 10
Feedback resistance R_f (MΩ)	1
Feedback capacitance C_f (nF)	82
Input resistance R_i (Ω)	100

The transfer function between the charge of the sensor and the amplifier voltage output is:

$$\frac{V_o}{Q} = -\frac{R_f s}{(R_f C_f s + 1)(R_i(C_p + C_c)s + 1)} \tag{B.1}$$

The two poles of the transfer function are $\omega_1 = 1/R_f C_f$ and $\omega_2 = 1/R_i(C_c + C_p)$, and the gain at the flat frequency band is determined by $1/C_f$. The Bode plot is shown in Figure B.5. The lower cutoff frequency is around 2 Hz and the flat region gain was selected to appropriately scale the measurement signal for the data acquisition system described in Section B.4. The effects of the charge amplifier on the collocated beam transfer function are shown in Section B.6.

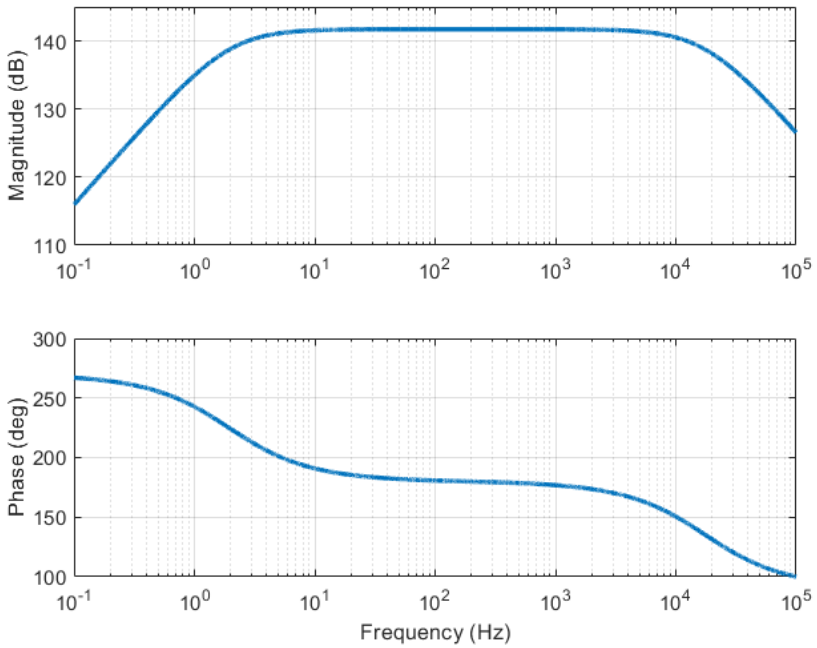

Figure B.5: Bode plot of the charge amplifier transfer function.

B.4 Microcontroller

The Texas Instruments C2000 Delfino MCU F28379D LaunchPad™ is used to implement the control method. It is an evaluation and development tool with a TMS320F28379D MCU and 80 pin connections. The MCU offers 200 MHz dual-core 32-bit CPUs with single-precision floating point, trigonometric, and complex math units, as well as two programmable control law accelerators which execute code independently of the CPUs. The MCU also provides 1 MB of flash memory, 16-bit or 12-bit ADCs, comparators, 12-bit DACs, and numerous other features and additional components for extending its functionality. The development board provides connections to 4 ADCs, 2 DACs, and various digital pins.

The experimental setup utilizes the 2 available 12-bit DACs to send the control and disturbance signals for amplification and actuation with the piezoelectric patch and stack actuators. In addition, one 16-bit ADC module with differential inputs is used to convert the piezoelectric sensor measurements fed through the charge amplifier. The differential input type uses 2 pins of a single ADC module to measure a differential signal, making it suitable for piezoelectric sensor measurements. The input voltage to each pin of the ADC must remain within 0-3 V, and should therefore be scaled using the feedback capacitance of the charge amplifier. Ideally, the full scale voltage range of the ADC should be utilized to maximize usage of the available resolution. At the same time, the ADC input signal should

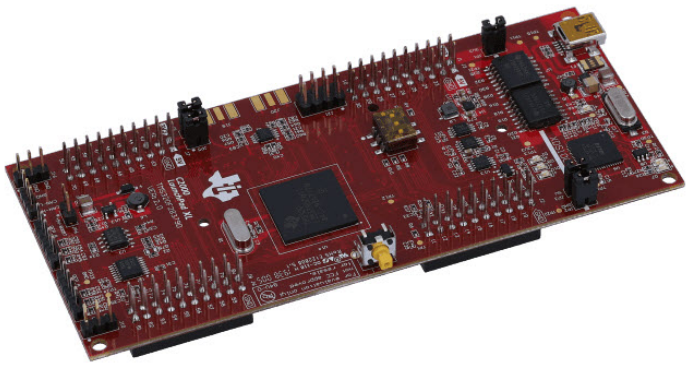

Figure B.6: F28379D development board.

be saturated at a certain voltage (e.g., by using a Zener diode) to prevent unintended ADC or MCU damage.

Compared to conventional data acquisition, monitoring, and control applications like the CompactRIO from NI, the TI Launchpad provides several advantages:

- It is a low-cost and portable testing tool.
- Code for the MCU can be generated using Matlab and Simulink embedded coder packages, making it incredibly easy to convert simulations from Simulink into code used for experimental testing with only slight modifications. An additional benefit is the availability of a vast amount of Matlab libraries, packages, and Simulink blocks that significantly simplify code generation for complex methods. Note that these functions and blocks should operate in discrete time.
- Monitoring and acquiring experimental data can be done simply through Simulink output blocks, or more preferably, the Data Inspector tool.
- Building and uploading code to the MCU is quite fast, which can be useful if the experiment requires many test runs with code adjustments in between.
- The MCU has numerous features which were not explored in this thesis, including the control law accelerators, enhanced pulse width modulation, and real-time parameter tuning.

Disadvantages of using the Launchpad and similar kits include:

- Low number of ADCs and DACs for I/O interfacing. Experiments that require many sensors can be implemented in a limited manner using sequential ADC inputs.

- Relatively limited input voltage range. Signal conditioning is thus required to prevent damages to the ADC and controller.
- Possibly insufficient processing speed for computationally complex applications.

In conclusion, the choice of hardware for control testing mostly depends on the computational and I/O requirements of the method, as well as personal preferences in regard to flexibility, portability, and the software used for code generation and monitoring (unless the code is manually written).

B.5 Code Generation and Monitoring with Simulink

This section serves as a basic guide for using the Simulink Embedded Coder Support Package for Texas Instruments C2000 processors. MathWorks documentation for setting up and using the package is readily available. The primary goal of this section is to use thesis examples to show the basic process and provide practical tips.

Once the packages are installed, the Simulink blocks used to interface with the controller should be available to use. The first step is to apply model and hardware settings using the 'Configuration Parameters' menu. This can be accessed from the main Simulink window by going to the 'Modeling' tab and selecting 'Model Settings'. In 'Configuration Parameters', under the 'Solver' tab, a fixed step size should be used with a suitable sample time and a discrete solver. The start and stop times of the test can also be set in this tab. Note that in some cases, monitoring may start late in the test run after the code is uploaded to the board, in which case a delay in the start time can be useful.

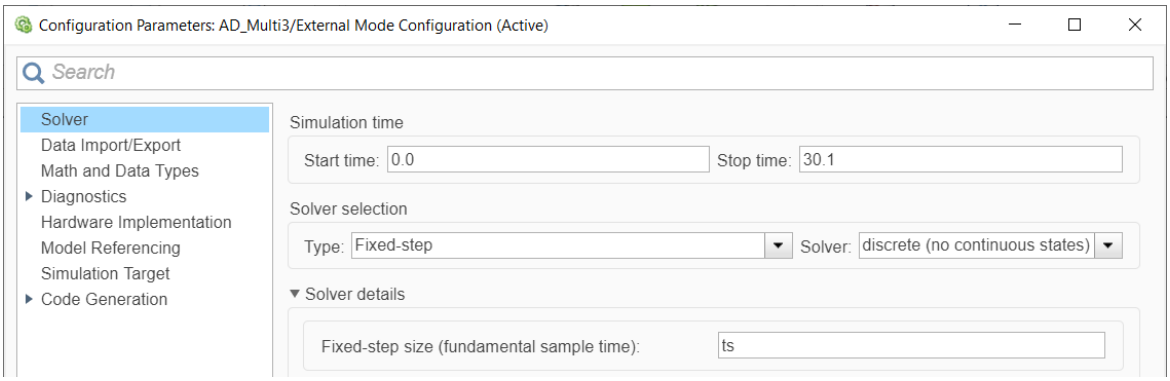

Figure B.7: Simulink solver settings for MCU code generation.

In the 'Configuration Parameters' menu, select the 'Hardware Implementation' tab. Here, the appropriate type of board should be selected. Under 'Hardware board settings', in the

'Build options' group, the 'Boot from flash' option should be checked in case the default memory provided by the MCU is not enough for the application. Next, go to the 'External mode' group and select the 'serial (using xcp)' communication interface. This enables data logging and monitoring with Simulink using the Data Inspector tool, which can also be used to export data to Matlab for processing.

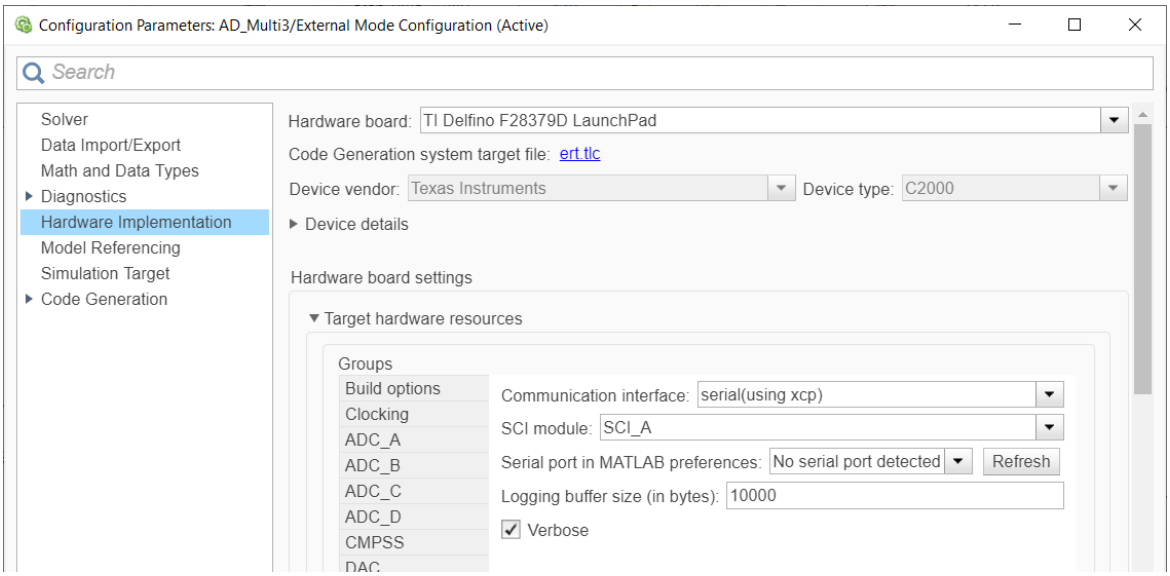

Figure B.8: Simulink hardware implementation settings for MCU code generation.

The model shown in Figure B.9 is a simple example of using a general purpose input/output (GPIO) pin. This was used to turn an LED on at the 8 second mark using a digital clock and a conditional switch. Note that in general, all blocks should operate in discrete time and as continuous alternatives will not be accepted by the code generator. Another thing to consider is to set all generated signal data types to 'single' in the 'Signal Attributes' tab found in the 'Block Parameters' menu for each block. since the processor operates with single precision. This has to be done for source blocks but not other blocks as they inherit the data type by default. An easy way to debug data types is by going to 'Debug' tab in the main Simulink window and selecting 'Base Data Types' under 'Information Overlays'. Finally, after connecting the LED to a GPIO pin on the board and ground, and selecting the corresponding GPIO number in the GPIOx block parameters menu, you can run the model by going to the 'Hardware' tab in the main Simulink window and selecting 'Monitor & Tune'. After the code has finished building and uploading, the LED should hopefully turn on after 8 seconds.

Next, Simulink implementation of the adaptive damping method for code generation is shown in Figure B.10. This is in many ways similar to the adaptive control loop shown in

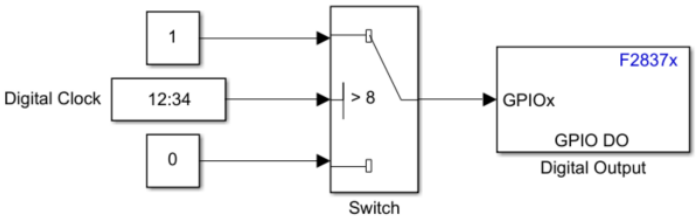

Figure B.9: Basic LED Simulink model.

Figure 2.13. Here, only 3 blocks are used to interface with the controller: 1 ADC block and 2 DAC blocks.

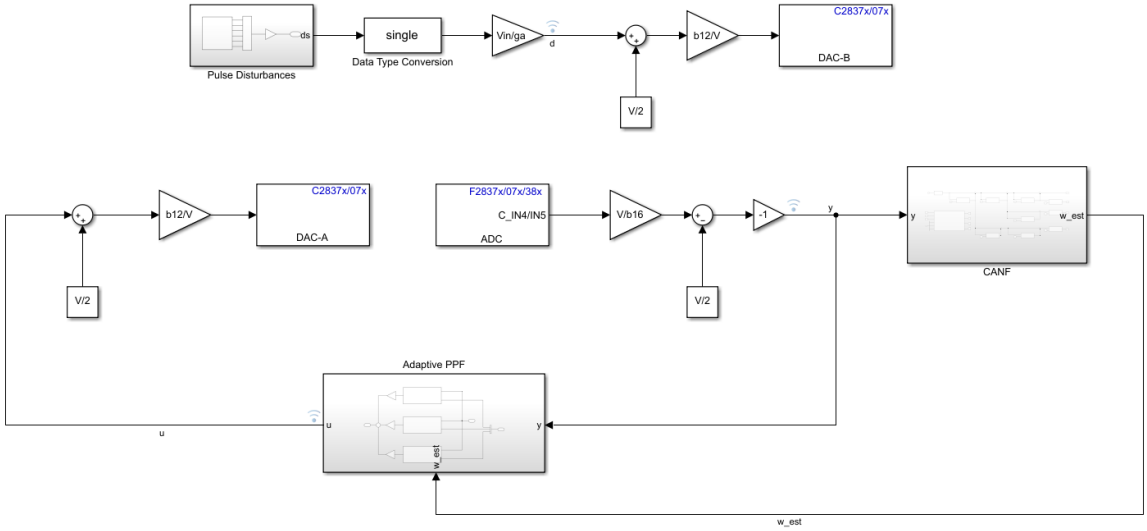

Figure B.10: Adaptive damping Simulink model.

In the top block group, a discrete disturbance signal is generated, converted to single data type, and multiplied by a gain value with V_{in} representing the desired input voltage to the stack actuator and ga representing the amplifier gain. The disturbance signal d is then logged by clicking on the signal path, selecting the 'Signal' tab from the main toolbar, and selecting 'Log Signals'. Logged signals can be monitored using the Data Inspector under the 'Hardware' tab. The disturbance is then offset by 1.5 V to ensure that a 0 V disturbance yields a 0 V amplifier output, and finally the disturbance voltage V_d is converted to bits. For the 12-bit DAC, this is done with the following equation:

$$b_d = V_d \frac{b_{12}}{V_{max}} = V_d \frac{2^{12}\ bits}{3\ V} \tag{B.2}$$

In the bottom block group, the same process is repeated for the control force signal sent from the PPF controller to the other DAC. Through the block parameters menu, the appropriate DAC channel can be selected corresponding to the pin connections. The DACs can also be forced to saturate on input overflow in case the input exceeds 3 V, which is definitely a safer option.

A 16-bit ADC with differential inputs is used to convert the conditioned sensor signal. The ADC module, resolution, sampling time, and input channels corresponding to the pin connections are all set inside the block parameters menu of the ADC. The measurements in bits are converted to volts and an offset is applied similarly to the DAC signals. The -1 gain is only required here because the sensor to ADC connections were physically flipped. The output measurement is then available for estimation and control.

Another important consideration is the implementation of discrete adaptive filters for PPF. A discrete time varying transfer function Simulink block can be used for this purpose with coefficient inputs obtained using the bilinear (Tusin) transform with a sampling period t_s:

$$s = \frac{2}{t_s}\frac{z-1}{z+1} \tag{B.3}$$

For the continuous second-order low pass filter used in PPF:

$$L(s) = \frac{\omega_f^2}{s^2 + 2\omega_f\zeta_f s + \omega_f^2} \tag{B.4}$$

The discretized transfer function using Equation B.3 is:

$$L(z) = \frac{\frac{\omega_f^2 t_s^2}{\omega_f^2 t_s^2 + 4 + 4\omega_f\zeta_f t_s}(1 + 2z^{-1} + z^{-2})}{1 + (\frac{2\omega_f^2 t_s^2 - 8}{\omega^2 t_s^2 + 4 + 4\omega_f\zeta_f t_s})z^{-1} + (\frac{\omega_f^2 t_s^2 + 4 - 4\omega_f\zeta_f t}{\omega_f^2 t_s^2 + 4 + 4\omega_f\zeta_f t_s})z^{-2}} \tag{B.5}$$

Figure B.11 shows the contents of the 'Adaptive PPF' block from Figure B.10. Figure B.11a shows the Simulink model of 3 PPF filters in parallel for damping 3 modes, and Figure B.11b shows the block diagram of a single adaptive PPF filter in discrete form. The coefficient inputs are given by Equation B.5 using the CANF frequency estimates to set the filter cutoff frequency.

Figure B.12 shows the contents of the 'CANF' estimation block from Figure B.10. This consists of the cascaded notch filter structure and an update block. Figure B.13 shows the bandpass and sensitivity filter structures used in the CANF. Similarly to the adaptive PPF case, these filters could be implemented using discrete time varying transfer function

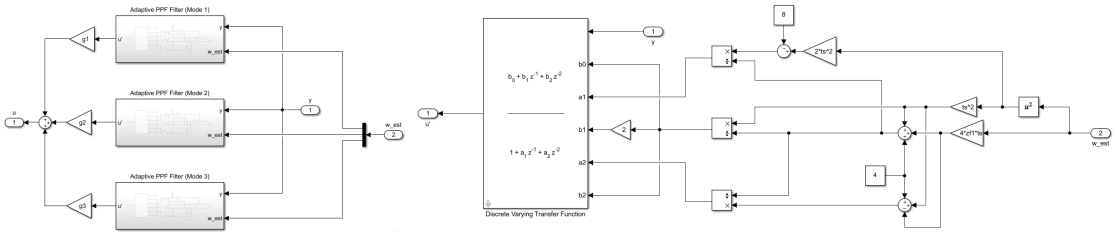

(a) Parallel PPF filters. (b) Adaptive PPF filter.

Figure B.11: Adaptive PPF Simulink models.

Simulink blocks, but direct implementation of the form given by Kwan and Martin [84] is preferred for consistency.

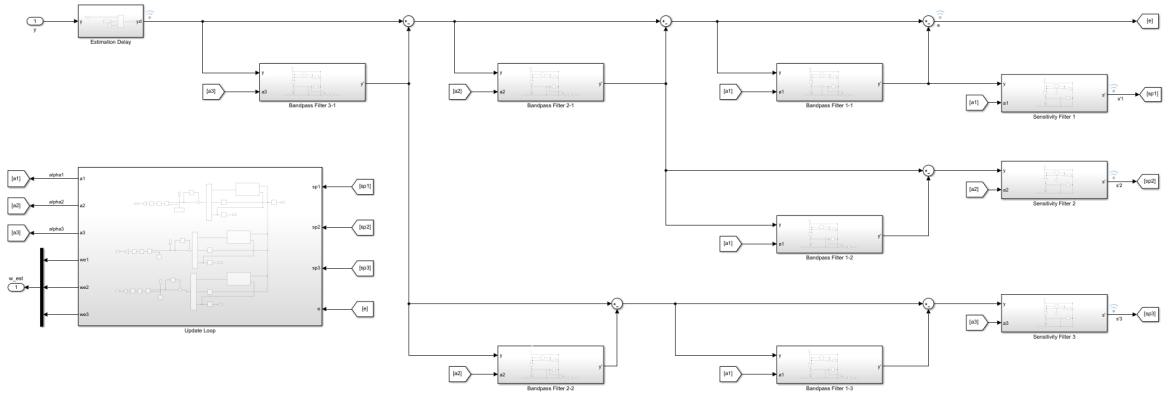

Figure B.12: CANF Simulink model.

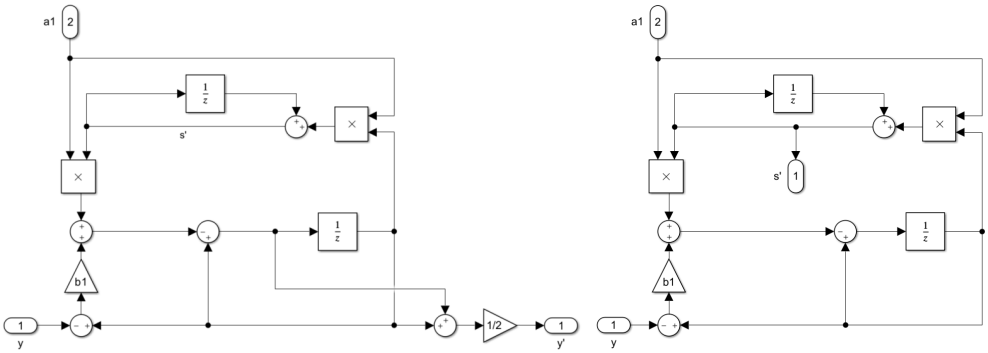

(a) Bandpass filter. (b) Sensitivity filter.

Figure B.13: CANF adaptive filter Simulink models.

Lastly, Figure B.14 shows the contents of the CANF update block which implements the update algorithm. A single update block diagram is shown here, but this is easily extended to the case of estimating multiple mode frequencies by adding an identical structure for each

frequency with its own parameters. The variable step size algorithm implementation is shown in Figure B.15.

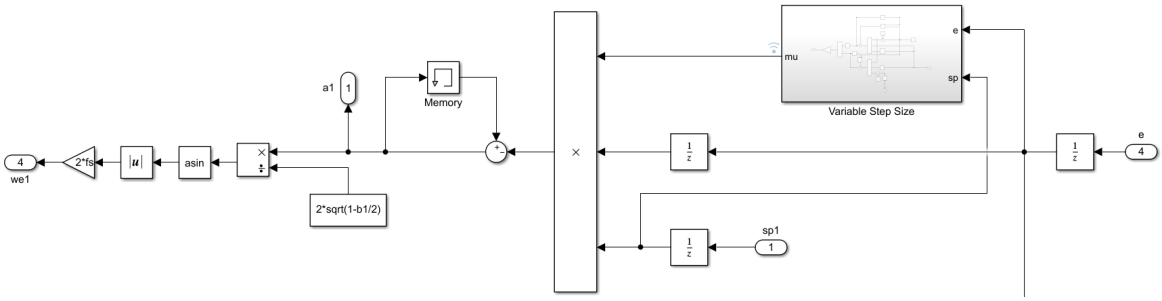

Figure B.14: ANF update Simulink model.

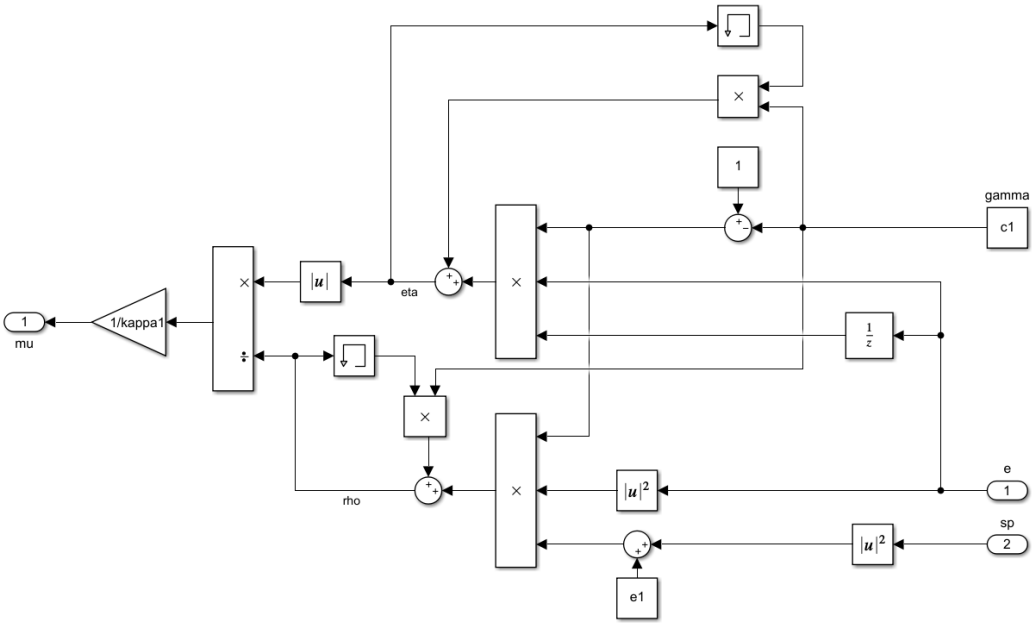

Figure B.15: ANF VSS Simulink model.

B.6 System Identification

With the experimental setup completed and the required code generated by Simulink, the beam with collocated piezoelectric transducers was identified. This was done using a chirp signal input with a frequency range that includes the modes to be damped. Note that the starting chirp frequency should be set at a reasonable value (e.g., 1 Hz), as lower values will require significantly more time for identification and should only be used if necessary.

Figure B.16 shows the identified frequency response of the system with different cases of signal conditioning. The frequency domain identification without any signal conditioning is as expected from the collocated system, although the gain should be adjusted to fit the ADC and DAC voltage range. The low frequency measurement is sufficient without using a charge amplifier, possibly because the ADC uses a switched capacitor input circuit. However, the time domain signal exhibits bias which also varies with time. A voltage amplifier circuit can be used to scale the gain and fix the time domain signal, although this significantly affects low frequency measurements and their coherence. Using the charge amplifier achieves good results in both time and frequency domains.

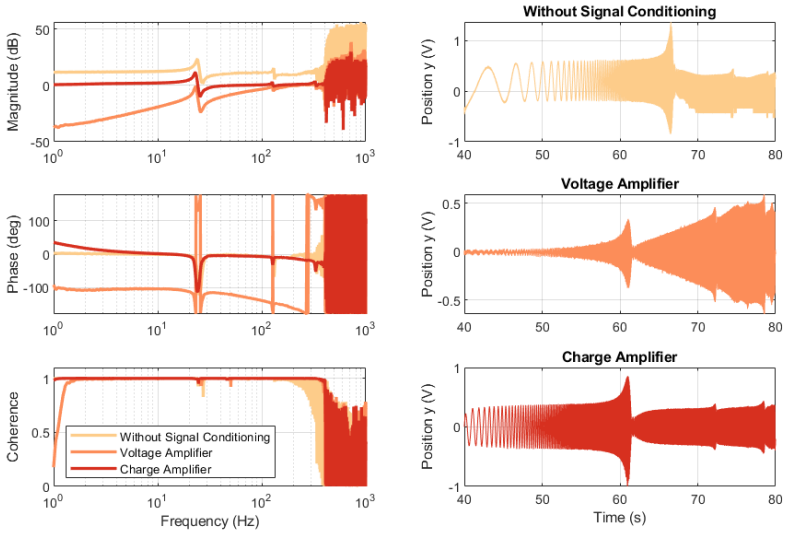

Figure B.16: Frequency and time response of the system with different cases of signal conditioning.

Figure B.17 shows the frequency response of the beam using the piezoelectric patch for sensing in two actuation cases. Patch actuation and sensing provides the expected collocated response, while piezoelectric stack actuation at the base of the beam gives a non-collocated response. It can also be seen that higher frequency modes are excited less by stack disturbances due to the negative slope in magnitude, which further explains the results in Figure 3.25 since the excitation and detection of the 3rd mode are relatively diminished compared to the first 2 modes.

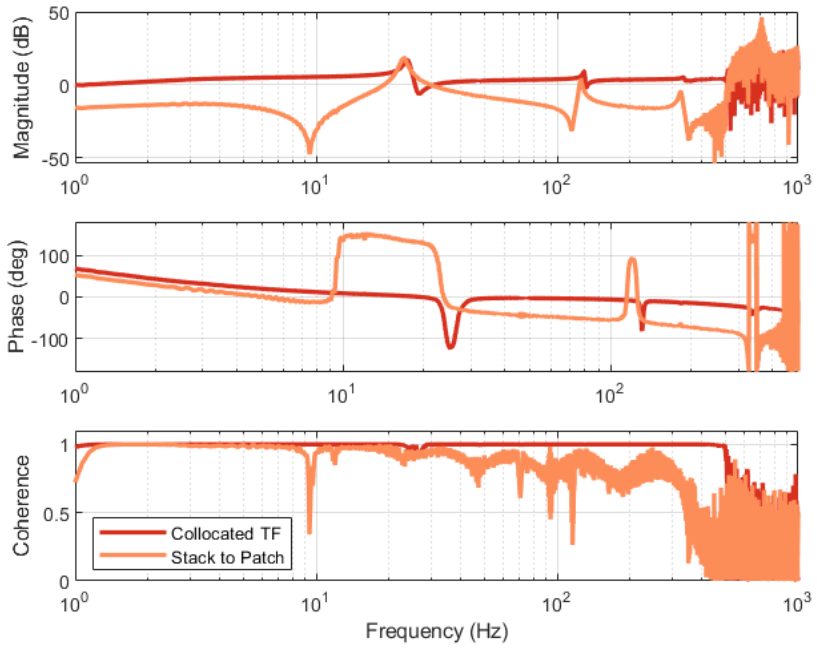

Figure B.17: Frequency response of the beam with different actuation points.

Appendix C

Code

C.1 Simulating Time-Varying Structures

The 'Varying Transfer Function' Simulink block from the Control System toolbox was used to simulate structures with time-varying mode frequencies. To obtain a transfer function with the form given by Equation 2.3, a sum of multiple 2nd order blocks were used. The Matlab script for generating the transfer function coefficients is given below:

```
% Manually set these parameters
Tf = 4;                     % Simulation time (s)
fs = 5000;                  % Sampling frequency (Hz)
k = 3;                      % Number of modes
% Mode damping ratios
z = [0.005, 0.005, 0.005];
% Mode frequency vector (see freqgen function)
w = 2*pi*[25, 50, 75, 150, 200, 250];
% Type of frequency variation (see freqgen function)
wtype = 'gradual';


ts = 1/fs;                  % Sampling time (s)
L = Tf*fs;                  % Length of signal
t = (0:L-1)'*ts;            % Time vector

% Time series of the mode frequencies and time varying TF coefficients
wn = freqgen(w,L,wtype);
for i = 1:k
    wa(i) = timeseries(wn(:,i),t);
    b0(i) = timeseries(0.02*wn(:,i).^2,t);
```

```
    a0(i) = timeseries(wn(:,i).^2,t);
    a1(i) = timeseries(2*z(i).*wn(:,i),t);
end
```

The function `freqgen` is shown below with instructions in the comments:

```
function wn = freqgen(w,L,wtype)

% Generates frequency vectors to simulate time varying modes
% ============================Inputs============================
% w: input frequency vector, dependent on wtype
% L: length of simulation signal
% wtype: type of frequency variation
%  'constant': frequency is constant throughout simulation
%               length(w) should be equal to # modes
%               example w for 2 modes: w = [10,20]
%  'instant':  frequency instantly changes
%               length(w) should be 2x # modes
%               frequency setpoints: odd w are initial values,
%                even w are final values
%               example w for 2 modes: w = [10,20,30,40]
%  'gradual':  frequency gradually increases then decreases
%               length(w) should be 2x the number of simulated modes
%               frequency setpoints: odd w are min values,
%                even w are peak values
%               example w for 2 modes: w = [10,20,30,40]
%  'hybrid1':  frequency gradually then instantly increases
%  'hybrid2':  frequency increases like hybrid1 then decreases
%               length(w) should be 3x the number of simulated modes
%               frequency setpoints: in sequences of triplets,
%                1st w is min value, 2nd is peak ramp value,
%                3rd is the "instant jump" value
%               example w for 2 modes: w = [10,20,30,60,70,80]
%
% ============================Outputs============================
% wn: generated frequency vector with length L

wlen = length(w);

switch wtype
    case 'constant'
        n = wlen;
        wn = zeros(L,n);
```

```
38          for k = 1:wlen
39              wn(:,k) = w(k);
40          end
41
42      case 'instant'
43          if mod(wlen,2) ~= 0
44              disp('Need 2 w values for each mode with this wtype');
45              return
46          end
47          n = floor(wlen/2);
48          wn = zeros(L,n);
49          for k = 1:n
50              wn(1:L/2,k) = w(2*k-1);
51              wn(L/2:L,k) = w(2*k);
52          end
53
54      case 'gradual'
55          if mod(wlen,2) ~= 0
56              disp('Need 2 w values for each mode with this wtype');
57              return
58          end
59          n = floor(wlen/2);
60          wn = zeros(L,n);
61          for k = 1:n
62              wn(1:L/2,k) = w(2*k-1):(w(2*k)-w(2*k-1))/(L/2):w(2*k)-...
63              (w(2*k)-w(2*k-1))/(L/2);
64              wn(L/2:L,k) = w(2*k):-(w(2*k)-w(2*k-1))/(L/2):w(2*k-1);
65          end
66
67      case 'hybrid1'
68          if mod(wlen,3) ~= 0
69              disp('Need 3 w values for each mode with this wtype');
70              return
71          end
72          n = wlen/3;
73          Lr = round(L/5);
74          wn = zeros(L,n);
75          for k = 1:n
76              wn(1:3*Lr,k) = ...
                    w(3*k-2):(w(3*k-1)-w(3*k-2))/(3*Lr):w(3*k-1)-...
77              (w(3*k-1)-w(3*k-2))/(3*Lr);
78              wn(3*Lr:5*Lr,k) = w(3*k);
79          end
80
```

```
81      case 'hybrid2'
82          if mod(wlen,3) ~= 0
83              disp('Need 3 w values for each mode with this wtype');
84              return
85          end
86          n = wlen/3;
87          Lr = round(L/3);
88          wn = zeros(L,n);
89          for k = 1:n
90              wn(1:Lr,k) = ...
                    w(3*k-2):(w(3*k-1)-w(3*k-2))/(Lr):w(3*k-1)-...
91              (w(3*k-1)-w(3*k-2))/(Lr);
92              wn(Lr:2*Lr,k) = w(3*k);
93              wn(2*Lr:3*Lr-1,k) = flip(wn(1:Lr,k));
94          end
95
96      otherwise
97          disp('Wrong wtype input, see function comments.')
98  end
```

C.2 Bairstow's Method

This code was used to simulate the recursive parametric system identification method for frequency estimation in the method comparison results of Section 4.2. The estimation method is discussed in detail in Appendix A.1. Bairstow's method is used to efficiently find the roots of the estimated polynomial given by Equation A.9. In Simulink, the 'Recursive Polynomial Model Estimator' block from the System Identification toolbox was used to estimate an AR model, and the coefficient estimates were then fed to a Matlab function block to run Bairstow's method recursively.

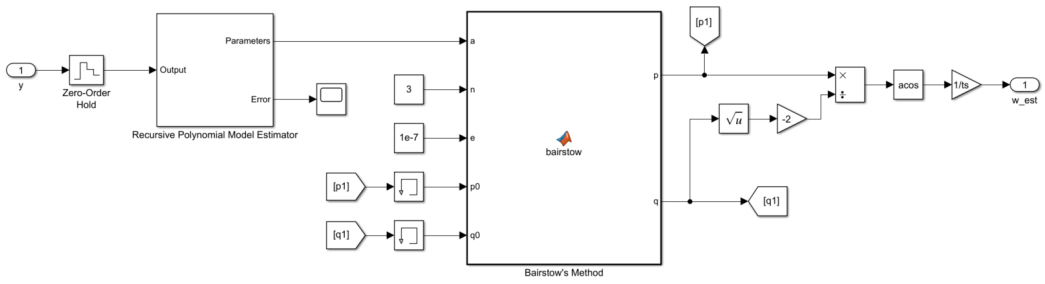

Figure C.1: Simulink implementation of recursive AR model estimation with Bairstow's root-finding algorithm.

```
function [p,q] = bairstow(a,n,e,p0,q0)
% Bairstow's method for root-finding
% ==============================Inputs==============================
% a: estimated polynomial coefficients
% n: number of estimated pole pairs/modes
% e: convergence tolerance
% p0 and q0: initial guesses for decoupled equation coefficients
% ==============================Outputs==============================
% p and q: decoupled equation coefficients used for frequency ...
    estimation

% MANUALLY initialize p and q (should be zeros(n,1) but that ...
    returns an error)
p = zeros(3,1);
q = zeros(3,1);

% # poles = 2x # modes
np = 2*n;

while true
    % Calculate b coefficients
    b = zeros(np+1,1);
    b(1) = a(1); b(2) = a(2) - p0(n)*b(1);
    for k = 3:np+1
        b(k) = a(k) - p0(n)*b(k-1) - q0(n)*b(k-2);
    end

    % Calculate c coefficients
    c = zeros(np,1);
    c(1) = b(1); c(2) = b(2) - p0(n)*c(1);
    for k = 3:np
        c(k) = b(k) - p0(n)*c(k-1) - q0(n)*c(k-2);
    end

    % Construct matrices
    Mp1 = [b(np), c(np-2); b(np+1), c(np-1)];
    Mp2 = [c(np-1), c(np-2); c(np)-b(np), c(np-1)];
    Mq1 = [c(np-1), b(np); c(np)-b(np), b(np+1)];
    Mq2 = [c(np-1), c(np-2); c(np)-b(np), c(np-1)];

    % Calculate change in p and q
    dp = det(Mp1)/det(Mp2);
    dq = det(Mq1)/det(Mq2);
```

```
42      pn = p0(n) + dp;
43      qn = q0(n) + dq;
44
45      % Check convergence and recurively calculate output coefficients
46      % p and q are sorted in reverse -> p(1) is the last value found
47      if (abs(pn-p0(n))/abs(p0(n)) < e) && (abs(qn-q0(n))/abs(q0(n)) ...
            < e)
48          p(n) = pn;
49          q(n) = qn;
50          % Recursively iterates for further factorization if needed
51          if n > 2
52              [prec,qrec] = bairstow(b(1:np-2),n-1,e,p0,q0);
53              p = p + prec;
54              q = q + qrec;
55          % Once only one 2nd order polynomial is left, the last ...
                values of p
56          % & q are simply the values of b
57          elseif n == 2
58              p(1) = b(2);
59              q(1) = b(3);
60          end
61          break;
62      end
63
64      % Set new initial values
65      p0(n) = pn;
66      q0(n) = qn;
67  end
```